NON-CANONICAL ROLE FOR INSULIN RECEPTOR SUBSTRATE-1 IN SIGNALING PATHWAYS OF THE LUNG

by

Heather Elizabeth Metz

B.S., Biological Sciences, University of Pittsburgh, 2006

Submitted to the Graduate Faculty of

The School of Medicine in partial fulfillment

of the requirements for the degree of

PhD in Cellular & Molecular Pathology

University of Pittsburgh

2015

UNIVERSITY OF PITTSBURGH

SCHOOL OF MEDICINE

This dissertation was presented

by

Heather Elizabeth Metz

It was defended on

November 13, 2015

and approved by

Marie C. DeFrances, M.D., Ph.D., Associate Professor

Wendy M. Mars, Ph.D., Associate Professor

Robert M. O'Doherty, Ph.D., Professor

Steven D. Shapiro, M.D., Professor

Dissertation Advisor: A. McGarry Houghton, M.D., Associate Member

Copyright © by Heather Elizabeth Metz

2015

NON-CANONICAL ROLE FOR INSULIN RECEPTOR SUBSTRATE-1 IN SIGNALING PATHWAYS OF THE LUNG

Heather Elizabeth Metz, PhD

University of Pittsburgh, 2015

Lung cancer is the leading cause of cancer deaths worldwide. In the United States alone, lung cancer accounts for ~160,000 deaths per year while the five-year survival rate remains stagnant at ~15%. Lung can be divided into different subsets including small cell and non-small cell lung cancer. Lung Adenocarcinoma (ADCA) accounts for over 50% of non-small lung cancer cases. Within this subset, *KRAS* is the most common activating mutation, accounting for ~35% of cases. *KRAS* mutant tumors have remained a largely un-targetable subtype, and a better understanding of the signaling pathways involved in the different ADCA subtypes will be necessary for the development of therapeutics. Insulin Receptor Substrate-1 (IRS-1) is a signaling adaptor protein that interfaces with many of the pathways that are activated in lung cancer, including phosphoinositol 3-kinase (PI3K), extracellular signal regulated kinase (MEK/ERK) and Janus Kinase (JAK) and Signal Transducer and Activator of Transcription (STAT). The central theme of this work is to describe novel roles for IRS-1 in the lung, including its integral role in the interplay between tumor cells and the surrounding tumor microenvironment. A key player in this interaction is the neutrophil, which can have pro-host and pro-tumor roles. We have found that neutrophils present in the tumor microenvironment cause degradation of the intracellular protein IRS-1, which in turn increases PI3K pathway activation leading to increased tumor proliferation. Independent study of IRS-1 loss with an *Irs-1*-deficient mouse model showed that Irs-1 loss induces an increase in neutrophil recruitment to the tumor. These two observations reveal a self-perpetuating cycle that causes increased tumor burden and mortality in mice and humans. Loss of *Irs-1* in our *Kras* mouse

model of lung adenocarcinoma induced activated JAK/STAT signaling and induced recruitment of immune cells to the tumor. Since neutrophils are essential for protection against invading pathogens, an indirect method of stopping this cycle must be used. Inhibiting JAK in our mouse model reduced inflammation, which in turn reduced tumor burden and prolonged survival. Overall, this work describes a novel role for IRS-1 as a mediator of cell growth and immune cell recruitment in lung adenocarcinoma.

TABLE OF CONTENTS

LIST OF TABLES

LIST OF FIGURES

PREFACE

ACKNOWLEDGEMENTS

I would like to first thank my mentor, McGarry Houghton, for all of his support and guidance throughout my PhD training as well as my time as a technician in his lab. I will forever be grateful for his mentorship, not only scientifically, but also in life.

I would also like to thank my doctoral committee: Marie DeFrances, Wendy Mars, Robert O'Doherty and Steve Shapiro. Your insightful guidance has greatly helped me through my development as a scientist.

I would like to thank the present and past members of the Houghton and Shapiro labs: Stephanie, Julia, Mark, Grace, Dee, Kyoung-Hee, Majd, Alyssa, Clint, Eduardo, Adriana, Shane, Robin, Dan, Lisa, Alyssa, Laura, Eleshia, Brittany, and Andy. Many of you have become the best friends I have ever had and I will always be grateful for the time I got to spend with each you.

I would also like to thank all of the collaborators that have helped make this work possible: Brenda Kurland, Kim Melton, Julie Randolph-Habecker and Sue Knoblaugh.

Finally, I would like to thank my friends and family: my parents Robin and George; my grandparents George and Shirley, George and Myrna; my siblings Andy, Megan and Katie; Mike, Brian, Bobby, David; my nephews Nathan and Gavin; my aunt Margie; Sarah, Eleshia, Amy, Jeanna, Elle, Nick, Bobby and Nelly. I couldn't have made it through without all the love and support you all have given me and I will forever be grateful.

1.0 INTRODUCTION

1.1 LUNG CANCER

1.1.1 Lung Cancer Statistics

Lung cancer continues to be the leading cause of cancer deaths worldwide [1]. In the United States, lung cancer accounts for 29% of male and 26% of female cancer deaths, totaling ~160,000 deaths per year. [2] Although in most western countries lung cancer death rates are decreasing, many Asian and African countries have increasing lung cancer rates due to recent changes in smoking prevalence [1]. In most developed countries, the five-year survival rate is less than 18% for women and less than 14% for men [3]. In developing countries, the five-year survival rate is only around 9% [3]. The recent decline in lung cancer deaths in Western countries is due to reduced smoking rates and not medical or scientific advancements for this disease, so continued research is necessary to better treat patients with this disease.

1.1.2 Brief History of Lung Cancer

The history of lung cancer is characterized by the emergence of a formerly extremely rare disease during the 20th century and its link to cigarettes. In the late 1800's lung cancer was noted to account for only 1% of cancers [4]. That number increased to 10-14% in the early 1900s and today accounts for more than 25% of cancers [2, 4]. The invention of the automated cigarette

machine in 1876 and World War I were major contributors to the increase in smoking prevalence. It is now accepted that cigarette smoke is the leading cause of lung cancer cases. This acceptance, however, took decades. The initial suspected agents of lung cancer were industrial air pollution, gas exposure from the war and mines, influenza and the least of these possibilities, smoking [2, 4]. Population studies of lung cancer and animal experiments beginning in the 1930's started to shed light on the link between cigarette smoke and cancer [4]. Unfortunately, for several decades cigarette use continued to rise as tobacco companies continued to market cigarettes and downplay potential harm. The Surgeon General's report of the hazards of cigarettes related to lung cancer was released in 1964 [4, 5]. Since the release of this report, smoking prevalence in the U.S. has decreased from 42% to 18% in 2012 [5]. Even with this decline, 5.6 million people currently under the age of 17 are expected to die from smoking-related causes later in life [5]. Although awareness of smoking dangers and decline in use has had significant improvements, the negative consequences arising from past and current use will carry on for decades.

While most lung cancer cases are smoking-related, there is a subset that occurs in non-smokers. Worldwide, 25% of lung cancer cases are non-smokers and in western countries about 10-15% [6, 7]. The statistics vary based on ethnicity and gender. Southeast Asian women have a higher prevalence, whereas, Western men have a lower prevalence of non-smoker lung cancer [7]. There are also differences in the types of lung cancer that non-smokers get. Non-small cell lung cancer, specifically adenocarcinoma, is the most common type in non-smokers [7]. The study of lung cancer in non-smokers has only begun in the past few years and the exact causes are still under investigation. Some of the suspected causes are: air pollution, smoke from cooking oil, radon, family history, history of tuberculosis, COPD, emphysema, chronic bronchitis,

hormone replacement and second hand smoke [7]. A number of genetic alterations also occur in non-smoker lung cancer cases including *EGFR*, *ALK*, *KRAS*, *HER2*, *BRAF*, and *PIK3CA* mutations [7].

1.1.3 Lung Cancer Pathology

Lung cancer is a heterogeneous disease that consists of two different subtypes: small-cell lung cancer (SCLC) and non-small cell lung cancer (NSCLC) making up 15% and 85% of cases respectively [8]. NSCLC is further divided into adenocarcinoma and squamous cell carcinoma subtypes. There has been a recent push among surgical pathologists to better classify tumor subtypes in patients because molecular-targeted therapies have been found to be effective in specific subtypes [9]. Two of the most common oncogenic drivers in lung ADCA are Kirsten rat sarcoma viral oncogene homolog (KRAS) and epidermal growth factor receptor (EGFR) [10]. Whereas EGFR-mutant patients have experienced modest improvement with therapy, KRAS-mutant tumors remain largely un-targetable [11]. To date, there are only a small number of FDA-approved targeted agents for NSCLC including bevacizumab (angiogenesis inhibitor), pemetrexed (chemotherapy drug), and erlotinib (EGFR inhibitor) [12-14]. The development of the tyrosine kinase inhibitor erlotinib, which targets EGFR has provided patient improvement in disease progression [12]. Other targeted agents including inhibitors of MEK and AKT pathways have provided less than 20% response rates in lung cancer patients [11]. There are a number of therapies currently in phase II and III clinical trials that target VEGFR, PDGFR, KIT, IGF-IR and EGFR. Unfortunately, there are still no targeted treatments for KRAS mutant patients.

1.2 INFLAMMATION AND CANCER

1.2.1 Inflammation and Cancer

The history of immunology has been characterized by competing pro-host versus anti-host theories. The field continues to evolve today as it is extended to investigation of tumor initiation and progression. In the early stages of immunology around the mid-1800's, it was observed that immune cells were present alongside bacterial cells and thus thought to have a pro-bacteria function [15]. This theory was challenged by Metchnikoff in the late-1800's to early-1900's, who's work was the first description of the phagocytic abilities of immune cells, providing a pro-host role for immune cells against infectious agents [16-18]. This same paradigm shifting development has begun in recent decades with regard to the role of inflammation and cancer. The first description of a link between inflammation and cancer was by Rudolf Virchow in 1863 when he noted leukocytes in neoplastic tissue and suggested that inflammation plays a role in the development of cancer [19, 20]. In the early 1900's Ehrlich proposed the theory that the immune system could eliminate cancers [21]. In the 1960's and 1970's Burnet and Thomas developed the theory of cancer immunosurveillance in which the immune system protected against tumor formation [22, 23]. Unfortunately, this theory was abandoned for more than twenty years based on experiments with a newly developed athymic nude mouse that showed no difference in tumor initiation and growth based on the immune system [21]. The development of knockout mice in the 1990's brought back interest in the immunosurveillance theory. Studies involving the loss of different immune cells and cytokines indicated the importance of the immune system in eliminating cancer formation [21]. Another line of thinking developed in the early 2000's as epidemiological studies gave evidence that chronic inflammation was related to an increase in

tumor development [24, 25]. It is now thought that acute inflammation can eliminate early cancer and chronic inflammation induces cancer development [26].

An important emerging concept in cancer biology is the role of the tumor microenvironment in tumor progression. Immune cells represent an important component of the tumor microenvironment. It has become evident that inflammatory responses increase tumor initiation and progression. Immune cells supply the tumor with different factors including growth factors, cytokines and reactive oxygen species that promote proliferation, survival, angiogenesis, invasion and metastasis [26-28]. Chronic inflammatory diseases have been correlated with development of cancers [19, 24, 26, 28]. Recent research has confirmed this observation, as many cancers are associated with chronic inflammation due to bacterial or viral infection and chemical and physical agents [19].

1.2.2 Neutrophils and Cancer

Neutrophils are a subset of leukocytes that are essential for protecting the host against invading pathogens [29]. They are the first line of defense against bacteria, fungi, protozoa, viruses [29]. Neutrophils are phagocytes that also release cytotoxic substances as well as proteinases into the extracellular environment. While this release is protective against pathogens, it also can cause damage of normal surrounding tissue [30]. Neutrophils are produced in the bone marrow where they are pre-packaged with granulocytic factors including proteinase-3, cathepsin G and Neutrophil Elastase and then are released into circulation with a life span of 1-3 days [29, 31]. Neutrophil Elastase is a major component of neutrophil function. It is released during degranulation and has a wide array of proteolytic activity against proteins and extra-cellular matrix components including elastin [32].

Neutrophils are capable of supplying the tumor with different factors including growth factors, cytokines and reactive oxygen species that promote proliferation, survival, angiogenesis, invasion and metastasis. [26-28]. An important observation in many cancer types, including NSCLC, is that elevated blood and intra-tumoral neutrophil counts correlate with poor patient outcomes [33]. Many of the trials providing evidence for this have only been published in recent years and it is still unclear how to use this observation to direct treatments in patients. Depleting neutrophils systemically could have severe negative consequences, as patients would become immune-compromised and susceptible to infection [30].

1.3 INSULIN RECEPTROR SUBSTRATE-1

1.3.1 Discovery of Insulin Receptor Substrate-1

The history of Insulin Receptor Substrate-1 (IRS-1) begins with a once fatal disease, diabetes. Diabetes first became a recognized disease in the early 1800's, and at this time patients had only weeks to live from time of diagnosis [34]. Almost 100 years later, it was discovered that insulin extracted from the pancreas could extend the lives of patients [35, 36]. Diabetes currently affects almost 27% of people over the age of 65 [34]. Insulin signaling has been a highly investigated field over the past several decades and many advancements have been made, including the development of synthetic insulin, characterization of the two different types of diabetes, as well as a thorough understanding of the cellular signaling cascade involved [34, 37, 38]. The intense study of insulin signaling has also revealed its role in cellular development, growth and metabolism [37]. The 3-dimensional structure of the insulin receptor was discovered in 1969 [39]. In 1985, Insulin Receptor Substrate-1 was identified as a 185 kD protein that becomes

phosphorylated due to cellular stimulation with insulin [40]. With the successful cloning of IRS-1 in 1991, it was then determined that IRS-1 coordinates signaling between the insulin receptor and PI3K [41]. To better understand the role of IRS-1 in signaling, an *Irs-1* null mouse was engineered. This mouse had low birth weight, displayed hyperglycemia and was insulin-resistant [42]. The development of this mouse precipitated the discovery of a related protein that had overlapping functions with IRS-1; it was named Insulin Receptor Substrate-2 (IRS-2) [42, 43]. An *Irs-2* null mouse was then engineered and this mouse displayed normal adult weight and development of type 2 diabetes [44]. An immense body of knowledge has since been added to the literature describing IRS protein signaling. The majority of research done on IRS proteins has, however, been in the setting of glucose metabolism and diabetes in metabolically active tissues such as muscle and adipose tissue.

1.3.2 Insulin Receptor Substrate-1 (IRS-1) Signaling 1 (Adapted from Metz, et al. Clinical Cancer Res, 2011.)

Insulin receptor substrates (IRS) are signaling adaptor proteins that function as intermediates of activated cell surface receptors, most notably for the insulin receptor (IR) and insulin-like growth factor receptor (IGF-IR) [41, 43, 45]. More recently, IRS proteins have been shown to signal downstream of integrin, cytokine, and steroid hormones receptors as well [46, 47], although these functions are poorly understood when compared with the “canonical” (IR- and IGF-IR–mediated) properties of IRS proteins. By mediating the activities of these receptors, IRS proteins interface with several signaling pathways, thereby impacting numerous aspects of cell behavior, including metabolism, motility, survival, and proliferation (Fig. 1). The majority of IRS protein research to date has centered upon the study of glucose metabolism and the pathogenesis of

diabetes. Reports pertaining to the roles of IRS proteins in cancer progression are beginning to emerge [48].

Six IRS proteins have been described; however, IRS-3 is expressed only in rodents [49], IRS-4 displays limited tissue expression (brain and thymus; [50]), and IRS-5 and IRS-6 are structurally dissimilar from the others [51]. Therefore, most of the attention has been focused on IRS-1 and IRS-2, both of which are widely expressed. IRS proteins share similar structural domains including an *N*-terminal pleckstrin homology domain and a phospho-tyrosine binding (PTB) domain, which is required for binding NPEY motifs in the juxtamembrane region of ligand-activated IR and IGF-IR [52]. The carboxy terminus contains numerous serine and tyrosine phosphorylation sites that bind PTB containing src-homology-2 (SH2) proteins, including p85, Grb2, Nck, the phosphotyrosine phosphatase SHP2, Fyn, and others [53]. Although IRS proteins are not catalytically active, they are capable of impacting numerous signaling cascades via interaction with SH2 proteins.

Despite sharing binding partners and structural similarities, IRS-1 and IRS-2 functions are not entirely overlapping. *IRS-1*$^{-/-}$ mice display low birth weight and glucose intolerance, but do not develop overt diabetes [42]. The generation of these mice led to the discovery of IRS-2, which was believed to compensate for the loss of IRS-1 and prevent additional metabolic derangements. *IRS-2*$^{-/-}$ mice have subsequently been shown to develop diabetes as a consequence of decreased β-cell function and insulin resistance [44]. Therefore, IRS-1 and IRS-2 possess both overlapping and unique properties, although their relative contribution to cancer growth and invasiveness has yet to be elucidated.

Though IRS proteins signal through many pathways, their predominant function seems to be activation and/or regulation of the phosphoinositide 3-kinase (PI3K) and extracellular signal

regulated kinase (ERK) pathways. PI3K is a heterodimer with separate regulatory (p85) and catalytic subunits (p110). In its resting state, PI3K exists as an inactive p85-p110 complex. Upon the activation of a receptor tyrosine kinase (RTK), meaning phosphorylation of its cytoplasmic tail, the p85-p110 complex is recruited to the receptor by interaction of an SH2 domain on p85 with phosphotyrosine residues on the RTK [54]. This interaction is believed to release the inhibitory effects of p85 on the catalytic p110 [55]. p110 is now able to interact with its lipid substrates, the phosphatidylinositols, and convert PIP2 to PIP3. Recruitment of PI3K by RTK also puts p110 in close proximity to these lipid substrates residing in the plasma membrane. The major exception to this schema is that PI3K can be activated by signal adapter proteins, such as IRS-1 and IRS-2, rather than by RTKs themselves [47]. Of note, IRS-mediated activation of PI3K requires that phosphorylated YMXM motifs occupy both SH2 domains within p85 [56].

Generation of PIP3 by activated PI3K near the plasma membrane results in interaction with, and subsequent phosphorylation of, its primary substrate, Akt [57]. Once activated, pAkt uses extensive downstream signaling pathways to enhance tumor viability in one of three ways: cell survival, cell proliferation (number), and cell growth (size; [58]). The avoidance of apoptosis, achieved by the direct phosphorylation of BAD by pAkt, is generally considered the predominant function of PI3K/Akt in cancer cells . However, PI3K/Akt also promotes tumor cell proliferation by causing an accumulation of cyclin D1, which regulates G1/S phase transition [59]. This is accomplished by inhibition of p27, p21, and glycogen synthase kinase-3β (GSK3β), which target cyclin D1 for proteasomal degradation, when active [60, 61].

PI3K activity seems to be regulated in two ways. The first is simply the activation of the p85 subunit, which maintains p110 in an inactive state at baseline. The second is the constitutively active negative repressor, phosphatase and tensin homolog (PTEN). PTEN

regulates the output of PI3K by dephosphorylating PIP3 back to PIP2 [62]. Mutation in PTEN is relatively common in cancers, and has been linked to PI3K hyperactivity in several, including prostate carcinoma, hepatocellular carcinoma (HCC), melanoma, renal-cell carcinoma, and glioblastoma, among others [63-67]. Interestingly, PTEN mutation is rare in some cancers, including lung cancer [68]. The common explanations for PI3K hyperactivity in the setting of preserved PTEN expression has been activation of PI3K by K-ras and genetic mutations within the PI3K pathway (e.g., PIK3CA), both of which possess the ability to by-pass regulatory machinery [69-71].

Although generally considered positive effectors of growth factor, IRS proteins may, in fact, function as homeostatic regulators of PI3K output in certain tissues. Supporting evidence of this theory includes the fact that IRS-p85 interaction takes place within the cytosol, pulling PI3K away from its lipid substrates and creating compartmentalization phenomena for signaling [72]. Furthermore, IRS proteins display low potency for ligand interaction. As an example, IRS-1-Grb2 binding results in nearly 10-fold less pathway output when compared with other common Grb2-binding partners [73].

1.3.3 Pro-Host and Pro-Tumor Roles for IRS-1 (Adapted from Metz, et al. Clinical Cancer Res, 2011.)

Preclinical studies have shown both protumor and prohost functions for IRS proteins in cancer. IRS-1 overexpression has been shown to induce malignant transformation in both embryonic mouse fibroblasts [74] and NIH3T3 fibroblasts [75, 76]. Such cells are capable of tumor formation in nude mice, a process displaying MEK/ERK hyperactivity and requiring IGF-IR, as embryonic fibroblasts derived from *IGF-IR*$^{-/-}$ mice are resistant to IRS-1–induced

transformation [77]. Oncogenic transformation by IRS-1 has not been described for other cell types.

Both IRS-1 and IRS-2 are commonly overexpressed in HCC, which is characterized by IR and IGF-IR signaling hyperactivity [78, 79]. IRS-1 overexpression in HCC cell lines prevents TGF-β–induced apoptosis [80]. In fact, transfection of these cells with a dominant-negative IRS-1 reverses their malignant phenotype [81].

The role of IRS-1 in breast cancer has been difficult to elucidate, as both prohost and protumor functions have been described. Simple overexpression of IRS-1 in MCF-7 breast cancer cells accelerates their growth, whereas IRS-1 gene silencing ultimately results in apoptosis, at least under serum-free conditions [82, 83]. IRS-1 and IRS-2 transgenic mice both display enhanced tumor growth, metastasis, and resistance from apoptosis [84]. These mice develop mammary gland hyperplasia early in life, and display unusual tumor histology, and not the typically encountered adenocarcinoma [85]. Thus, these overexpression studies may not be representative of pathophysiologic properties of IRS proteins in human cancers. As such, IRS-1–silenced tumor xenografts actually displayed increased metastasis [86], consistent with a prohost role for IRS-1. Additionally, studies of IRS-1 in human breast cancer show that IRS-1 expression is lost in clinically advanced cases [87].

We have recently described a prohost role for IRS-1 in lung cancer [88]. While investigating the role of neutrophil elastase in lung cancer, we observed that neutrophil elastase–deficient tumors in the Lox-Stop-Lox-K-ras (LSL-K-ras) model of lung adenocarcinoma [89] accumulated intracellular IRS-1 protein, whereas neutrophil elastase–sufficient tumors contained scant IRS-1. We were able to show that IRS-1 is an intracellular proteolytic target for neutrophil elastase, which induced cellular proliferation and pAkt production upon the degradation of IRS-

1. Ultimately, we discovered that the loss of IRS-1 functioned to increase the pool of bio-available PI3K, rendering p85 free to interact with the more potent growth factors present in lung cancer cells, especially the platelet-derived growth factor (PDGF) and receptor (PDGFR) complex [90]. Consistent with this concept, IRS-1 gene silencing in lung cancer cells resulted in cellular proliferation and pAkt production, whereas IRS-1 overexpression induced cell cycle arrest. Furthermore, a correlation of the presence of neutrophil elastase with the absence of IRS-1 was established in human lung adenocarcinomas. Thus, IRS-1 is capable of both growth promoting and growth regulatory functions in cancers, depending on the cell of origin.

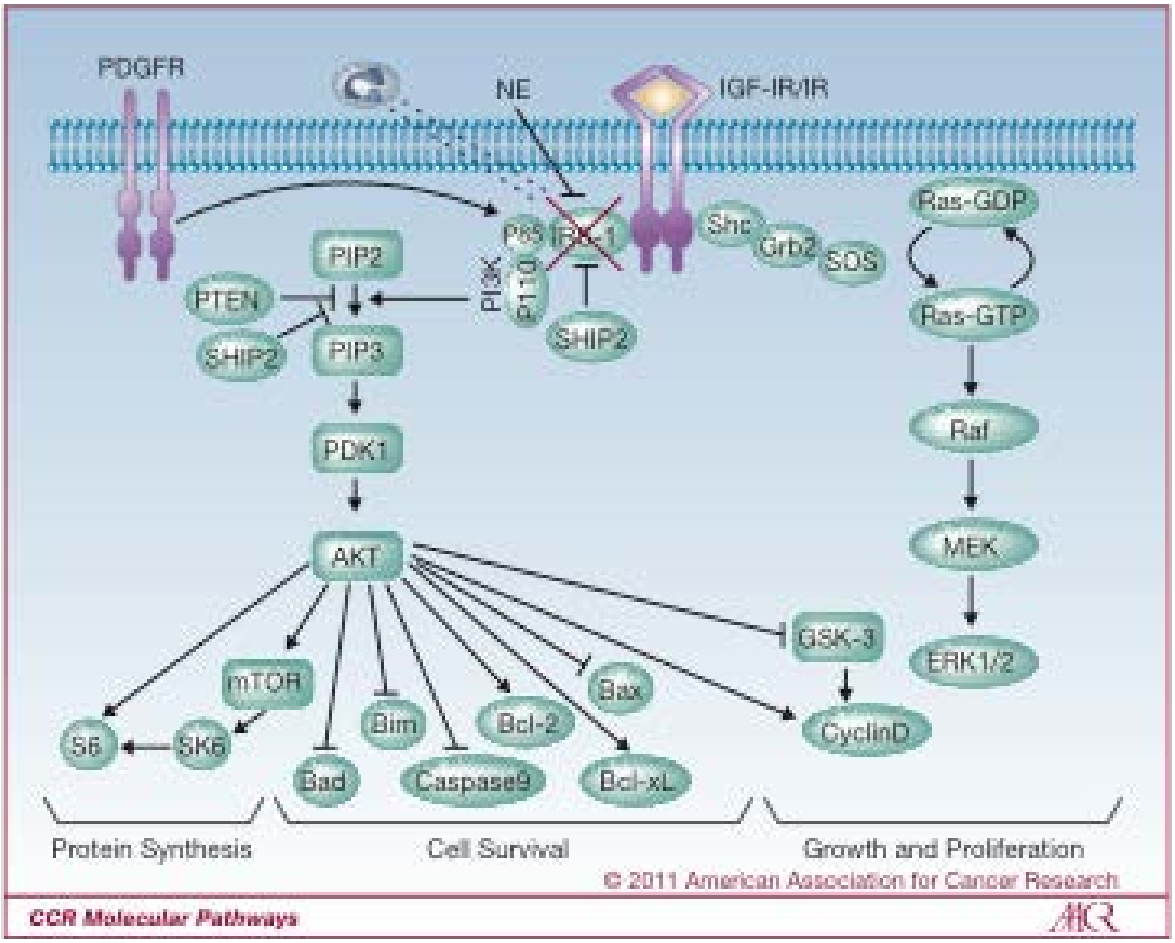

Figure 1. IRS-1 signaling. (Metz, et al. Clinical Cancer Res, 2011.): IRS-1 regulates downstream signaling of IR/IGF-IR. IRS-1 is a homeostatic regulator of PI3K signaling in lung tumor cells.

IRS-1 has serine and tyrosine phosphorylation sites that bind SH2 domain–containing proteins including p85, Grb2, and SHIP2, among others. IRS-1 recruits PI3K and MEK/ERK via interaction with the regulatory p85 subunit and GRB2, respectively. The catalytic subunit of PI3K, p110, is now available to convert PIP2 to PIP3. PIP3 activates PDK-1, which subsequently phosphorylates AKT, enhancing cell survival, proliferation, and growth. Downstream effectors of AKT inhibit apoptosis via inhibition of Bad, Bim, Bax, and caspase 9, and activation of BCL-XL and Bcl-2. Tumor cell proliferation is promoted by the inhibition of GSK3, which targets cyclin D1 for proteasomal degradation. Increased protein synthesis results from activation of the mTOR pathway. The MEK/ERK pathway also promotes proliferation via interaction of IR/IGF-IR with IRS or Shc proteins. A feedback loop exists between the PI3K/AKT signaling pathway and IRS-1, in which IRS-1 is degraded through the ubiquitin-proteasome degradation pathway. The above pathways have been well established in metabolically active tissues including adipose and muscle. The above figure, however, describes an alternative to those established paradigms. In lung cancer cells, the PI3K/AKT pathway is weakly activated by IRS-1. IRS-1 acts homeostatically to prevent activation of PI3K by more potent mitogens, including PDGF. Therefore, the loss of IRS-1 increases the amount of available PI3K, which can then be activated by these mitogens causing much greater pathway activation. As shown, neutrophil elastase (NE) can enter tumor cells and degrade IRS-1 during tumor-associated neutrophilic inflammation allowing other RTKs to control PI3K signaling.

1.3.4 IRS-1 Mouse Model

A second generation *Irs-1* null mouse was engineered a few years after the original IRS-1 knockout mouse. This new mouse was designed with an *Irs-1* gene flanked by two loxP sites,

allowing for its targeted removal in specific tissues [91]. LoxP sites are the target of an Adenoviral Cre recombinase (Adeno Cre) that removes the gene during a recombination event [92]. This mouse model thus presents the opportunity to selectively delete *Irs-1* from a specific tissue with the administration of AdenoCre. For a lung model, the AdenoCre would be delivered either intranasally or intratracheally, directing the virus into the lungs where it would then infect the cells of the lung and delete *Irs-1*. This mouse can also be crossed with other genetically modified mice in order to study the effects of combined genetic mutations.

1.4 JANUS KINASE (JAK) AND SIGNAL TRANSDUCER AND ACTIVATOR OF TRANSCRIPTION (STAT) SIGNALING

1.4.1 JAK/STAT

It has become clear that Janus Kinase (JAK) and Signal Transducer and Activator of Transcription (STAT) signaling play an important role in tumor growth and development [93, 94]. The JAK/STAT pathway is known for its major role in the initiation and resolution of inflammation [93]. The discovery of STATs and JAKs came about through the study of interferons, cytokines that mediate signals between host cells and the immune system in response to pathogens, in the late 1980's and early 1990's by two independent groups [95]. These investigators noted that a protein mediator functioned to relay signals from extracellular cytokines through cytokine receptors and transmit the signal to the nucleus to induce transcription. This protein mediator became known as a STAT. Between the late 1980's and late 1990's several different STATs and JAKs were described [96-102]. Since their discovery, JAKs and STATs have been heavily investigated. Studies identified the roles of JAKs and STATs as

mediators in immune modulation through cytokine signaling [103]. Aberrant JAK/STAT signaling has been found to play a role in tumorigenesis through the modulation of immune responses around the tumor site [104]; and currently, several JAK inhibitors are in clinical trial [103].

1.4.2 JAK/STAT Signaling

The JAK/STAT pathway is characterized by signaling from extracellular growth factors through cell-surface receptors mediating phosphorylation and dimerization of STATs leading to nuclear localization of STATs and increased gene expression. Signaling becomes activated through a combined interaction between the cytokine receptor, JAK and STAT proteins. The receptor first dimerizes and allows for JAK binding and phosphorylation. The activated JAK then induces phosphorylation of the receptor providing a site for STAT binding (SH2 site). JAK is then able to phosphorylate STAT on a tyrosine residue (around residue 700). Activated STATs form dimers and translocate to the nucleus. STAT dimers are transported to the nucleus through binding of transportin. The combinations include STAT1: STAT1, STAT3: STAT3, STAT4: STAT4, STAT5: STAT5, STAT1: STAT2 and STAT1: STAT3. Tetramer combinations are also possible [105, 106].

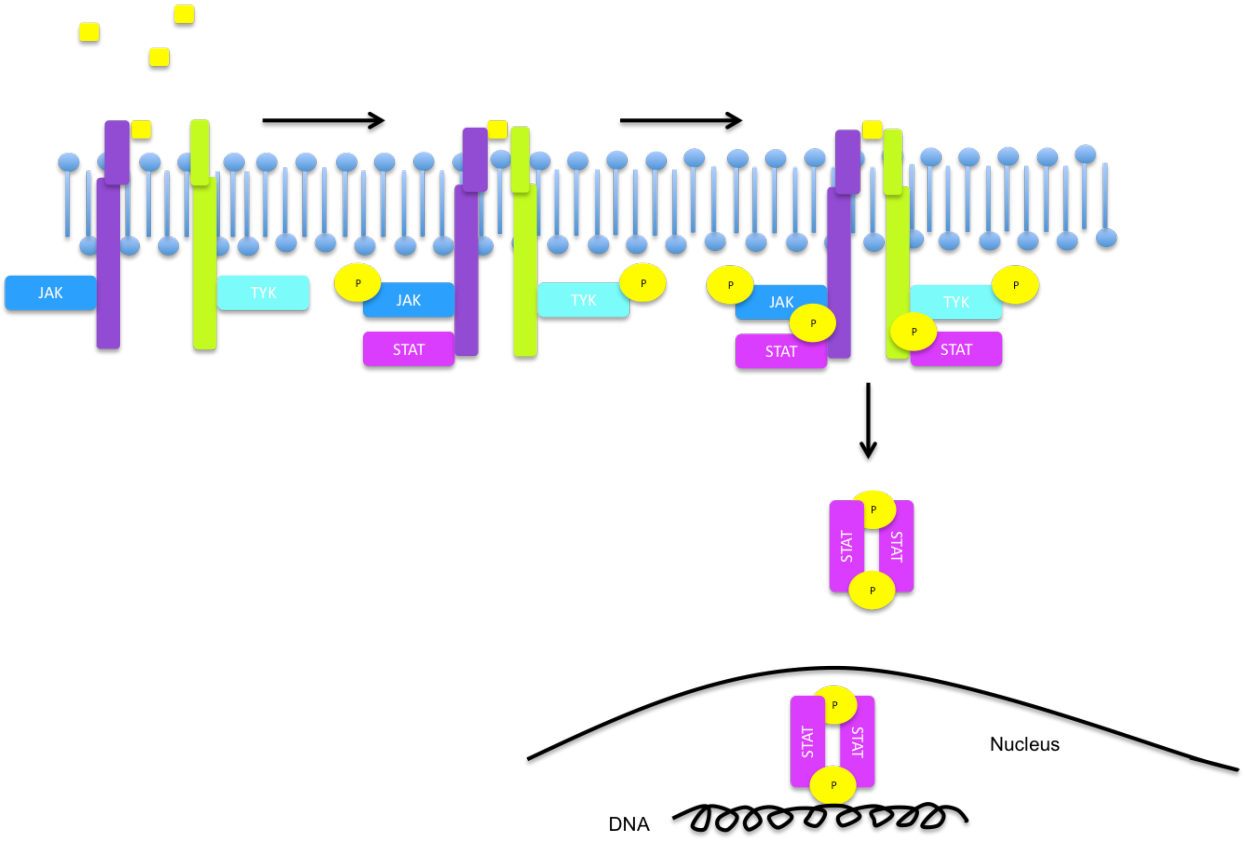

Figure 2. JAK/STAT signaling: Ligand binding to cytokine receptors triggers activation of JAKs. The JAKs then phosphorylate the receptor, which induces recruitment of STATs to the receptor which are in turn phosphorylated by JAKs. The STAT molecules then dimerize and are transported to the nucleus where they activate transcription.

There are almost 40 cytokine receptors that signal through the JAK/STAT system [107]. One such receptor that has been found to play a role in lung adenocarcinoma is the IL-22 receptor [108]. The IL-22 receptor consists of a dimer between Il-22R1 and IL-10R2, which is activated by the cytokine IL-22 [109]. In the lung, IL-22 predominantly comes from T cells including Th1, Th17 and Th22 cells. Release of IL-22 from these cells is driven by IL-6 and IL-23, whereas TGFB inhibits IL-22 production [109].

Deregulated JAK/STAT signaling can be found in many different tumor types and presents the opportunity for different levels of therapeutic intervention [110]. A meta-analysis of

17 clinical trials revealed that STAT3 activation predicts poor outcomes in NSCLC patients [111]. Roughly half of lung adenocarcinoma cases have activated STAT3 signaling [112, 113]. A study investigating the role of JAK inhibition in different NSCLC cell lines demonstrated its growth inhibitory effect in several cell lines but only in 3-dimensional soft agar and xenograft assays [114]. This study also demonstrated that STAT3 activation in these cell lines is dependent on JAK2 and not on oncogenic drivers and therefore, inhibitors of pathways activated by driver mutations may not effectively reduce tumor growth [114]. JAK inhibition may provide a promising strategy for treating certain lung cancer patients.

1.5 KRAS

1.5.1 Description of KRAS

Kirsten rat sarcoma (*KRAS*) is one of the most commonly mutated genes in lung cancer, found in about ~30% of lung adenocarcinoma cases [115]. *Kras* is an oncogene that was first discovered as a transforming retrovirus in animals. *Ras* was first identified in the mid-1960s when studies by Harvey and Kirsten showed that a rat leukemia virus induced sarcomas in infected rodents [116, 117]. These viruses became known as the Harvey murine sarcoma virus (HRAS) and the Kirsten murine sarcoma virus (KRAS). Scolnick, in the mid-70's, showed that these viruses transduced normal sequences from the rat genome [118, 119]. In the late 70's and early 80's several groups studied the role of DNA from transformed cells in animal and human tissue and found that DNA had transforming potential [120]. These studies were revolutionary to the field of cancer research.

There are 3 human *RAS* genes; *H-RAS*, *N-RAS* and *K-RAS* which all function through regulation of GDP/GTP exchange, transmitting signals from extracellular ligands through cell surface receptors including RTK's, non-RTK's and GPCR's [121]. The *RAS* genes are present in many different tissue types and have both overlapping and divergent roles [122]. *KRAS* is the most common activating mutation in cancer [123]. RAS is a small GTPase that alternates between a GTP-bound active state and a GDP-bound inactive state [124]. Oncogenic RAS becomes constitutively activated in the GTP-bound state [123]. This RAS activation then leads to increased signaling through RAF/MEK/ERK, PI3K/AKT/mTOR and RalGEF/RAL/NFκB pathways [124]. Over-activation of these pathways induces cellular proliferation and increased tumorigenesis [124].

It has become evident that different types of *KRAS* mutations cause different effects with regard to downstream signaling and subsequent cellular behavior. There are a few common *KRAS* mutations, including mutations in codon 12, 13, 10 and 61, with the most prevalent of these being a mutation in codon 12 [125]. Recent work has demonstrated that depending on which codon is mutated, KRAS toggles between signaling through MEK, AKT or RalA/B and that these differences in signaling impact patient survival [126]. Investigation of NSCLC cell lines has revealed that mutant-KRAS-G12D mutations signal through AKT and MEK pathways, whereas mutant-KRAS-G12C signals through RalA/B and MEK and wildtype KRAS signal through MEK [126].

1.5.2 Kras Mouse Model of Lung Adenocarcinoma

Several generations of mouse models have been developed to study KRAS mutation [124, 127]. In the late 1990's, the development of a null Kras mouse was attempted. However, it was noted

that all offspring were heterozygous for the *Kras* gene. It was thus found that homozygous deletion of *Kras* is embryonic lethal due to cardiac, neurological, hematological as well as liver defects in embryos [122, 128]. It became evident that having a functional *Kras* gene is necessary for development and laid the groundwork for future Kras mouse models. A few years later, a mouse model was developed in which a latent form of mutant *Kras-G12D* was inserted and later became active upon spontaneous recombination events [129]. In this model, embryos expressed normal Kras to ensure normal development until birth and later developed tumors with the accumulation of recombination events inducing mutant Kras expression. These mice most notably developed lung tumors that ranged from hyperplasia to adenocarcinoma [129]. The disadvantage of this model is non-synchronous tumor initiation and development, which is a confounding factor for careful study of tumor growth and development. To address this issue, the same group developed a system that would allow for conditional expression of mutant Kras. In this system, a Lox-Stop-Lox (LSL-) sequence flanks the *K-ras-G12D* sequence, preventing its expression until activation is desired [89]. An adenoviral Cre recombinase (AdenoCre) is administered intranasally to the mouse and upon entry removes the stop codon, allowing for expression of the mutant gene. Once activated, mice displayed a progression from atypical adenomatous hyperplasia (AAH), epithelial hyperplasia (EH) and finally adenomas in a predictable time course based on dose of AdenoCre [89]. The LSL-Kras model has become a gold standard for lung cancer research and has since been combined with many other mouse models, including ones in which genes are mutated, deleted or overexpressed in order to more fully understand the complexities of this disease in a controlled manner.

1.6 IDIOPATHIC PULMONARY FIBROSIS (A LUNG CANCER RELATED DISEASE)

1.6.1 Idiopathic Pulmonary Fibrosis Pathology

Patients with idiopathic pulmonary fibrosis (IPF) are more likely to have lung cancer than non-IPF patients [130]. IPF is a debilitating disease characterized by scarring of the lung and loss of function due to deregulated fibroblast repair response to epithelial injury [131]. IPF is the most common interstitial lung disease with only a 3 to 5 year survival rate [132]. The exact mechanisms and causes of IPF are still unclear. It is thought that cigarette smoking, viral infections and environmental factors such as asbestos lead to the development of IPF [133]. IPF is characterized by persistent inflammation and wound healing processes during which fibroblasts deposit extracellular matrix causing dense fibrotic tissue accumulation in the lung [134]. Sadly, there are currently no effective treatments for IPF [130]. A better understanding of the mechanism for development of fibrotic lung tissue will be necessary for the successful development of new therapies for this disease.

1.6.2 Neutrophils and Fibroblasts

The lungs have resident fibroblasts that function in tissue homeostasis by secreting factors that maintain the extracellular matrix. In the setting of wound healing, fibroblasts develop an activated phenotype and are called myofibroblasts. These myofibroblasts release matrix metalloproteinases that function in tissue remodeling, secrete collagen that leads to scarring and express alpha-smooth muscle actin, which allows for its contractile properties [135]. There are three phases of would healing that include: an immune response, proliferation of fibroblasts and

activation to myofibroblasts and finally deposition and remodeling of the extracellular matrix [136]. The final phase is point at which scarring can occur. There is some evidence that neutrophils can affect fibroblast activity. There is clinical data to suggest that neutrophils and Neutrophil Elastase are related to IPF pathology [134]. Further studies into the role of neutrophils in fibroblast activation may illuminate this complex disease.

2.0 NOVEL PRO-HOST ROLE FOR INSULIN RECEPTOR SUBSTRATE-1 IN *KRAS*-MUTANT LUNG ADENOCARCINOMA

Heather E. Metz[1,2,7], Julia Kargl[7], Stephanie E. Busch[7], Kyoung-Hee Kim[7], Brenda F. Kurland[4,5], Shira R. Abberbock[4], Julie Randolph-Habecker[8], Sue E. Knoblaugh[8], Jay K. Kolls[3], Morris F. White[6], and A. McGarry Houghton[7,9]

From the Departments of [1]Medicine, [2]Pathology, [3]Pediatrics, and the [4]University of Pittsburgh Cancer Institute, University of Pittsburgh School of Medicine, Pittsburgh, PA; Department of [5]Biostatistics, University of Pittsburgh Graduate School of Public Health, Pittsburgh, PA; [6]Division of Endocrinology, Boston Children's Hospital, Boston, MA; [7]Clinical Research Division and [8]Experimental Histopathology Shared Resource, Fred Hutchinson Cancer Research Center, Seattle, WA and [9]Division of Pulmonary and Critical Care, University of Washington, Seattle, WA.

Manuscript in preparation.

2.1 INTRODUCTION

Lung cancer continues to be the leading cause of cancer deaths worldwide [1]. In the United States alone, lung cancer accounts for more than 160,000 deaths per year with five-year survival rates of just ~15% [2, 3]. Lung cancer is a heterogeneous disease that is typically subdivided into two major subtypes: small-cell lung cancer (SCLC) and non-small cell lung cancer (NSCLC), which constitute approximately 15% and 85% of cases, respectively. NSCLC is further sub-classified by the existence of multiple histologic subtypes, most of which are designated as lung adenocarcinoma (L-ADCA, ~60%) or squamous cell carcinoma (L-SCCA, ~20%) [8]. In contrast to L-SCCA, L-ADCA is characterized by the presence of driving mutations in key oncogenes, such as the epidermal growth factor receptor (*EGFR*) and the Kirsten rat sarcoma viral oncogene homolog (*KRAS*) [10]. Whereas *EGFR*-mutant cancers can be addressed with novel targeted therapies, *KRAS*-mutant tumors remain largely un-targetable [11].

Numerous studies have been performed that address the impact of a specific driving mutation on the function of a particular signaling pathway. However, the impact of alterations in the signaling pathway machinery within these aberrantly functioning pathways, have not been adequately studied. Of the numerous proteins that are involved in pathway signaling, the insulin receptor substrate-1 (IRS-1) is somewhat unique in that it interfaces with many different pathways, including the phosphoinositol 3-kinase (PI3K) and extracellular signal regulated kinase (MEK/ERK) pathways, as well as the JAK/STAT signaling pathway [53, 137-142]. IRS-1 is afforded this promiscuity as a result of possessing numerous binding domains, including an N-terminal pleckstrin homology (PH) domain, a phospho-tyrosine binding (PTB) domain and a carboxy-terminus with multiple serine and tyrosine phosphorylation sites. IRS-1 is a signaling adaptor protein best known for mediating canonical signaling from both the insulin receptor (IR)

and the insulin-like growth factor receptor (IGF-IR) [45]. The majority of research investigating the function of IRS proteins has naturally been performed in the setting of glucose metabolism and diabetes in metabolically active tissues, including muscle and adipose tissue. In this context, IRS-1 has been appropriately characterized as a positive effector of growth factor [47, 56]. However, the impact of IRS-1 on pathway activity in cancer cells, where aberrant signaling is frequently encountered, has not been adequately addressed.

An emerging concept in cancer biology is the role of the tumor microenvironment (TME) on tumor progression, and the role of aberrant pathway signaling in sculpting the TME. Immune cells represent a major component of the TME, frequently comprising over half of the cells in resected tumor specimens. It has become evident that inflammatory responses increase tumor initiation and progression, as immune cells are capable of supplying tumors with the growth factors, cytokines, and reactive oxygen species required to promote proliferation, survival, angiogenesis, invasion and metastasis [26-28]. The mechanisms by which cancers generate tumor-promoting microenvironments must be further explored in order to identify novel therapeutic agents that address the TME.

Given the prominent role of IRS-1 in signaling pathways commonly hyperactive in L-ADCA, we undertook an independent study of this protein within the adenocarcinoma subtype. Surprisingly, we identified a counter-paradigmatic and pro-host role for IRS-1 specifically in *KRAS* mutant L-ADCA via alterations in cancer cell signaling that subsequently impacted the cellular composition of the TME.

2.2 MATERIALS AND METHODS

2.2.1 Mice

Lox-Stop-Lox-K-ras (*LSL-K-ras*) and *Irs-1*$^{fl/fl}$ (Morris White, Boston Children's) mice on a pure SVEV background (backcrossed >10 generations) were used in these studies. The mice were housed in a pathogen free barrier facility at the Fred Hutchinson Cancer Research Center (FHCRC) and experiments were performed in accordance with approved IACUC protocols.

2.2.2 Intratracheal administration of AdCre

A titer of $4x10^7$ pfu AdCre (University of Iowa Viral Vector core) was administered intratracheally (IT) to sex-matched anesthetized mice between 8 and 10 wks of age via a 22g intravenous (IV) catheter placed in the trachea.

2.2.3 Assessment of mortality

LSL-K-ras/Irs-1$^{+/+}$ and *LSL-K-ras/Irs-1*$^{fl/fl}$ mice (n>25 per group) were followed from the date of AdCre administration until death or signs/symptoms of impending mortality. This time interval was used to calculate overall survival. Differences in survival were measured using the Kaplan-Meier method.

2.2.4 BAL fluid analysis

At 8, 12 and 16 weeks post-AdCre, mice were sacrificed and bronchial alveolar lavage (BAL) fluid was collected by inserting a 22g IV catheter into the trachea. Lungs were then lavaged with 0.75ml saline 4 times. The BAL fluid was centrifuged at 3,000 r.p.m. for 3 minutes. Red blood

cells (RBC) were lysed using a RBC lysis buffer (Biolegend, San Diego, CA). Total cell counts were obtained using a hemocytometer. Cytospins were made from each suspension and manual differentials were generated using Hema-3 staining (Thermo Fisher Scientific, Waltham, MA).

2.2.5 Histology and immunohistochemistry

At 8, 12 and 16 weeks post-AdCre, the mice were sacrificed and the lungs were harvested. A split lung inflation technique was performed in which the left lung was ligated, removed and frozen, while the right lung was subsequently inflated with 2X Zinc Fixative (BD Biosciences #552658, San Diego, CA) at 25cm H_2O pressure via intratracheal catheter for 15 minutes. Lungs were removed and fixed in 2x Zinc Fixative for 72 hours. Lungs were then paraffin embedded. 5-µm paraffin-embedded sections were stained for hematoxylin and eosin (H&E), IRS-1 (abcam #52167, Cambridge, MA), Ly-6G (Biolegend #127601, San Diego, CA), Phopho-Stat3 (pTyr705) (D3A7) (Cell Signaling # 9145, Danvers, MA), and IL-22 receptor alpha 1 (IL22RA1) (Millipore # 06-1077, Temecula, CA). Staining was preformed using the avidin-biotin HRP technique with 3,3′-diaminobenzidine (DAB) as the chromogenic substrate as previously described [143].

Slides were scanned using Eclipse 80i microscope (Nikon Instruments Inc., Melville, NY). Total lung and tumor area was determined from H&E stained slides using NIS-Elements Advanced Research software (Nikon). Tumor area % was calculated as follows: ((tumor area/ total lung area) x 100). Phospho-Stat3 and IL22RA1 stained lung tissue were scored using a grid at 40X magnification. Results are expressed as number of positively stained cells per high-powered field (hpf) from a total of 5 hpf per slide.

2.2.6 Therapeutic studies in mice

Mutant *K-ras* expression was induced in *LSL-K-ras* and LSL-K-ras/Irs-$1^{fl/fl}$ mice using AdCre, as described above. After allowing 8 wks post-AdCre for tumors to develop, mice (n=8 per group) received either the JAK inhibitor AZD1480 (30 mg/kg) (AstraZeneca) or vehicle control via oral gavage. Mice were treated with drug or vehicle 6 days per week for 3 weeks. In a separate experiment, LSL-K-ras/Irs-$1^{fl/fl}$ mice were treated with either the neutrophil-depleting Ly-6G 1A8 monoclonal antibody or Rat IgG2a 2A3 isotype control (BioXCell, West Lebanon, NH) beginning at 6 wks post-AdCre for 4 weeks at a dose of 500µg 3 times per week.

2.2.7 Quantitative PCR (qPCR)

Frozen mouse lungs were homogenized in Trizol (Invitrogen, Carlsbad, CA) and total RNA was extracted using chloroform and isopropanol precipitation. cDNA was generated from 2µg total RNA using a SuperScript cDNA synthesis kit (Invitrogen, Carlsbad, CA). qPCR was performed using a StepOnePlus Real-Time PCR Machine (Applied Biosystems) and Taqman primer/probe sets (Applied Biosystems). Reactions were run in triplicate and GAPDH was used as the endogenous housekeeping gene. Delta-CT values were used for data analysis and expressed as fold change from control.

2.2.8 Cells

A549 (ATCC # CCL-185) and 201T (Obtained from University of Pittsburgh Cancer Institute [144]) human lung adenocarcinoma cell lines were used for in vitro experiments. Cells were maintained in Dulbecco's modified essential medium (DMEM) plus 10% fetal calf serum (FCS) and 1x penicillin-streptomycin (Gibco).

2.2.9 shRNA transfection

A549 and 201T cells were transfected with control and IRS-1 Lentiviral Transduction particles (Sigma-Aldrich SHC001V and TRCN0000039910 NM_005544.1-4044s1c1). Cells were plated in 96-well plate (4,000 cells per well) in DMEM containing 10% serum and allowed to adhere overnight. 5 µl of transduction particles were added to each well for 18 hours. Plates were washed 2x with PBS and fresh 10% serum DMEM was added. One day later, puromycin was added to wells and cells were selected for 10 days.

2.2.10 IL-22 treatment

A549 and 201T cells were plated at 250,000 cells per well in 6-well plates in DMEM containing 10% serum and allowed to adhere overnight. Plates were then washed with PBS twice and serum free DMEM was added. 18 hours later 25ng of IL-22 (eBioscience # 14-8229-63) was added to the existing serum-free media for various timepoints (10, 15. 30 and 60 minutes). Cells were washed twice with PBS, frozen in liquid nitrogen, lysed with 2x cell lysis buffer plus protease/Phosphatase inhibitor Cocktail (Cell Signaling # 9803 and # 5872).

2.2.11 In vitro JAK inhibiton

Cells were plated at 250,000 cells per well in 6-well plates in DMEM containing 10% serum and allowed to adhere overnight. Plates were then washed with PBS twice and serum free DMEM was added. A JAK inhibitor (Millipore #42009918) diluted in DMSO was added to the serum free media along with DMSO control for 2 hours. After 2 hours, 10ng of IL-22 (eBioscience # 14-8229-63) was added to the existing serum-free media plus inhibitor and DMSO control for 15 minutes. Cells were washed twice with PBS, frozen in liquid nitrogen, lysed with 2x cell lysis buffer plus protease/Phosphatase inhibitor Cocktail (Cell Signaling # 9803 and # 5872).

2.2.12 Immunoblotting

Protein concentrations were calculated using a BCA Protein Assay Kit (Pierce #23225) and were separated using NuPAGE 4-12% Bis-Tris gels (Life Technologies) followed by transfer to PVDF membranes. Membranes were blocked for either 2 hours at room temperature or overnight at 4C in 5% milk in PBS-tween. Primary antibodies were incubated either overnight at 4C or for 2 hours at room temperature followed by secondary antibody for 1 hour at room temperature. Membranes were incubated in SuperSignal West Pico Chemiluminescent Substrate (Thermo Scientific Rockford, IL) for 5 min. and then developed using an x-ray film processer. Primary antibodies include; IRS-1 (1:250, Cell Signaling # 2382), pSTAT3 (1: 1,000 Cell Signaling #9271), STAT3 (1:1,000 Cell Signaling #9145), pAKT (ser473) (1:250 Cell Signaling # 9271), AKT (1-1,000 Cell Signaling # 9272), pGSK-3B (ser9) (1:1,000 Cell Signaling #9336), GSK-3B (27C10) (1:1,000 Cell Signaling #9315), PI3K-p85 (1:1,000 Millipore #06-497), IL-22 Receptor (1:1,000 Thermo Scientific #PA5-19987). GAPDH (1:10,000 Cell Signaling #2118) and Ponceau stain (Sigma #P3504) was used as load control.

2.2.13 Human Tissue Microarray (TMA)

A lung adenocarcinoma cohort on tissue microarray was obtained from the University of Pittsburgh Cancer Institute (UPCI). The TMA consists of 135 cases. Each case is annotated as either KRAS mutant, EGFR mutant, or WT for both EGFR and KRAS. Survival data and known prognostic factors (age, tumor stage, mutational status, etc.) were available through the UPCI cancer registry. Patient identifiers were removed and the study was therefore considered “not human subjects” research (IRB exempt).

FFPE sections were stained with an IRS-1 antibody (Santa Cruz #sc-720, Dallas, TX). Digital images of IHC-stained (with IRS-1 antibody) TMA slides were obtained at 20x magnification (0.5 μm per pixel) using a whole slide scanner (ScanScope AT, Aperio) fitted with a 20x/0.75 Plan Apo objective lens (Olympus, Center Valley, PA, USA). Images were saved in SVS format (Aperio), managed with server software (ImageServer, Aperio), and retrieved with a file management web interface (Spectrum, Aperio).

Under pathologist supervision, the TMA cores were annotated using Aperio's annotation software (ImageScope v12.2, Aperio). For automated image classification, image areas from TMAs were annotated that represented five user-defined Image Classes (tumor, stroma, inflammation, other, and clear glass) and ranged in morphologic appearance and staining intensity of DAB and hematoxylin (counterstain). These image areas were used as input parameters for the histologic pattern recognition training software (Genie Training, Aperio) to produce a Genie Training Set. The effectiveness of the Genie Training Set was visualized on the TMA image test regions (TMA spots) using the image classifier algorithm (Genie Classifier, Aperio), which overlaid an image markup pseudo colored for each Image Class. Annotated image areas from the TMA were adjusted (adding or removing image areas) for each Image Class to improve the classifier accuracy. For example, if the Genie Classifier algorithm over-classified regions of stroma as tumor, additional stromal annotations were added to the Genie Training algorithm to better represent the stromal Image Class. This process of adjusting annotations, re-running the Genie Training algorithm, and visually inspecting pseudo colored markup images output by Genie Classifier was iteratively repeated until a Genie Training Set was developed to classify the TMA slides optimally, as visually validated by a pathologist. The optimized Genie Classifier was then run on the TMAs.

IHC staining was evaluated within tumor areas only of each TMA spot that had been manually annotated, and a separate analysis was performed on areas from each TMA spot that had been classified as tumor by the Genie Classifier. The Color Deconvolution algorithm (Aperio) was used to isolate individual stains for quantification: the red, green, and blue (RGB) OD color vectors were measured for each stain using default software settings for hematoxylin and DAB. The average RGB OD values (Hematoxylin: 0.65, 0.704, 0.286; DAB: 0.268, 0.57, 0.776) were utilized in the Color Deconvolution software to define each stain component in the final analysis settings. Staining was quantified by the following metrics: the percentage of tumor with IRS-1 staining (% Strong, Medium, and Weak Positivity), and the Score. The H-Score was calculated by a simple formula involving the positive percentages. Score = 1.0*(%Weak) + 2.0* (%Medium) + 3.0*(%Strong).

H&E stained sections were obtained from the UPCI and were scored for myeloid and lymphocytic cell inflammation. The specimens were scored as follows for each: absent = 0, sparse cellular content = 1, moderate cellular content = 2, heavy cellular infiltration = 3.

2.2.14 Statistical Analysis

Statistical Analysis. For human TMA, overall survival (OS) was calculated from the date of diagnosis to the date of death or last confirmation of vital status. Associations between overall survival and clinical and novel predictors were assessed using the log-rank test and by Cox proportional hazards regression. Recursive partitioning, a tree-based survival analysis method, was used to identify an optimal IRS-1 H-score cutpoint in a univariate survival model [Breiman et al 1984 book]. Dichotomized IRS-1 and clinical predictors with strong associations with survival in our data or in the literature (sex, age, mutational phenotype [K-ras, EGFR, Wild-

type], TNM stage, smoking status [never/former/current]) were considered for a multivariable Cox regression model. Statistical analyses were conducted using SAS/STAT software, version 9.4 (SAS Institute, Inc., Cary, NC) and R version 3.1.3 (R Foundation for Statistical Computing, Vienna, Austria) including the rpart package.

Kaplan-Meier survival curves were generated using Prism Software. For all other studies, both in vitro and in vivo, either Student's t-tests (two-sided, two-sample) or one-way ANOVA (with Tukey Post-Test) were used, as appropriate. Data expressed as mean ± SEM. A P value < 0.05 was considered significant.

2.3 RESULTS

2.3.1 K-RAS mutant, IRS-1^{low} lung adenocarcinomas display reduced patient survival

To evaluate the significance of IRS-1 protein content on L-ADCA patient outcomes, we stained and analyzed a human tissue microarray (TMA) consisting of 135 primary tumor specimens that had been annotated for *KRAS* and *EGFR* mutation status, and for which detailed outcomes data was available. Immunohistochemistry for IRS-1 was performed and the staining was quantified using an Aperio Genie system. Tumor, stromal and inflammatory compartments were scored independently. H-scores were generated by assessing the IRS-1 staining intensity specifically within the tumor compartment. Examples of H&E-stained, IRS-1-stained and Genie overlay of IRS-1^{high} and IRS-1^{low} cases are shown in Figure 1A-C. The analysis was performed on 124 specimens, as inadequate tissue precluded an assessment of IRS-1 staining on the remaining 11 cases.

As a continuous variable, IRS-1 expression did not predict overall survival (OS) (hazard ratio=0.99, 95% CI 0.98-1.00, p=0.14). Threshold effects were explored using recursive partitioning, identifying an H-score cutpoint of 130 (Figure 1D, log-rank test p-value = 0.01). Evaluated in subgroups by mutational status, the prognostic signal for dichotomized IRS-1 appeared to be driven by tumors with *KRAS* mutations (Figure 1E). In these patients, median OS was 50 months for IRS-1^{low} (95% confidence interval 30-84 months) and 131 months for IRS-1^{high} (71-131 months). *EGFR* mutant and Wild-type subgroups did not demonstrate IRS-1 as a strong prognostic factor (Figure 1F-G). The effect of IRS-1 persisted in a multivariable model including established prognostic factors: controlling for clinical stage (as a continuous variable with Stages 1A-4 all represented, though 63% were stage 1) and smoking status (never, former, current smoker), the hazard ratio for dichotomized IRS-1 was 2.4 (95% CI 1.4-4.3): patients with IRS-1^{low} tumors had a hazard of death 140% greater than those with IRS1^{high} (Wald test p-value=0.002). Thus, we have concluded that IRS-1 deficiency confers decreased survival in L-ADCA patients, particularly for those with *KRAS* mutant tumors.

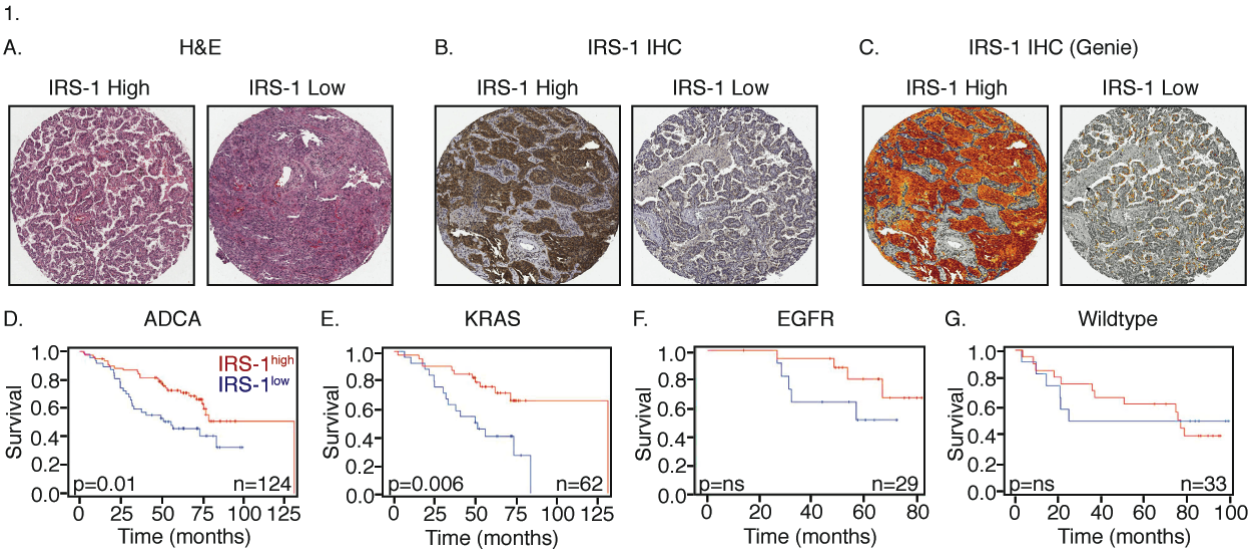

Figure 3. IRS-1 predicts patient survival in lung adenocarcinoma: (A-B) Representative images of IRS-1^{low} ((H-score < 130) and IRS-1^{high} (H-score >130) human lung adenocarcinoma TMA sections stained for (A) H&E and (B) IRS-1. (C) Example of tumor compartment specific quantification of IRS-1 staining using Aperio Genie. (D-G) Kaplan-Meier estimates of overall survival for the (D) entire lung adenocarcinoma cohort (N=124, *P*=0.01, (E) *KRAS* mutant cases (N=62, *P*=0.006), (F) *EGFR* mutant cases (N=29, *P*=NS), and (G) Non-*KRAS*, non-*EGFR* mutant cases (N=33, *P*=NS). All *P* values determined from log-rank tests.

2.3.2 K-ras/Irs-$1^{fl/fl}$ mice display increased tumor burden and decreased survival

To further interrogate the phenotype identified in the human TMA study, we generated Lox-Stop-Lox (LSL) *K-ras/Irs-*$1^{+/+}$ and *LSL-K-ras/Irs-*$1^{fl/fl}$ mice on a pure 129.SvJ genetic background. Mice were treated with Adenoviral Cre recombinase (AdCre) at 8 weeks of age to activate mutant *Kras* expression and studied over a time course ranging from 4- to 20-weeks post-AdCre. Similar to the findings in human L-ADCA, Kaplan-Meier survival curve analysis demonstrated a statistically significant reduction in survival for *LSL-Kras/Irs-*$1^{fl/fl}$ mice when

compared to the Irs-1 sufficient group ($p<0.0001$) (Figure 2A). *LSL-Kras/Irs-1*$^{fl/fl}$ mice displayed a median survival of 13.57 weeks, as compared to a median survival of 19.86 weeks (mice censored at 20 weeks) in the *LSL-K-ras/Irs-1*$^{+/+}$ control group. Additionally, tumor burden was quantified at 4-, 8-, and 12-weeks post-AdCre (Figure 2B-D). Statistically significant increases in tumor burden were observed in IRS-1 deficient mice at the 8- and 12-week time points, representing a doubling and tripling of the tumor burden identified in control mice and the two time points, respectively.

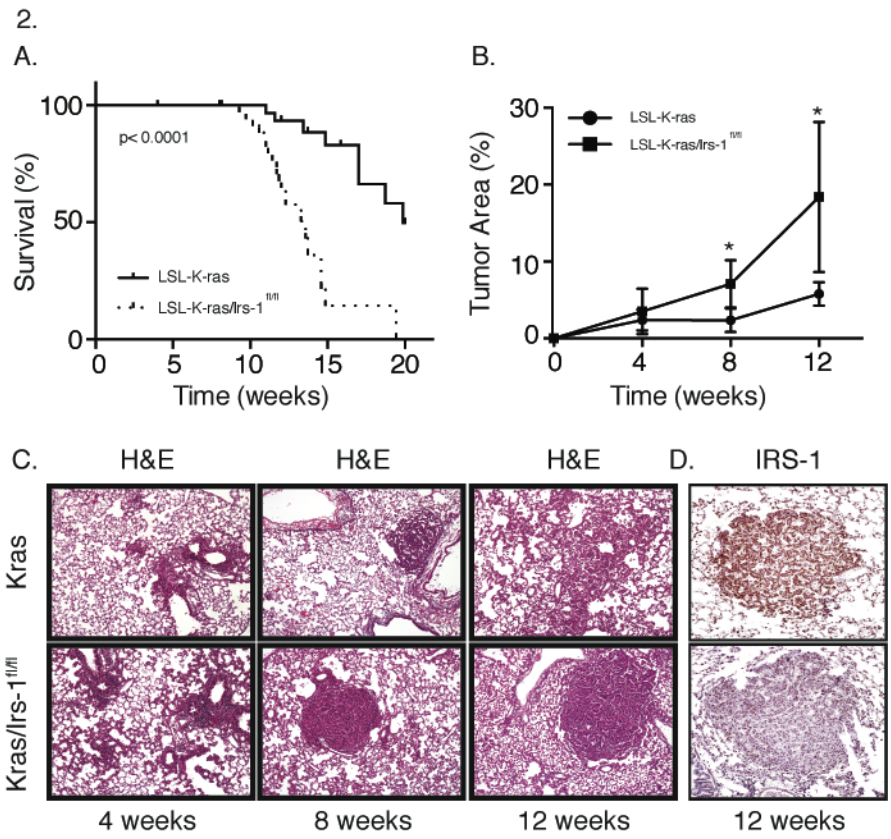

Figure 4. Increased tumor burden and mortality in *LSL-Kras/Irs-1$^{fl/fl}$* mice: Kaplan-Meier estimates of overall survival for AdCre-treated *LSL-Kras-Irs-1$^{+/+}$* (N=40) and *LSL-Kras/Irs-1$^{fl/fl}$* (N=45) mice. P<0.0001, log-rank test. (B) Tumor area percent (% of lung tissue occupied by tumor) for *LSL-Kras-Irs-1$^{+/+}$* and *LSL-Kras/Irs-1$^{fl/fl}$* mice at 4-, 8-, and 12-weeks post-AdCre. N=6 each group. Bars ± SEM. **P*<0.05. (C) Representative H&E stained images for *LSL-Kras-Irs-1$^{+/+}$* and *LSL-Kras/Irs-1$^{fl/fl}$* mice 4-, 8-, and 12-weeks post-AdCre. (D) Representative Irs-1 stained images for *LSL-Kras-Irs-1$^{+/+}$* and *LSL-Kras/Irs-1$^{fl/fl}$* mice at 12-weeks post-AdCre.

2.3.3 Increased neutrophilic inflammation in LSL-Kras/Irs-1$^{fl/fl}$ mice

Surprisingly, the most striking initial phenotypic difference apparent in the *LSL-K-ras/Irs-1$^{fl/fl}$* mice was a dramatic increase in inflammatory cell content in the bronchial alveolar lavage (BAL) fluid (Figure 3A-B). Further investigation revealed robust increases in macrophage, and

especially in neutrophil content (Figure 3A-B). At 12 weeks, neutrophils were ~5 fold higher in *LSL-K-ras/Irs-1*$^{fl/fl}$ mice and Ly6G staining revealed the presence of tumor-associated neutrophils (Figure 3C). RNA was isolated from *LSL-Kras* and *LSL-K-ras/Irs-1*$^{fl/fl}$ frozen lung tissue and subject to qPCR to assess for differential expression of CC and CXC chemokines known to recruit myeloid lineage cells to the TME. *LSL-Kras/Irs-1*$^{fl/fl}$ mice displayed significant increases in most of these chemokines when compared to *LSL-Kras* mice (Figure 3D). Specifically, we identified statistically significant increases in CCL-2, -3, -4, and CXCL-1, -2, and -5, consistent with the BAL cellular content data.

To verify a tumor-promoting role for tumor associated neutrophils, we treated both cohorts of mice with an Ly6G antibody, which reduced both tumor associated neutrophilic inflammation and tumor growth (not shown), consistent with prior reports.

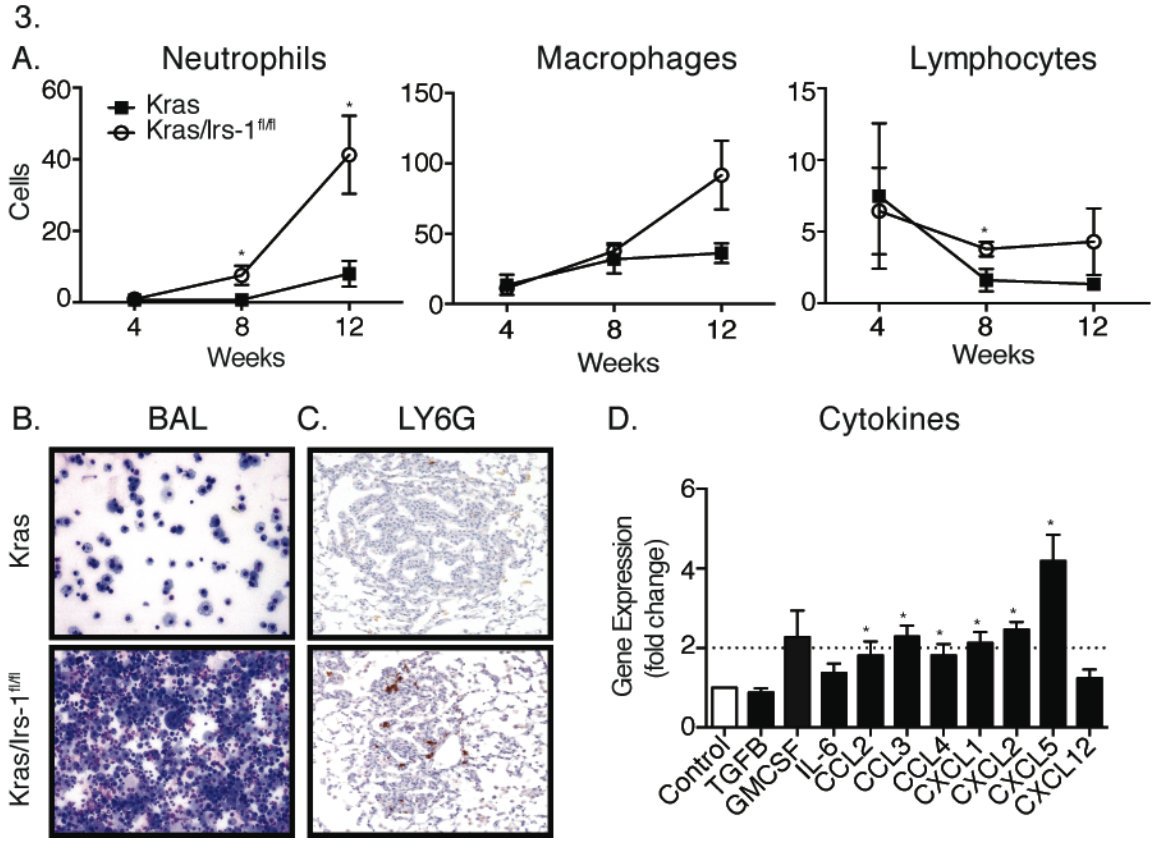

Figure 5. Increased tumor-associated inflammation in *LSL-Kras/Irs-1*$^{fl/fl}$ mice: (A) Bronchoalveolar lavage (BAL) fluid content of neutrophils, macrophages, and lymphocytes from *LSL-Kras-Irs-1*$^{+/+}$ and *LSL-Kras/Irs-1*$^{fl/fl}$ mice at 4-, 8-, and 12-weeks post-AdCre. N=6 each group. Bars ± SEM. **P*<0.05. (B) Representative Hema-3 stained cytospins performed on BAL fluid from *LSL-Kras-Irs-1*$^{+/+}$ and *LSL-Kras/Irs-1*$^{fl/fl}$ mice at 12-weeks post-AdCre. (C) Representative anti-Ly6G (neutrophil marker) stained sections from *LSL-Kras-Irs-1*$^{+/+}$ and *LSL-Kras/Irs-1*$^{fl/fl}$ mice at 12-weeks post-AdCre. (D) Real-time PCR values for the listed genes from *LSL-Kras-Irs-1*$^{+/+}$ and *LSL-Kras/Irs-1*$^{fl/fl}$ mice at 8-weeks post-AdCre. N=4 each group. Results expressed as fold change from *LSL-Kras-Irs-1*$^{+/+}$ values ± SEM. *P<0.05.

2.3.4 L-22 is required for increased chemokine response in IRS-1 deficient cancer cells

In order to further evaluate the differences in chemokine production observed between Irs-1 deficient and Irs-1 sufficient mice, we generated IRS-1 deficient A549 (*KRAS* mutant) lung adenocarcinoma cells using shRNA approaches. We were not able to observe an increase in cytokine or chemokine production in a microarray study of IRS-1 silenced A549 cells under standard serum conditions (Table 1). We then reasoned that a factor present in the TME, but not present in cancer cells in tissue culture might be responsible for the in vivo observations in *LSL-Kras/Irs-1*$^{fl/fl}$ mice. Initially, we confirmed that Th17 cytokines were present in the *LSL-Kras* mouse model, as has been reported [145], by using flow cytometry to document the presence of Th17 cells (produce both IL-17 and IL-22) within the TME (not shown). Additionally, we confirmed the presence of Th17 cells in the TME of human L-ADCA specimens, also using flow cytometry (not shown). Next, we tested the ability of IL-6, IL-17A and IL-22 to induce greater CC and CXC chemokine expression from IRS-1 deficient cancer cells in vitro, as they are all known to do so under the appropriate conditions. A549 cells permanently silenced for IRS-1 (shIRS-1) and vector control (shCon) A549 cells were stimulated with the above cytokines and qPCR was performed to assess for differences in cytokine and chemokine production (Figure 4A). Aside from an IL-6 response in the no stimulation and IL-6 treatment groups, only IL-22 generated an increase in cytokine and chemokine production in IRS-1-deficient cells. Since survival differences in human L-ADCA were limited to the *KRAS* mutant group, we repeated these experiments in 201T L-ADCA cells, which harbor WT KRAS alleles. TGFB was induced by IL-6, IL17A and IL-22 treatments, but other cytokines and chemokines were not upregulated by IRS-1 deficiency in the absence of *KRAS* mutation (Figure 4B).

Table 1: IRS-1-deficient A549 cells do not display chemokine production under unstimulated conditions. Microarry analysis was performed on siSCR and siIRS-1 A549 cells cultured under normal conditions.

TargetID	logFC	AveExpr	adj.P.Val	sig
CCL2	-0.1562683	9.10078158	0.96716921	0
CCL3	-0.1363696	7.07592982	0.96689674	0
CCL4	-0.058377	6.94923138	NA	0
CCL5	-0.0632319	8.03806188	0.96861682	0
CXCL1	-0.1259055	8.70077323	0.97606147	0
CXCL2	-0.0789665	7.97277147	0.9794449	0
CXCL3	-0.006735	7.13675063	0.99486831	0
CXCL5	-0.0444819	10.8112367	0.97900473	0
CXCL12	-0.0590391	6.97727587	NA	0
IL17A	-0.0068752	7.05417357	NA	0
IL17F	-0.0341823	6.87502109	NA	0
IL22	0.00628651	6.95704633	NA	0
IL6	-0.0145917	7.10357395	0.99180646	0
TGFB1	-0.0552148	6.95129392	NA	0
CSF2	-0.0094949	7.0602362	NA	0

4.

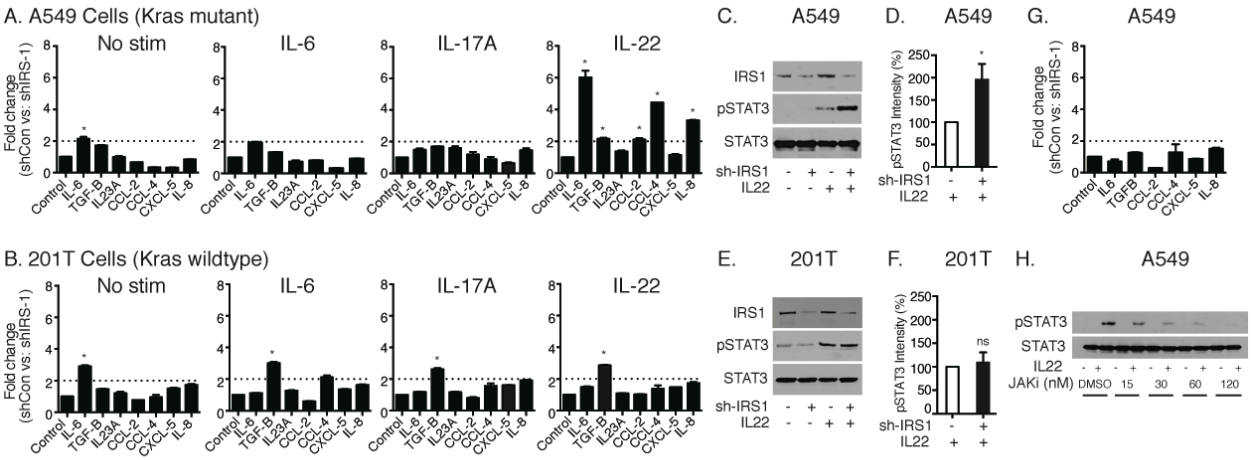

Figure 6. IRS-1 deficiency enhances IL-22 signaling: (A-B) Real-time PCR values for the listed genes from lentiviral shControl and shIRS-1 transfected (A) A549 and (B) 201T cells treated with either IL-6, IL-17A, or IL-22. Results expressed as fold changed in gene expression from shControl values ± SEM. *P<0.05. (C) Western blot for control and IRS-1 silenced A549 cells (*KRAS* mutant) both with and without IL-22 stimulation probed for IRS-1, STAT3, and pSTAT3. (D) Band densitometry comparing pSTAT3 content from lane 3 vs. lane 4 from (C) above. Quantification performed on an N=4 blots. Bars ± SEM. *$P<0.05$. (E) Western blot for control and IRS-1 silenced 201T cells (*KRAS* WT) both with and without IL-22 stimulation probed for IRS-1, STAT3, and pSTAT3. (F) Band densitometry comparing pSTAT3 content from lane 3 vs. lane 4 from (E) above. Quantification performed on an N=4 blots. Bars ± SEM. (G) Real-time PCR values for listed genes from control and IRS-1 silenced A549 cells pre-treated with a JAK inhibitor (Calbiochem #420099) and stimulated with IL-22. Results expressed as fold change from control values. Bars ± SEM. (H) Western blot probed for STAT3 and pSTAT3 from A549 cells treated with a JAK inhibitor over the indicated concentrations and stimulated with IL-22.

2.3.5 IL-22 stimulation causes exaggerated pSTAT3 production in KRAS mutant, IRS-1 silenced cells

IL-22 is a known inducer of JAK/STAT signaling. To investigate the impact of IRS-1 deficiency on IL-22 induced JAK/STAT signaling, we treated shIRS-1 and shCon A549 and 201T cells with IL-22, both with and without the presence of a JAK inhibitor. As expected, IL-22 stimulation increased the production of pSTAT3 when compared to non-IL-22 stimulated control cells, for all conditions. Predictably, the addition of a synthetic JAK inhibitor (Calbiochem #420099) abrogated pSTAT3 production and cytokine/chemokine induction under all conditions. Notably, IRS-1 silenced A549 cells (KRAS mutant) displayed an even greater increase in pSTAT3 production upon IL-22 stimulation than did IRS-1 sufficient A549 cells (Figure 4C and E). In contrast, IL-22 induced pSTAT3 production was similar in magnitude between IRS-1 silenced and vector control 201T cells (KRAS WT). To demonstrate that this mechanism was operative in vivo, FFPE sections from *LSL-Kras/Irs-1*$^{+/+}$ and *LSL-K-ras/Irs-1*$^{fl/fl}$ mice were subjected to IHC for pSTAT3 (Figure 5A). Tabulation of the slides confirmed increased pSTAT3 production in *LSL-K-ras/Irs-1*$^{fl/fl}$ mice (Figure 5B), when compared to controls, thereby validating the in vitro findings with respect to pSTAT3.

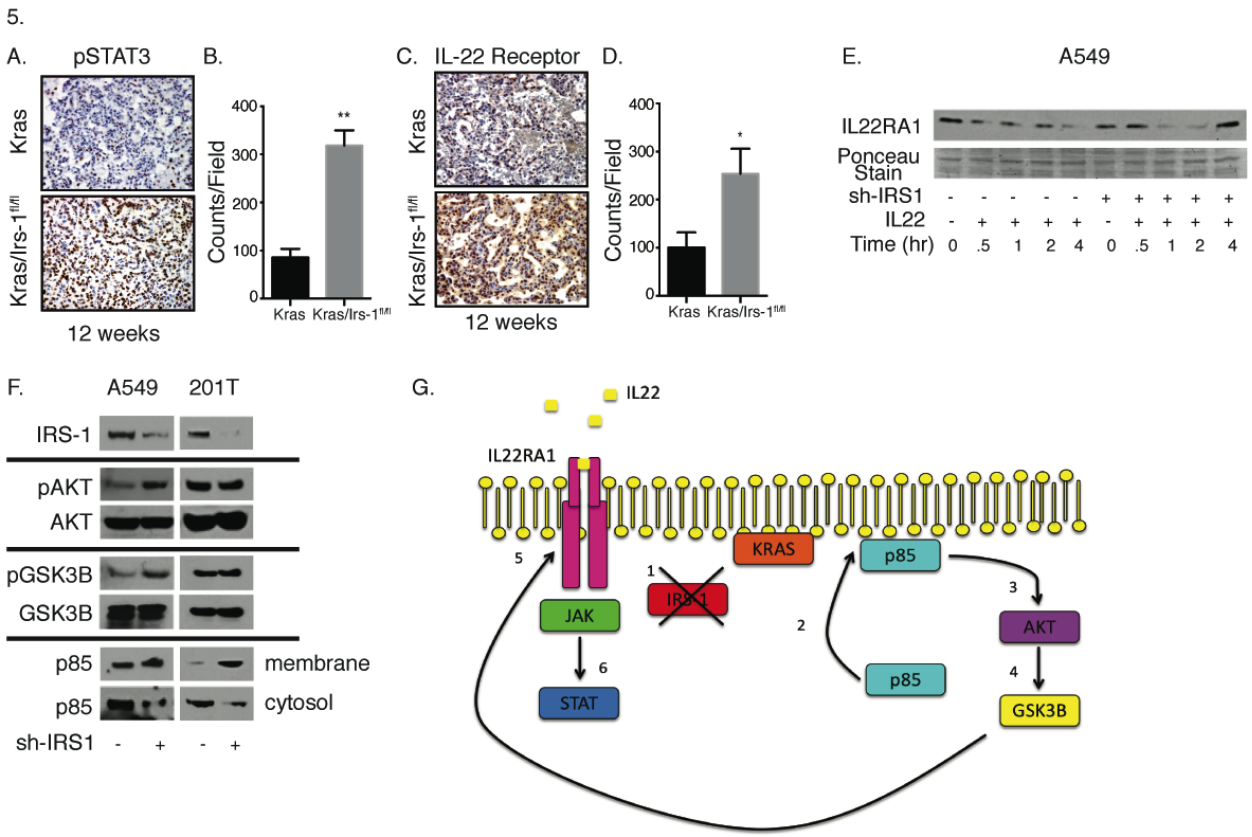

Figure 7. Increased IL-22RA1 content in IRS-1 silenced cells: (A) Representative images for pSTAT3 stained sections from *LSL-Kras-Irs-1*$^{+/+}$ and *LSL-Kras/Irs-1*$^{fl/fl}$ mice at 12-weeks post-AdCre. (B) Quantification of staining in (A) from N=6 in each group. Bars ± SEM. **P*<0.05. (C) Representative images for IL22RA1 stained sections from *LSL-Kras-Irs-1*$^{+/+}$ and *LSL-Kras/Irs-1*$^{fl/fl}$ mice at 12-weeks post-AdCre. (D) Quantification of staining in (C) from N=5 in each group. Bars ± SEM. **P*<0.05. (E) Control and IRS-1 silenced A549 cells pre-treated with cycloheximide prior to IL-22 stimulation. Western blot probed for IL22RA1 was performed on membrane fraction. (F) Representative Western blots for the indicated proteins from control and IRS-1 silenced A549 and 201T cells. (G) Illustrative diagram depicting the proposed mechanism by which IRS-1 deficiency results in exaggerated pSTAT3 production in response to IL22. The p85 subunit of PI3K, typically located both within the cytosol and at the cell membrane, is preferentially redistributed to the cellular membrane in the absence of IRS-1. In the presence of

mutant KRAS, increased bioavailability of p85 results in increased pAkt, and subsequently pGSK-3B production. pGSK-3B is known to prolong IL22RA1 half-life via protective phosphorylation of its cytoplasmic tail. Increased IL22RA1 half-life results in enhanced pSTAT3 production in response to IL22 stimulation.

2.3.6 IRS-1 deficiency prolongs IL-22RA1 half-life via pGSK-3B production

The increased production of pSTAT3 by IRS-1 deficient cancer cells as compared to IRS-1 sufficient cancer cells was observed while using an equivalent concentration of IL-22. This suggests that the production of pSTAT3 induced by each molecule of IL-22 is greater for IRS-1 silenced cells compared to controls. The most logical mechanism to explain these observations would be a prolongation of the IL-22R half-life in IRS-1 deficient cells. IHC for IL-22RA1 was performed on FFPE sections from LSL-K-ras/Irs-$1^{fl/fl}$ mice and appropriate controls. Similar to the findings with respect to pSTAT3, LSL-K-ras/Irs-$1^{fl/fl}$ tumor displayed greater than twice the IL-22RA1 staining when compared to LSL-K-ras/Irs-$1^{+/+}$ controls (Figure 5D). To demonstrate this more clearly, IRS-1 silenced and vector control A549 cells were treated with cycloheximide to inhibit all protein synthesis prior to IL-22 stimulation and subsequent tracking of IL-22RA1 cycling. The control cells show the natural life cycle of the IL-22RA1 following IL-22 stimulation. IL-22RA1 signal is gradually lost from the membrane as it is internalized following activation, tagged for degradation, and eventually completely absent in the membrane fraction (Figure 5E). Since the cells have been treated with cycloheximide, they are incapable of repopulating the cell surface with new receptor. In contrast, by the conclusion of the experiment in IRS-1 deficient cells, the IL-22RA1 membrane content has been restored, as the receptor has been recycled to the membrane, never having been degraded.

Recently, pGSK-3B has been shown to phosphorylate the cytoplasmic tail of IL-22RA1, which inhibits the ability of ubiquitinases to tag the receptor for degradation [146]. This results in a prolongation of IL-22RA1 half-life. Since IRS-1 is a homeostatic binding partner of the p85 subunit of phospho-inositol 3-kinase (PI3K), and well known to impact PI3K signaling, we investigated the impact of IRS-1 deficiency on pAKT and pGSK-3B production in KRAS mutant and KRAS WT cells. IRS-1 silencing had little effect on pAKT and pGSK-3B production in KRAS WT 201T cells (Figure 5F). However, IRS-1 deficiency in the presence of mutant KRAS actually increased both pAKT and pGSK-3B (Figure 5F). Alteration in the sub-cellular location of the PI3K machinery is the most likely explanation for this counter-intuitive finding. IRS-1 is a signaling adaptor protein, and is therefore able to interact with p85 within the cytosol, following phosphorylation by a cell surface receptor. This is in contrast to traditional receptor tyrosine kinases that interact with p85 near the inner leaflet of the cellular membrane, where lipid substrates are abundant. In the absence of IRS-1, the subcellular location of p85 relocates predominantly to the cell membrane, regardless of whether or not mutant K-RAS is present (Figure 5F). Similar observations were previously made in adipocytes [147]. Taken together, these data suggest that pAKT and pGSK-3B production is increased when p85 is located nearest to the phospho-inositols, if a continuous signaling mutated protein is present.

2.3.7 JAK inhibition reduces inflammation and tumor burden in LSL-K-ras/Irs-1fl/fl mice

Although the increased tumor-associated inflammation and tumor burden identified in LSL-K-ras/Irs-$1^{fl/fl}$ mice was the result of a multi-step process, all of these steps culminated in JAK/STAT activation. Therefore, we administered a JAK antagonist, AZD 1480, to both LSL-K-

ras/Irs-1$^{+/+}$ and LSL-K-ras/Irs-1$^{fl/fl}$ mice in attempts to identify a novel therapeutic strategy for the K-ras mutant, IRS-1 low tumor subtype. Mice received either AZD 1480 or vehicle control via oral gavage 6 days per week for 3 weeks, starting 8-weeks post-AdCre. Analysis of the BALF inflammatory cell content revealed that LSL-K-ras/Irs-1$^{fl/fl}$ mice possessed substantially reduced inflammation that was similar in magnitude to that observed in LSL-K-ras/Irs-1$^{+/+}$ mice (Figure 6D and F). AZD 1480 significantly reduced the tumor burden in both groups of mice, where the tumor burden was reduced to 5.8% in the LSL-K-ras/Irs-1$^{+/+}$ mice and 3.8% in the LSL-K-ras/Irs-1$^{fl/fl}$ mice (Figure 6 A-C). Mechanistically, JAK inhibition reduced CC and CXC chemokine expression, as expected (Figure 6G and H). These results provide evidence that JAK inhibition is capable of reducing tumor burden in K-ras mutant mice, and additionally capable of abrogating the enhanced tumor-promoting inflammation afforded by IRS-1 deficiency.

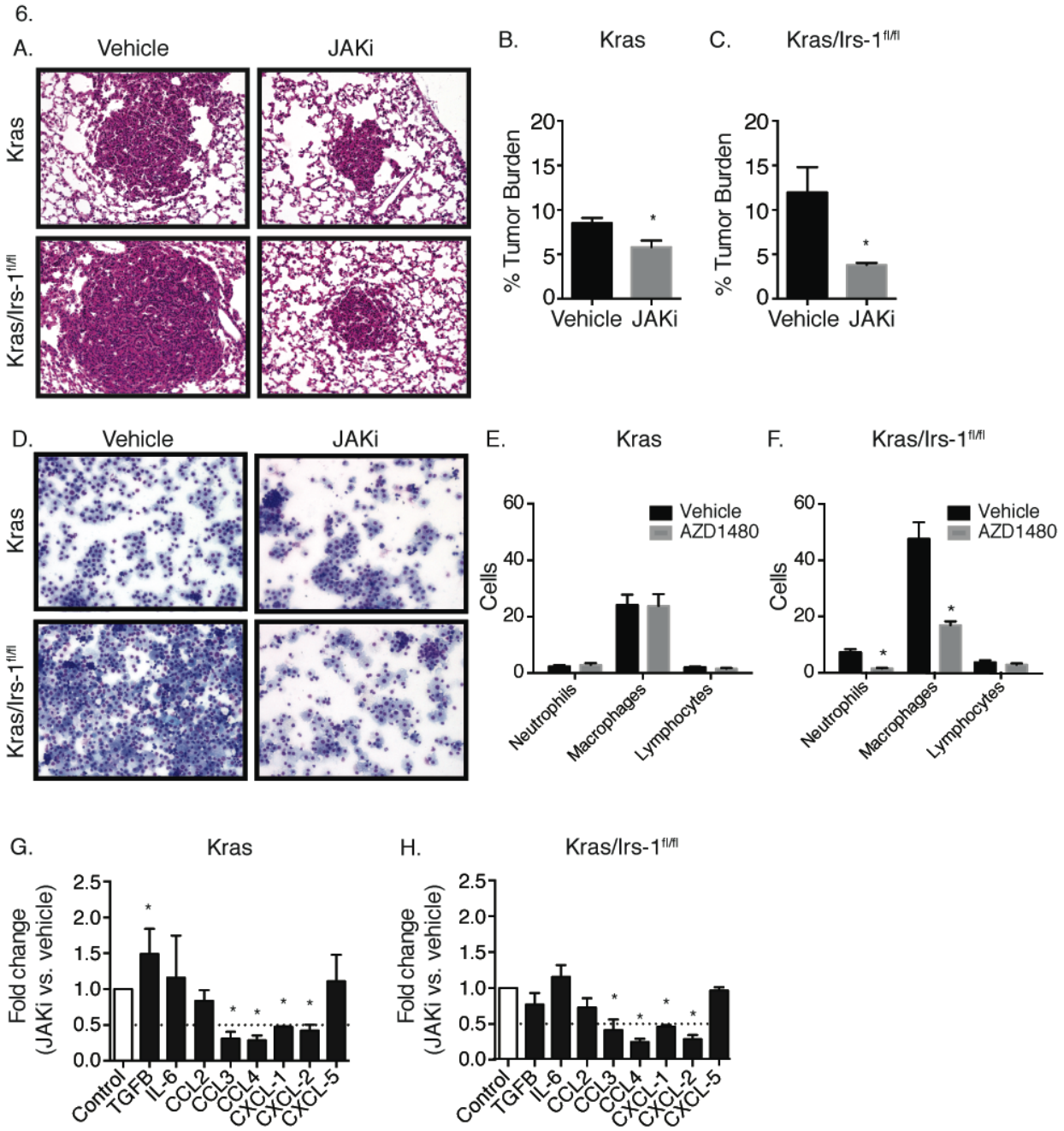

Figure 8. JAK inhibition reduces tumor burden and inflammation in *LSL-Kras/Irs-1$^{fl/fl}$ mice:* (A) Representative H&E stained sections from *LSL-Kras-Irs-1$^{+/+}$* and *LSL-Kras/Irs-1$^{fl/fl}$* mice treated with AZD1480 (JAK inhibitor) or vehicle control for a total of 6-weeks beginning at 8-weeks post-AdCre. (B-C) Tumor area percent (% of lung occupied by tumor) for (B) *LSL-Kras-Irs-1$^{+/+}$* and (C) *LSL-Kras/Irs-1$^{fl/fl}$* mice treated with either AZD1480 or vehicle control, as above. N>4

each group. Bars ± SEM. *P<0.05. (D) Representative images of, and (E-F) quantification of Hema-3 stained cytospins of BAL fluid from *LSL-Kras-Irs-1*$^{+/+}$ and *LSL-Kras/Irs-1*$^{fl/fl}$ mice on therapy with either AZD1480 or vehicle control. (G-H) Real-time PCR values for the listed genes from (G) *LSL-Kras-Irs-1*$^{+/+}$ and (H) *LSL-Kras/Irs-1*$^{fl/fl}$ mice treated with either AZD1480 or vehicle control, as above. Results are expressed as fold change from vehicle control ± SEM. N=3 each group. *P<0.05.

2.3.8 K-RAS mutant, IRS-1^{low} human lung adenocarcinomas contain increased myeloid cell inflammation

To validate the mechanistic findings in LSL-K-ras/Irs-1$^{fl/fl}$ mice, we re-analyzed our human lung adenocarcinoma TMA for immune cell content. Specifically, we scored all *K-RAS* mutant cases in our TMA for myeloid cell infiltration and lymphocyte infiltration (both on a semi-quantitative score from 0-3, where absent = 0, mild = 1, moderate = 2, and heavy = 3). These scores were also combined to give a total immune cell content score. *K-RAS* mutant, IRS-1^{low} cancers possessed ~30% greater content of inflammatory cells, and ~40% increased myeloid cell infiltration, but no significant difference in lymphoid inflammation was identified, consistent with the findings in the *K-ras* mouse model (Supplementary Figure 1).

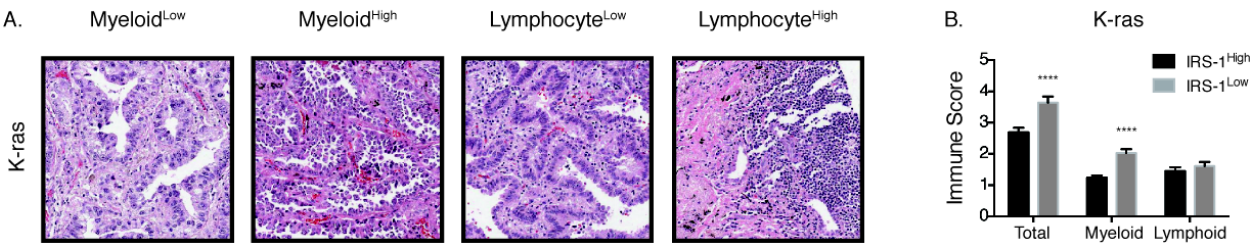

Figure 9. KRAS-mutant, IRS-l^{Low} human lung adenocarcinomas have increased myeloid cell infiltration: (A) Representative H&E images from myeloid and lymphocyte high and low cases. (B) Quantification of total, myeloid and lymphoid inflammation between IRS-1 ^{High} and IRS-1^{Low} patients.

2.4 DISCUSSION

It has become clear that inflammatory responses can promote tumor initiation and progression. Numerous studies have uncovered elaborate mechanisms by which aberrant immune cell function promotes tumorigenesis. Yet, the mechanisms by which these immune cells have been recruited and by which their function has been polarized, remain poorly understood. Here, we show that deficiency of a homeostatic protein, IRS-1, skews cancer cell signaling towards a pro-inflammatory phenotype.

We began this study of IRS-1 in lung cancer by identifying that IRS-1 deficient lung adenocarcinomas displayed reduced survival, but that this phenotype was restricted to the *KRAS* mutant L-ADCA subtype. Controlled experiments in mice reproduced the phenotype observed in humans and uncovered a pro-inflammatory phenotype highlighted by enhanced pSTAT3 production, excessive CC and CXC chemokine expression, and consequential increases in inflammatory cell content. We suspect that most, but not all, of the differences in tumor burden

were the result of increased tumor-promoting inflammation, and were able to diminish tumor burden using a neutrophil depleting antibody, as has been reported several times previously. Moreover, antagonism of the JAK/STAT pathway abrogated increases in inflammation and tumor burden afforded by IRS-1 deletion. Mechanistically, IRS-1 deficient cells display an altered sub-cellular distribution of the PI3K machinery, favoring a plasma membrane location. Under certain circumstances, such as the presence of mutant *KRAS*, abundant PI3K within close proximity to its lipid substrates can enhance PI3K pathway activity, as observed here. In this case, increased pGSK-3B production increased the half-life of IL-22RA1, ultimately causing enhanced pSTAT3 production, CXC chemokine expression, and increased pro-tumor inflammatory cell infiltration.

The importance of the Th17 cytokines IL-17 and IL-22 in solid tumor malignancies has been highlighted by several recent publications. Though we were unable to identify a role for IL-17A specifically in the context of IRS-1 deficiency, IL-17A-deficient mice were recently shown to display reduced tumor burden and tumor-associated inflammation in the *LSL-Kras* model employed here [145]. Notably, IL-22 has recently been shown to play dual roles in cancer. Early in the process of tumorigenesis, IL-22 is essential for epithelial cell repair, and actually retards tumor formation. In contrast, in established lesions in pro-inflammatory colon cancer models, IL-22 drives myeloid cell infiltration and tumor burden via JAK/STAT mediated amplification of CC and CXC chemokine production [148], similar to our findings. Whether reduced IRS-1 protein content is encountered in other malignancies, and if this impacts IL-22 signaling, is an active area of study in our laboratory.

This is the first definitive report of a pro-host role for IRS-1 in any human cancer type and is paradigm shifting in nature. Traditionally, IRS-1 is considered a positive effector of

growth factor and presumed to promote tumor growth via PI3K activation, which is likely the case in certain malignancies. Several IHC based studies have correlated IRS-1 staining with poor outcomes, including myosarcoma, leiomyosarcoma, lipsarcoma, rhabdomyosarcoma, and hepatocellular carcinoma [149]. The only prior study of IRS-1 in human lung cancer reported that 46% of NSCLC cases had diminished IRS-1 content by IHC, though outcomes data were not available [150]. Notably, we denoted 38% of L-ADCA on the TMA as being IRS-1 low, consistent with the prior study. Taken together, these studies strongly suggest that approximately 40% of L-ADCA tumors display reduced IRS-1 content at the protein level. Specifically within the *KRAS* mutant group, 37% of cases were defined as IRS-1 low, such that ~10% of all L-ADCA is comprised of this unique subtype. Furthermore, these findings may shed light as to why initial clinical trials employing IGF-1R antagonists have not produced positive results. IGF-1R inhibition would be expected to reduce the pTyr-IRS-1 cellular content, which would reduce IRS-1:p85 interaction as only pTyr-IRS-1 binds to p85. Thus, IGF-1R inhibition may generate a relatively deficient IRS-1 state, which in the presence of mutant KRAS, may produce untoward effects.

One potential shortcoming of the current study is that we have not identified the mechanism by which IRS-1 protein content is reduced in human L-ADCA. It unlikely to be the result of a mutation, as IRS-1 mutations were not reported in the lung adenocarcinoma TCGA dataset. There is one prominent polymorphism known to occur in IRS-1 that impacts p85 binding (G972R), though it has not been described to impact protein levels. The remaining mechanistic possibilities include epigenetic silencing, post-transcriptional silencing, or post-translational degradation. We previously identified a significant correlation between neutrophil elastase staining and reduced IRS-1 staining on serial sections of 38 human lung adenocarcinomas using

IHC. However, we have not directly identified the mechanism by which IRS-1 protein content is reduced in this context in human disease.

The results reported here highlight a novel concept with respect to pathway signaling in cancer cells. Whereas the focus of aberrant pathway signaling has logically centered upon hyperactive mutant proteins (K-RAS, PIK3CA, B-RAF, etc.), this report clearly demonstrates that signaling intermediaries can drastically impact cell behavior when their content is reduced. Signaling intermediates are numerous, and mutated versions of many of these proteins are not frequently encountered. However, relative deficiencies of promiscuous signaling proteins, such as IRS-1, can impact pathway output in a manner that is difficult to predict. Furthermore, reductions in pathway intermediates should be considered in the context of mutant oncogenes, as the impact on cell behavior can be impacted by unique combinations.

KRAS mutant, IRS-1^{low} lung adenocarcinomas represent a unique subtype in which JAK/STAT activation is excessive, and drives tumor-promoting inflammation. Since the constellation of events instigated by IRS-1 deficiency culminates in pSTAT3 production, we used a JAK inhibitor to show that this tumor subtype is particularly susceptible to this therapeutic strategy. Since *KRAS* mutant, IRS-1^{low} lung adenocarcinomas represent 10% of all lung adenocarcinomas, JAK inhibition may represent a viable therapeutic option, especially when considering the intractable nature of *KRAS* mutant cancers. Lastly, the ability of JAK inhibition to reduce myeloid cell infiltration and tumor burden in *LSL-Kras* mice suggests that this may be a viable strategy to address myeloid derived suppressor cell (MDSC) content in solid tumors, a strategy for which there are no approved therapies.

3.0 IRS-1 AND CELLULAR PROLIFERATION

The work in Chapter 2 was preceded by studies involving the role of IRS-1 in cellular proliferation. A paper entitled, *Neutrophil elastase-mediated degradation of IRS-1 accelerates lung tumor growth* [88] (Appendix B) describes a role for IRS-1 in lung adenocarcinoma in which IRS-1 is degraded by Neutrophil elastase and the loss of this protein induces cellular proliferation. Overall, this work showed that Neutrophil elastase increases tumor burden and decreases survival in mice, neutrophil elastase degrades IRS-1 within the cell inducing proliferation through activation of more potent receptors and also that human lung adenocarcinoma cases display an inverse correlation between neutrophil elastase and IRS-1 presence.

My specific contributions to this paper involved performing experiments for the in vitro mechanism of this phenotype. I performed experiments in which neutrophil elastase-sufficient and –deficient mouse neutrophils were co-cultured with LSL-K-ras tumor-derived cell lines and then thymidine incorporation assays were used to evaluate cellular proliferation. Exposure to neutrophil elastase increased cellular proliferation (Appendix B, Figure 11 a). I then performed experiments in which LSL-K-ras cell lines and human lung adenocarcinoma cell lines (A549 and 201T) were exposed to different concentrations of neutrophil elastase. Thymidine incorporation and cell count assays as well as western blots were then performed. Exposure to 40nM and 80nM neutrophil elastase increased cellular proliferation (Appendix B, Figure 11 b-e). Western blots

displayed increased pAKT in three different cell lines at increasing concentrations of neutrophil elastase (Appendix B, Figure 11g). MAPK, however, was not increased with exposure to neutrophil elastase (Appendix B, Figure 11 f). A proliferation assay was performed on A549 cells pre-treated with a PI3K inhibitor (LY294002) and a MAPK inhibitor (U0126) (Appendix B, Figure 11 f). The results of this displayed the reliance on AKT signaling for proliferation due to neutrophil exposure, as the PI3K inhibitor reduced proliferation back to baseline. I also performed a proliferation assay of neutrophil elastase-treated A549 cells that were also pre-treated with Dynasore, an inhibitor of endosome formation (Appendix B, Figure11 j). Cells treated with Dynasore did not proliferate upon neutrophil elastase treatment, indicating that neutrophil elastase must enter the cell in an endosomal compartment in order to have an effect.

The hypothesis evolved from here into an investigation of the PDGF receptor. I performed co-immunoprecipitation experiments involving the p85 subunit of PI3K and the PDGF receptor (Appendix B, Figure 12 c, d). Results indicated that p85 is in fact bound to the PDGF receptor more readily with exposure to neutrophil elastase. I then performed a PDGF receptor knock-down experiment in A549 cells and evaluated proliferation using a thymidine uptake assay (Appendix B, Figure 12 e, f). Silencing of the PDGF receptor reduced neutrophil elastase-induced proliferation significantly.

We then investigated the role neutrophil elastase had on Insulin Receptor Substrate-1. I performed an experiment in which recombinant IRS-1 protein was mixed with neutrophil elastase in a test tube and then run on a gel and probed for IRS-1 (Appendix B, Figure 13 a). IRS-1 was degraded with increasing concentrations of neutrophil elastase. I then treated A549 cells with neutrophil elastase and ran the whole lysate on a gel and probed for IRS-1 (Appendix B, Figure b). IRS-1 was also degraded in vitro with increasing concentrations of neutrophil

elastase. I then performed a proliferation assay using siRNA to silence IRS-1 in A549 cells where it was found that loss of IRS-1 increased cellular proliferation (Appendix B, 13 c). I also overexpressed IRS-1 in A549 cells and found that overexpression greatly reduces proliferation (Appendix B, 13 d).

Another paper I was involved in entitled, *Neutrophil Elastase Promotes Myofibroblast Differentiation in Lung Fibrosis* [151], describes a role for IRS-1 in fibroblast proliferation. Briefly, this paper shows that neutrophil elastase-deficient mice have reduced lung fibrosis from asbestos exposure and reduced myofibroblast levels. Neutrophil elastase was found to increase fibroblast proliferation and increase myofibroblast differentiation. For this paper, I performed experiments in which proliferation was evaluated for both neutrophil elastase exposure and knock-down of IRS-1 (Appendix C, Figure A-D and I-J). These experiments indicated that neutrophil elastase induces proliferation in fibroblast cells and that loss of IRS-1 specifically produces this effect.

These two papers led to the independent evaluation of IRS-1 in lung adenocarcinoma (Chapter 2). We were interested in further elucidating the mechanism responsible for increased proliferation upon IRS-1 loss. To our surprise, IRS-1 loss did more than just induce proliferation; it also activated a signaling cascade culminating in increased chemokine production and thus increased immune cell recruitment to the tumor microenvironment. Taking a broader and also a more controlled look at IRS-1 allowed us to identify a population of people who currently do not have any targeted therapies available to them (KRAS-mutant, IRS-1^{Low} L-ADCA) and hypothesize that they may benefit from JAK inhibitor therapy based on a mouse pre-clinical trial.

4.0 SUMMARY AND FUTURE DIRECTIONS

The overarching goal of this work was to investigate novel roles for IRS-1 in the lung, including its role as a key mediator of homeostasis in cancer cells and fibroblasts, as well as its role in regulating immune cell recruitment to the tumor microenvironment. The studies described in chapters two and three, and appendix B and C reveal a counter-intuitive role for IRS-1 in which its loss induces cellular proliferation. Chapter three and appendix B describe a novel role for IRS-1 in which an intracellular adaptor molecule within a tumor cell regulates immune cell content in the tumor microenvironment as a whole. These studies have identified a population of patients within the lung adenocarcinoma subtype and provide possible therapeutic targets for this deadly disease.

Chapter three and appendix B investigate the loss of IRS-1 in cancer cells, which occurs through degradation by Neutrophil Elastase (NE) secreted from neutrophils in the tumor microenvironment. The goal of this study was to determine if NE affected tumor progression. A model combining the Kras mouse model of lung adenocarcinoma and an NE-deficient mouse displayed increased survival and decreased tumor burden in Kras-NE-deficient mice. It was also noted that Kras-NE-deficient mice had increased pAkt production. IRS-1 is a key player in AKT signaling and was reduced in Kras-NE-sufficient mice. In vitro experiments demonstrated that NE directly degrades IRS-1 and that once IRS-1 is lost, p85 can bind more potent growth factor receptors, thus increasing cellular proliferation.

Chapter two represents the follow-up to this study, in which IRS-1 loss was independently evaluated without other confounding factors contributed by NE. The goal of this study was to evaluate the role of IRS-1 in cellular proliferation. A study using a human lung adenocarcinoma tissue microarray stained for IRS-1 revealed significant survival differences between IRS-1^{High} and IRS-1^{Low} patients in the KRAS subtype. Kras and Kras, Irs-1-deficient mice were employed to evaluate this phenotype further. Kras, Irs-1-deficient mice displayed increased mortality and tumor burden. A surprising finding in the study was an increase in immune cells in the BAL fluid in Kras, Irs-1-deficient mice. Further interrogation revealed that loss of IRS-1 increased the release of chemokines by tumor cells through increased JAK/STAT signaling in the setting of IL-22 stimulation. The link between IRS-1 loss and increased JAK/STAT signaling is through an increase in pAKT as was described in chapter three and appendix B. This increase in pAKT causes downstream phosphorylation of pGSK3β, which in turn stabilizes the IL-22 receptor allowing for elevated JAK/STAT signaling. This work also demonstrated that JAK inhibition reduced tumor burden, chemokine production and inflammation in our mouse model.

Future directions for this study could be extended to clinical trials in lung adenocarcinoma patients, with a specific focus on the *KRAS* mutant subtype. There are several JAK inhibitors currently in clinical trial for pancreatic cancer, acute myeloid leukemia, psoriasis inflammatory bowel disease and rheumatoid arthritis [103]. Another important consideration would be the impact of different KRAS mutations on the signaling we have described. Ihle et al. describe KRAS point mutations that have different consequences for downstream signaling as well as patient survival [126]. It was shown that KRAS-G12D had increased PI3K and MEK signaling but KRAS-G12C and KRAS-G12V had increased Ral signaling [126]. It would be

informative to evaluate the specific KRAS mutations present in our TMA cohort and compare each to IRS-1 levels and survival outcomes. Understanding which specific KRAS mutation affects which signaling pathway would help direct patient care.

Another interesting follow-up would be to investigate the role of immune checkpoint inhibitors in the Kras and Kras, Irs-1-deficient mouse model. Cytotoxic T lymphocytes (CTL) are $CD8^+$ T cells that are capable of killing tumor cells. Tumor cells evade this destruction by expressing immune checkpoint ligands including programmed death-1 ligand (PD-L1) that neutralizes the CTL's ability to kill by interacting with the programmed death-1 (PD-1) receptor [152]. Immune checkpoint inhibitors have recently been developed that aim to block the interaction of PD-1 and PD-L1, thus allowing the immune system to recognize and eliminate cancer cells. There are currently three PD-1/PD-L1 inhibitors for lung cancer including nivolumab, pembrolizumab and MPDL3280A [153]. It would be interesting to evaluate these drugs in KRAS mutant lung adenocarcinoma in combination with JAK inhibition.

IL-22 presents another target for potential therapy. We found that IL-22 in the tumor microenvironment activated JAK/STAT signaling through the IL-22 receptor and caused an increase in tumor burden and decrease in survival. Blocking either IL-22 or the IL-22 receptor may reduce this response. A neutralizing antibody against IL-22 is currently in clinical trial for psoriasis and rheumatoid arthritis [154]. Mouse models of IL-22 and IL-22 receptor deficiency display many negative side effects, so further investigation using models systems will be necessary to properly target these entities without harming the host [154].

Chapters two and three describe a pro-tumor role for the neutrophil. This concept should be taken into consideration with regard to patient treatment following chemotherapy. Many patients develop neutropenia following chemotherapy and are given a granulocyte colony-

stimulating factor (G-CSF) drug such as filgrastim, which stimulates the bone marrow to product neutrophils [155]. A study of lung tumor progression in KRAS and KRAS IRS-1-deficient mice treated with a G-CSF drug would be an informative study to address the pro-host versus pro-tumor role of neutrophils.

Appendix C investigates the role of Neutrophil Elastase in fibroblast proliferation and differentiation. In this study C57BL/6 controls and C57BL/6 $NE^{-/-}$ mice were administered asbestos intratracheally. The $NE^{-/-}$ mice did not develop fibrosis in response to asbestos and had significantly less fibroblast and myofibroblast content in the lungs. In vitro studies revealed that NE degrades IRS-1 in fibroblasts as it did in cancer cells as described in appendix B. This loss of IRS-1 increased pAKT production and proliferative signaling in the fibroblasts. A synthetic small molecule inhibitor of Elastase, ONO-5046, was given to asbestos treated mice and reduced the fibrotic phenotype of the C57BL/6 control mice.

This study provides another non-canonical role for IRS-1 in a non-cancer cell type. Fibroblasts are an important component of the tumor microenvironment. There is evidence that fibroblasts play a role in cancer progression [156]. A study of lung adenocarcinoma patients indicated that carbonic anhydrase IX expression by cancer associated fibroblasts correlated with lower patient survival rates [157]. An interesting follow-up study for appendix C would be to evaluate fibroblast behavior in a cancer model. The tumor microenvironment consists of many different components all contributing to cancer progression in various ways and it will be important to gain a better understanding of these interactions.

In summary, the findings described in this dissertation provide novel roles for IRS-1 as a pro-host molecule. The consequences of IRS-1 loss that have been described will hopefully lead

to future experiments that will help advance patient care by providing novel targets for therapeutic intervention.

APPENDIX A

ABBREVIATIONS

A1AT, Alpha-1 antitrypsin

ADCA, Adenocarcinoma

AdenoCre, Adenoviral cre recombinase

ALK, Anaplastic lymphoma kinase

αSMA, alpha smooth muscle actin

AKT, protein kinas B (PKB)

BAL, bronchoalveolar lavage

CG, cathepsin G

ECM, extracellular matrix

EGFR, Epidermal growth factor receptor

FSP-1, fibroblast specific protein-1

Grb2, Growth factor receptor-bound protein 2

HCC, Hepatocellular carcinoma

HER2, Human epidermal growth factor receptor 2

IGF-1R, Insulin-like growth factor-1 receptor

IPF, idiopathic pulmonary fibrosis

IR, Insulin receptor

IRS-1, insulin receptor substrate-1

IRS-2, insulin receptor substrate-2

JAK, Janus kinase

KRAS, Kirsten rat sarcoma viral oncogene homolog

MMP, Matrix metalloproteinase

MEK/ERK, Extracellular signal regulated kinase

NE, Neutrophil Elastase

NSCLC, Non-small cell lung cancer

PDGF, Platelet derived growth factor

PDGFR, PDGF-receptor

PI3K, phosphoinositol-3 kinase

PIP3, Phosphatidylinositol (3,4,5)-trisphosphate

PI3KCA, phosphoinositol-3 kinase, catalytic subunit (p110)

PMN, polymorphonuclear neutrophils

PMF, primary mouse fibroblasts

PMSF, phenylmethylsulfonyl fluoride

PTB, Phosphotyrosine-binding domain

PTEN, Phosphatase and tensin homolog

RALA/B, Ras-related protein

RTK, Receptor tyrosine kinase

SH2, Src Homolygy 2

SCLC, Small cell lung cancer

STAT, Signal transducer and activator of transcription

TiO2, titanium dioxide

TGF-ß, transforming growth factor beta

VEGFR, vascular endothelial growth factor

APPENDIX B

NEUTROPHIL ELASTASE-MEDIATED DEGRADATION OF IRS-1 ACCELERATES LUNG TUMOR GROWTH

A. McGarry Houghton,[1,4,5] Danuta M. Rzymkiewicz,[6] Hongbin Ji,[7] Alyssa D. Gregory,[1,4] Eduardo E. Egea,[1,4] Heather E. Metz,[1,4] Donna B. Stolz,[2,5] Stephanie R. Land,[3,5] Luiz A. Marconcini,[6] Corrine R. Kliment,[1] Kimberly M. Jenkins,[1,4] Keith A. Beaulieu,[1,4] Majd Mouded,[1,4] Stuart J. Frank,[8] Kwok K. Wong,[9] and Steven D. Shapiro[1,4,5]

[1]Department of Medicine, University of Pittsburgh School of Medicine, Pittsburgh, PA 15213

[2]Department of Cell Biology & Physiology, University of Pittsburgh School of Medicine, Pittsburgh, PA 15213

[3]Department of Biostatistics, University of Pittsburgh School of Medicine, Pittsburgh, PA 15213

[4]Division of Pulmonary, Allergy, and Critical Care Medicine, University of Pittsburgh School of Medicine, Pittsburgh, PA 15213

[5]University of Pittsburgh Cancer Institute, University of Pittsburgh School of Medicine, Pittsburgh, PA 15213

[6]Division of Pulmonary and Critical Care Medicine, Brigham and Women's Hospital, Boston, MA 02115

[7]Institute of Biochemistry & Cell Biology, Shanghai Institute for Biological Sciences & Chinese Academy for Sciences, Shanghai, China

[8]Division of Endocrinology, Diabetes, and Metabolism, University of Alabama at Birmingham, Birmingham, AL 35294.

[9]Ludwig Center at Dana-Farber/Harvard Cancer Center, Departments of Medicine and Medical Oncology, Dana-Farber Cancer Institute & Harvard Medical School, Boston, MA 02115.

Address correspondence to A.M.H. Email: (houghtonm@dom.pitt.edu)

Modified from Houghton, A.M., et al., *Neutrophil elastase-mediated degradation of IRS-1 accelerates lung tumor growth.* Nat Med, 2010. **16**(2): p. 219-23.

B.1 SUMMARY

Lung cancer is the leading cause of cancer death worldwide [158]. Recent data suggest that tumor-associated inflammatory cells may modify lung tumor growth and invasiveness [28, 159]. To determine the role of neutrophil elastase (NE or *Elane*) on tumor progression, we utilized the *LSL-K-ras* model of murine lung adenocarcinoma [89] to generate *LSL-K-ras/Elane*$^{-/-}$ mice. Tumor burden was markedly reduced in *LSL-K-ras/Elane*$^{-/-}$ mice at all time points following induction of mutant K-ras expression. Kaplan-Meier life survival analysis demonstrated that while 100% of *LSL-K-ras/Elane*$^{+/+}$ mice died, none of the mice lacking NE died. NE directly induced tumor cell proliferation in both human and mouse lung adenocarcinomas by gaining access to an endosomal compartment within tumor cells where it degraded insulin receptor substrate-1 (IRS1). Co-immunoprecipitation studies showed that as NE degraded IRS1, there was increased interaction between PI3K and the potent mitogen platelet derived growth factor receptor (PDGFR) thereby skewing the PI3K axis toward tumor cell proliferation. The inverse relationship identified between NE and IRS1 in *LSL-K-ras* mice was also identified in human lung adenocarcinomas, thus translating these findings to human disease. This study identifies IRS1 as a key regulator of PI3K within malignant cells. Additionally, this is the first description of a secreted proteinase gaining access to a cell beyond its plasma membrane and altering intracellular signaling.

B.2 RESULTS AND DISCUSSION

Lung cancer is the leading cause of cancer related deaths worldwide with dismal ~15% five-year survival rates despite therapeutic advances over the preceding decades [158]. A better understanding of tumor-associated inflammation may identify novel therapeutic targets.

Neutrophils are known to infiltrate tumors, however, only recently have they been thought to modify tumor growth and invasiveness [28, 89, 159-163]. We have previously shown that lung cancer cells elaborate CXC chemokines driving neutrophil recruitment. Hence, tumor-associated neutrophils don't necessarily represent a means of host defense. Indeed, there have been reports that neutrophil infiltrates within tumors correlate with poor clinical outcomes [164, 165].

The purpose of this study was to determine if the most potent neutrophil proteinase, NE, played a role in tumor progression. NE is a neutrophil-specific serine proteinase with broad substrate specificity. Its expression is limited to promyelocyte stages of bone marrow development where it is packaged into azurophil granules [166]. The main function of NE is to eliminate pathogens within neutrophils [167, 168]. However, upon activation, neutrophils translocate NE to the cell surface and secrete small amounts of enzyme from individual granules [169].

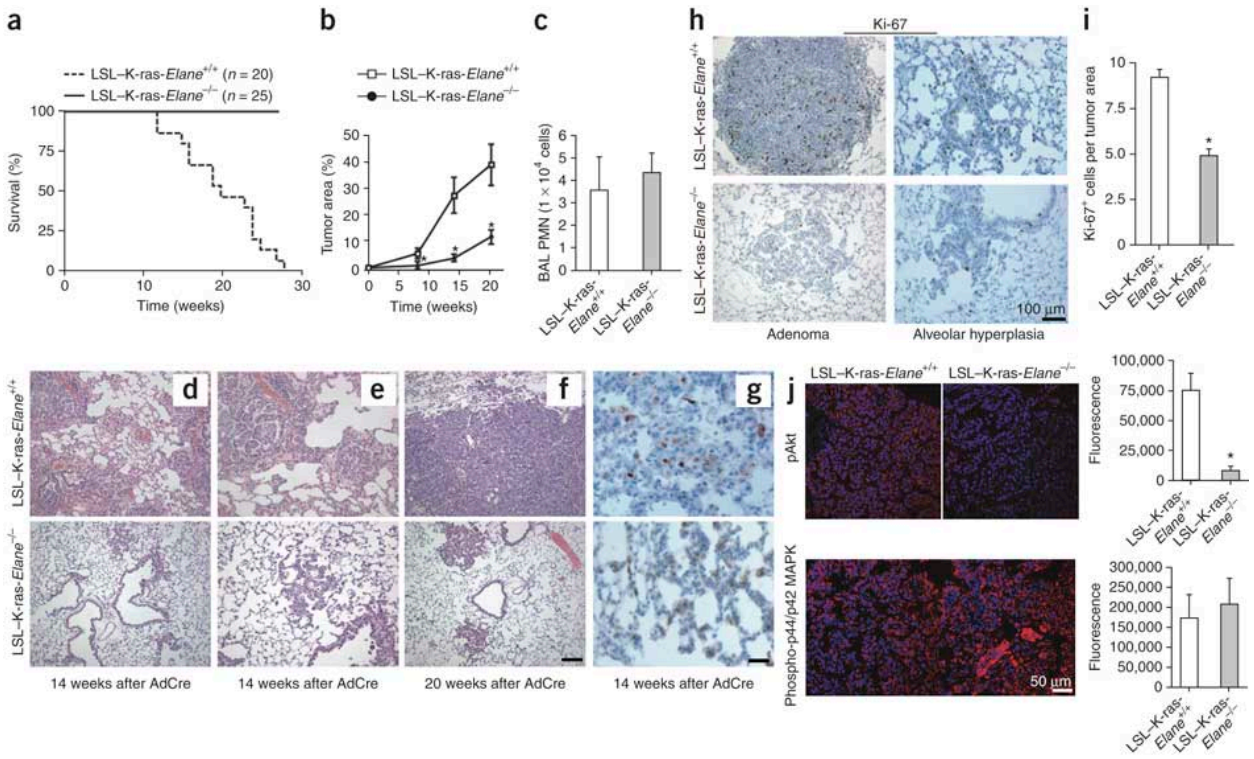

Figure 10. NE promotes lung tumor growth: **(a)** Kaplan-Meier Survival curve for AdenoCre recipient *LSL/K-ras/Elane*$^{+/+}$ and *LSL/K-ras/Elane*$^{-/-}$ mice; *P*=0.006, log-rank test. **(b)** Tumor area (%) for both groups at 8, 14, and 20 weeks post-AdenoCre. N=5 mice per group. Bars ± SEM. **P*<0.01. **(c)** BALF neutrophil counts for AdenoCre recipient *LSL/K-ras/Elane*$^{+/+}$ and *LSL/K-ras/Elane*$^{-/-}$ mice at the 14-week time point. N=5 mice per group. Bars ± SEM. *P*=NS. Representative H&E images at 14 weeks **(d, e)** and 20 weeks **(f)** post-AdenoCre. **(g)** Representative images for anti-p40^{phox} (anti-neutrophil) IHC at 14 weeks post-AdenoCre. (**h**) Representative Ki-67 IHC 14 weeks post-AdenoCre. **(i)** Ki-67 (+) cells per tumor area for N=5 mice per group at the 14-week time point. Bars ± SEM. **P*<0.01. **(j)** Representative IF images and quantification for pAkt and phospho-MEK/ERK from both groups of mice 14 weeks post-AdenoCre. Bars ± SEM. *P*<0.01 for pAkt.

We subjected Lox—Stop—Lox K-ras^{G12D}/Elane$^{-/-}$ (*LSL-K-ras/Elane*$^{-/-}$) and control (*LSL-K-ras/Elane*$^{+/+}$) mice to 5×10^6 pfu intratracheal adenoviral cre recombinase (AdenoCre) to activate mutant K-ras expression[4]. During the 28 weeks following AdenoCre administration, all *LSL-K-ras/Elane*$^{+/+}$ but none of the *LSL-K-ras/Elane*$^{-/-}$ mice died. Survival analysis demonstrated a significant (P=0.006) advantage for *LSL-K-ras/Elane*$^{-/-}$ mice (Fig. 1a). NE-deficiency is not completely protective, as we have subsequently identified death beyond 30 weeks in independent studies. Tumor burden was markedly reduced in *LSL-K-ras/Elane*$^{-/-}$ mice at all time points (Fig. 1b,d–f). The differences observed represent a reduction in tumor growth and differentiation (less mature lesions), as tumor number was equivalent in the two groups (Supplementary Table 1). NE-mediated effects on tumor growth are not model specific, as similar reductions in tumor growth were observed in the Lewis Lung carcinoma model using WT and *Elane*$^{-/-}$ mice (Supplementary Fig. 1).

Immunohistochemical (IHC) analyses and lung lavage cell counts demonstrated equivalent neutrophil content and distribution in *LSL-K-ras/Elane*$^{-/-}$ and *LSL-K-ras/Elane*$^{+/+}$ mice (Fig. 1c,g), thereby excluding a role for NE in neutrophil trafficking. We also excluded the unlikely possibility that *LSL-K-ras* tumors produced NE using casein zymography (not shown).

We identified significant reductions in tumor cell proliferation in *LSL-K-ras/Elane*$^{-/-}$ mice (Fig. 1h,i) using Ki-67 IHC. Immunofluorescence (IF) staining demonstrated differential activity in the PI3K pathway (pAkt), but specifically not in MEK/ERK (Fig. 1j). Proteinases can release growth factors sequestered within extracellular matrix for use by tumors [169, 170] which could account for these findings. However, we were unable to detect differences between the groups for relevant growth factors (not shown).

We examined the possibility that NE could directly induce tumor cell proliferation and performed co-culture experiments utilizing WT and *Elane*$^{-/-}$ PMN to demonstrate an essential requirement for NE in PMN-mediated tumor cell proliferation (Fig. 2a). Neutrophils only release ~2% of their NE content upon activation resulting in modest concentrations (~50 nM) just beyond the cell surface [171]. Dose response curves in *LSL-K-ras* tumor-derived cell lines (Fig. 2b) confirmed that modest concentrations of NE (40-80 nM) induced cellular proliferation, while excessive concentrations caused cell death (Fig. 2b). We reproduced NE-induced proliferation in two human lung adenocarcinoma cell lines, A549 (K-ras mutant) and 201T (K-ras WT)(Fig. 2c–e). The effects of NE required catalytic activity, as inactive NE (heated or synthetic inhibitor) failed to induce proliferation (Supplementary Fig. 2).

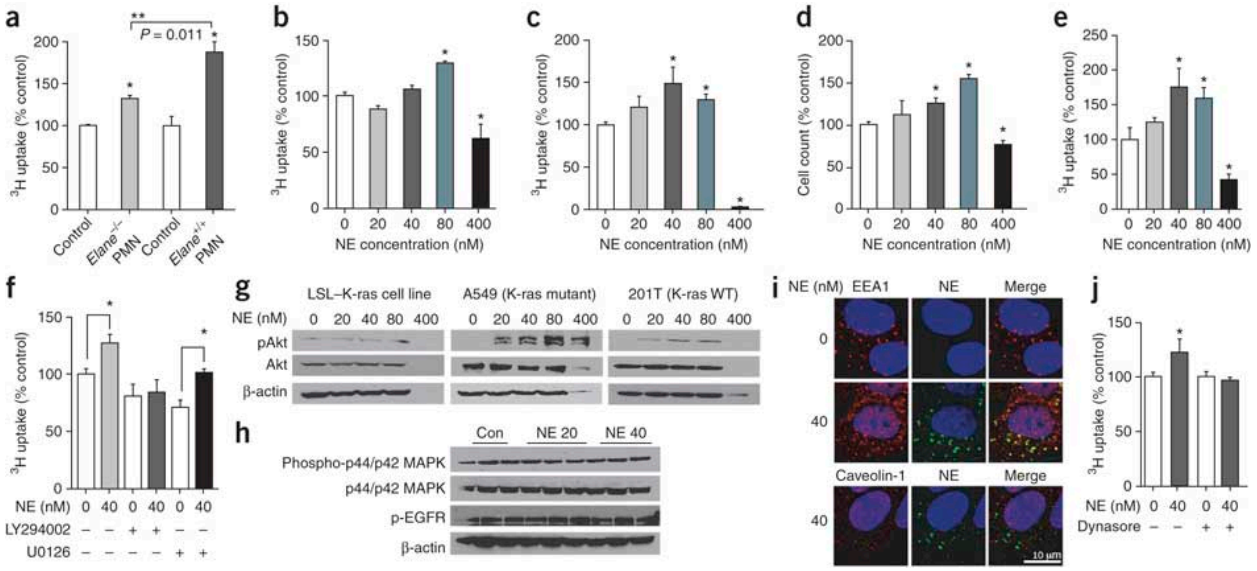

Figure 11. Neutrophil Elastase induces tumor cell proliferation: (a) ^{3}H uptake for LSL–K-ras tumor–derived cell lines[5] incubated with WT or*Elane*$^{-/-}$ PMNs for 2 h. Results show a representative experiment in triplicate. Data represent means ± s.e.m. **P* < 0.05 compared to control. ***P* = 0.011, analysis of variance. (b) ^{3}H uptake for LSL–K-ras cells stimulated with neutrophil elastase (NE) or vehicle for 60 min. Data from a representative experiment in triplicate. Data represent means ± s.e.m. **P* < 0.01 compared to NE = 0 (vehicle). (c–e) ^{3}H uptake (c) and cell counts (d) for A549 cells and ^{3}H uptake for 201T cells (K-ras WT) (e). Results are from representative experiments in triplicate. Data represent means ± s.e.m., **P* < 0.05 compared to NE = 0 (vehicle). (f) ^{3}H uptake for A549 cells stimulated with neutrophil elastase in the presence or absence of 1.0 μM LY294002 or 10 μM U0126 for 60 min. Results are from a representative experiment in triplicate. Data represent means ± s.e.m. **P* < 0.05. (g) Western blots of pAkt, Akt and β-actin for neutrophil elastase–exposed lysates of A549, 201T and LSL–K-ras cells. (h) Western blot of phospho-p44/p42 MAPK, p44/p42 MAPK, phosphorylated epidermal growth factor receptor (pEGFR) and β-actin for neutrophil elastase–exposed A549 lysates. (**i**) Confocal images for early endosomal antigen-1 (EEA-1), caveolin-1

and neutrophil elastase from A549 cells exposed to Alexa Fluor 488–conjugated neutrophil elastase or vehicle. Nuclei were counterstained with DAPI. (**j**) ^{3}H uptake for A549 cells stimulated with neutrophil elastase ± 40 μM dynasore. Results are from a representative experiment in triplicate. Data represent means ± s.e.m. *$P < 0.05$.

Dependence of NE-induced proliferation upon PI3K was demonstrated using an inhibitor (LY294002), whereas inhibition of the MEK/ERK pathway (U0126) had no effect (Fig. 2f). NE exposure induced pAkt (Fig. 2g), as expected for a PI3K dependent process. Phospho-p44/42-MAPK production was not affected (Fig. 2h).

Alexa488-labeled NE was utilized to identify the site of NE and tumor cell interaction. Surprisingly, NE gained access to tumor cells beyond their plasma membrane. The enzyme was localized to early endosomal antigen-1^{+} (EEA1) endosomes (but not calveolae) (Fig. 2i), known to shuttle cargo from clathrin pits to other cellular locations [172]. Endosomal NE was required for cell proliferation, as inhibition of endosome formation (using dynasore[90]) prevented proliferation (Fig. 2j).

Of growth factors known to activate PI3K, the PDGF/PDGFR complex is an attractive candidate to drive tumor cell proliferation. It's a potent inducer of pAkt via PI3K, is not found in lung epithelial cells, but is highly expressed in non-small cell lung cancer (NSCLC) [173]. Both the ligand and the receptor are produced in NSCLC thereby creating a potent autocrine loop for PI3K activation. *LSL-K-ras* tumors also express PDGF and PDGFR (Fig. 3a).

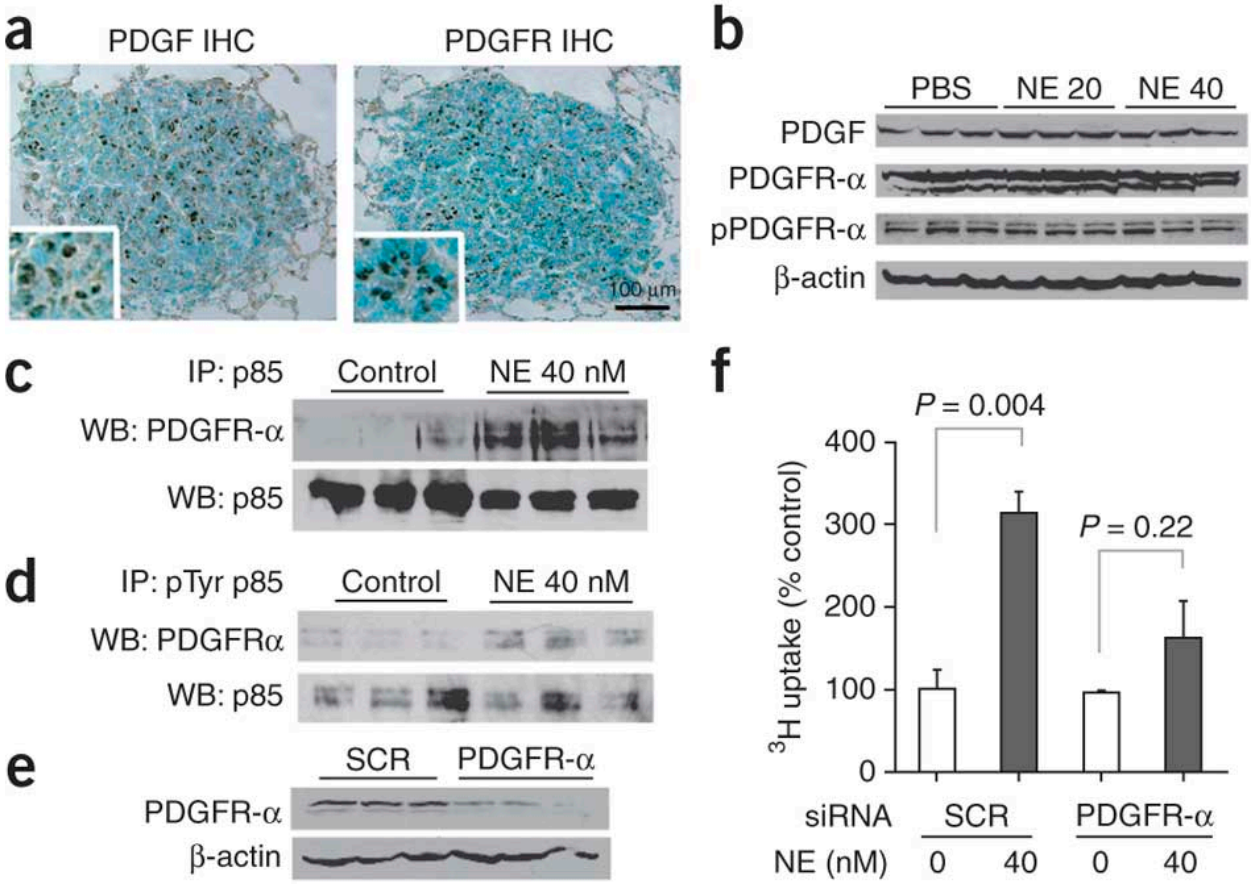

Figure 12. Neutrophil Elastase-induced proliferation is dependent upon PDGFR-PI3K signaling: (a) Representative images for PDGF and PDGFR immunohistochemistry (IHC) of LSL–K-ras tumors. Insets, high magnification showing PDGF and PDGFR staining within cells with tumor morphology. (b) Western blots for PDGF, PDGFR-α, pPDGFR-α and β-actin from neutrophil elastase–exposed A549 cell lysates. Results from a representative experiment in triplicate. (c,d) Immunoprecipitation (IP) of p85 (c) and phospho-tyrosine p85 (d) from A549 cell lysates followed by western blotting (WB) for PDGFR-α. Membranes were stripped and probed for p85. (e) Representative blot for PDGFR-α after siRNA treatment with scrambled siRNA (SCR) versus PDGFR-α–specific siRNA. (f) ^{3}H uptake for PDGFR-α–silenced A549 cells exposed to neutrophil elastase or vehicle. Results from a representative experiment in triplicate. Data represent means ± s.e.m.

Treating A549 cells with NE at cell-proliferative concentrations didn't alter the quantity of PDGF, PDGFR, or p-PDGFR (Fig. 3b). NE-exposure did increase interaction (co-immunoprecipitation) between the p85 subunit of PI3K and PDGFR (Fig. 3c,d). Gene silencing confirmed dependence of NE-induced proliferation on PDGFR (Fig. 3e,f).

The PI3K axis is uniquely regulated within each cell type [69]. We reasoned that NE must degrade a homeostatic binding partner of p85. Loss of such a binding partner would create an opportunity for PDGF/PDGFR to recruit and activate p85. We identified a number of potential NE-substrates within the PI3K pathway, including IRS1, an adaptor protein known to bind p85 [46]. In fact, IRS1 and PDGF have been shown to differentially regulate PI3K activity in adipocytes, generating opposing effects on cell behavior despite activating the same p85 subunit [72].

NE rapidly hydrolyzed IRS1 at 1:100 molar concentrations (Fig. 4a). Cell proliferative concentrations of NE eliminated IRS1 within A549 cells (Fig. 4b). Silencing of *IRS1* gene expression induced tumor cell proliferation (Fig. 4c). Marked IRS1 over-expression reduced tumor cell growth and abrogated the proliferative effects of NE, confirming that IRS1 loss is a required event in this process (Fig. 4d). Hence, independent of NE, IRS1 is capable of regulating tumor cell proliferation.

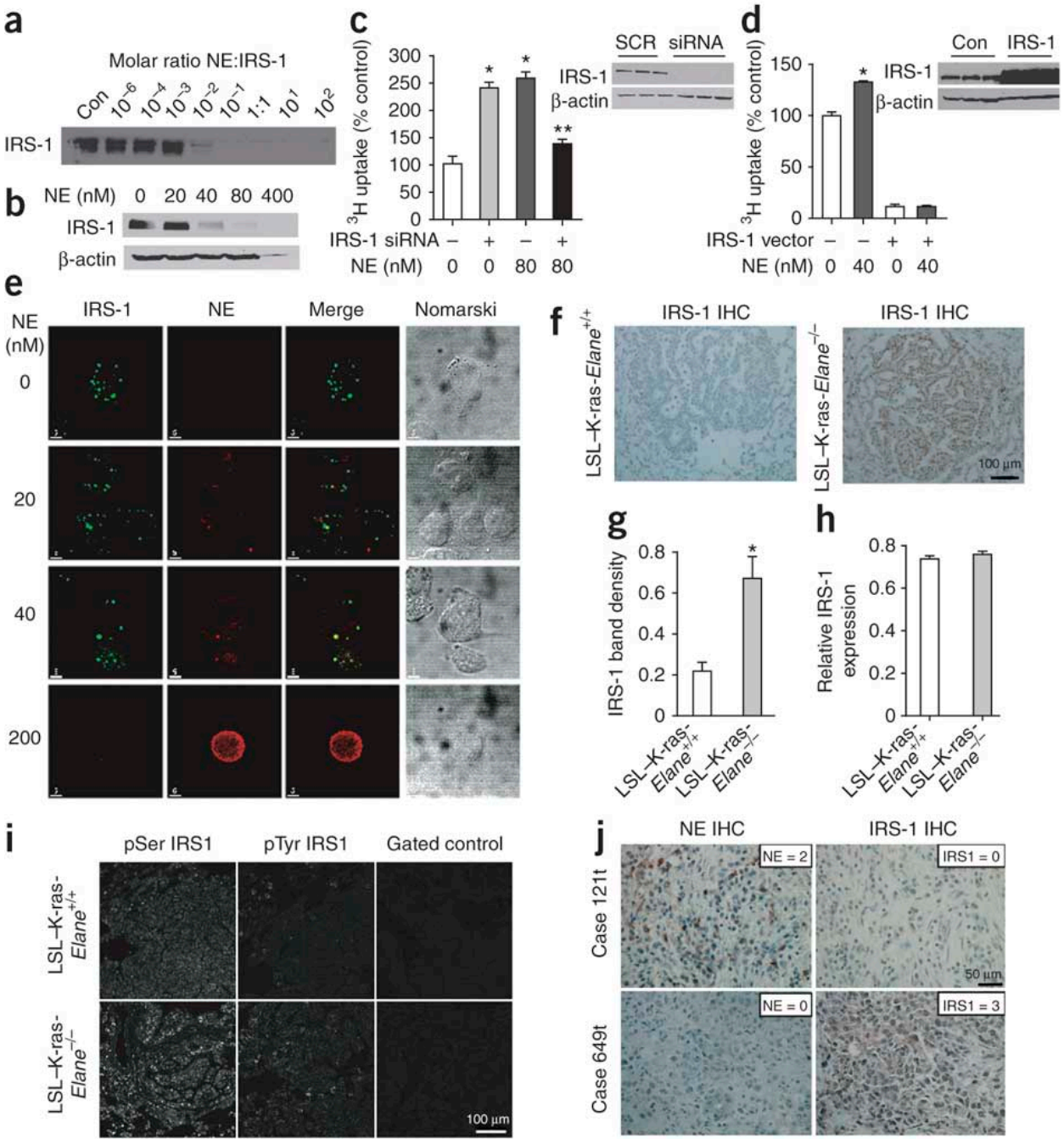

Figure 13. Neutrophil Elastase colocalizes with and degrades IRS-1: (a) Western blot for IRS-1 after incubation of recombinant IRS-1 protein with NE over a range of molar ratios. Con, control. (b) Western blots for IRS-1 and β-actin in neutrophil elastase–exposed A549 cell lysates. (c) ^{3}H uptake for IRS-1–silenced (or SCR control) A549 cells subsequently exposed to neutrophil elastase or vehicle. Results are from a representative experiment in triplicate. Data

represent means ± s.e.m. *P < 0.001 compared to control. **P < 0.05 compared to a neutrophil elastase concentration of 80 nM. Inset, western blot of IRS-1 in SCR siRNA– and IRS-1 siRNA–treated lysates. (d) ^{3}H uptake for IRS-1–overexpressing A549 cells exposed to neutrophil elastase or vehicle. Results are from a representative experiment in triplicate. Data represent means ± s.e.m. *P < 0.01. Inset, western blot of IRS-1 western blot in IRS-1 vector– and control-treated lysates. (e) Confocal images for IRS-1 and neutrophil elastase from A549 cells exposed to neutrophil elastase (or vehicle) and labeled by antibody-mediated labeling. (f) Representative IRS-1 immunohistochemistry images from LSL–K-ras-*Elane*$^{+/+}$ and LSL–K-ras-*Elane*$^{-/-}$ mice 14 weeks after AdenoCre transduction. (g) IRS-1 western blot of tumor homogenates from both groups 14 weeks after AdenoCre transduction (n = 5). Results are presented as relative band density ± s.e.m. *P < 0.001. (h) Real-time PCR for *Irs1* in tumor homogenates from both groups 14 weeks after AdenoCre transduction (n = 4). Results are expressed as glyceraldehyde 3-phosphate dehydrogenase CT/IRS-1 cycle threshold ± s.e.m. (i) Representative immunofluorescence images for pSer307 and pTyr608 IRS-1 from LSL–K-ras-*Elane*$^{+/+}$ and LSL–K-ras-*Elane*$^{-/-}$ tumors 14 weeks after AdenoCre transduction. (j) Representative images of human lung adenocarcinoma specimens for NE = 2 and IRS-1 = 0 (Case 121t) and NE = 0 and IRS-1 = 3 (Case 649t) (see Online Methods for scale system). The empirical probability of discordance was 0.88, which was significantly greater than chance (0.5), P < 0.001.

IRS1 isn't located on the cell surface nor sequestered in the ECM. Therefore, NE: IRS1 interaction must occur within the cell, a distinct possibility given the trafficking studies presented in Fig. 2i. Confocal microscopy of NE-exposed A549 cells co-localized NE and IRS1 within tumor cells (Fig. 4e). Remarkably, Irs1 protein was significantly reduced in *LSL-K-ras/Elane*$^{+/+}$

compared to *LSL-K-ras/Elane*$^{-/-}$ tumors *in vivo* (Fig. 4f,g). However, *Irs1* mRNA levels were equivalent between the two groups by qPCR (Fig. 4h), consistent with degradation of the protein.

IRS1 has been reported to function in both pro-tumor and pro-host capacities [48]. The phosphorylation status of IRS1 may dictate behavior, with pTyr IRS1 functioning as a positive effector of growth factor and pSer producing a regulatory factor [174]. IRS1 accumulation in *LSL-K-ras/Elane*$^{-/-}$ tumors was predominantly serine-phosphorylated (Fig. 4i), consistent with this hypothesis.

Han *et al*. reported that IRS1 staining was absent in 43.6% of Stage I NSCLC, correlating with increased tumor size [150]. We performed NE and IRS1 IHC on 38 human lung adenocarcinomas to confirm an inverse relationship between NE and IRS1 (Fig. 4j). We used likelihood ratio tests to demonstrate that the proportion of discordant views (NE and IRS1 were considered discordant when either one was present but the other was absent/faint in the same view) was statistically significant (P<0.001).

These results may partially explain PI3K hyperactivity in NSCLC despite infrequent mutation in PTEN, the constitutive negative repressor of PI3K [69]. Our findings suggest that IRS1 is a key regulator of PI3K. We propose that the downstream consequences of p85 binding by IRS1 are fundamentally different (more homeostatic) than those for potent growth factors such as PDGFR. If IRS1 levels were depleted (NE-mediated degradation), or its ability to bind p85 altered (G972R polymorphism[175]), increased cancer susceptibility may result. In fact, G972R confers increased prostate cancer risk [176]. Aberrant autocrine loops (PDGF—PDGFR) would be required to significantly skew the net function of PI3K. Consistent with this hypothesis, NE didn't induce proliferation in lung epithelial cells (PDGFR^{-}) but did in fibroblasts (PDGFR^{+}) (Supplementary Fig. 3).

NE exists within neutrophil azurophil granules for rapid transit to phagolysosomes where it kills bacteria during acute infection [167, 168]. If “dumped” into ECM, NE causes tissue destruction. In the lung, unopposed NE degrades elastin resulting in emphysema [177]. NE may also cause cell death at high concentrations, but these concentrations are not likely achievable in vivo. At physiologic concentrations, NE was actively transported to a sub-cellular location and increased cell proliferation. The ability of a secreted proteinase to enter another cell and alter cell signaling represents a new concept in proteinase biology, and expands the list of both potential substrates and functions for proteinases.

Small molecule inhibitors of NE have been developed for, although never adequately tested in, COPD. To demonstrate the plausibility of NE-inhibition as cancer therapy, we treated *LSL-K-ras* mice with the NE inhibitor, ONO-5046, or vehicle, for 14 weeks post-AdenoCre. Administration of the inhibitor reduced lung tumor growth by three-fold ($P<0.05$) (Supplementary Fig. 4). The results presented here might spur enthusiasm to test these agents in NSCLC, especially in light of the recent finding that emphysema predisposes to the development of lung cancer [178, 179]. NE may explain the link between the two diseases. As neutrophils and NE are recruited to the lungs of smokers to promote emphysema, sub-clinical nodules would become more aggressive. Hence, NE inhibition might be an attractive approach to treat both diseases, which currently account for ~300,000 deaths per year in the U.S. alone [158, 180].

B.3 METHODS

B.3.1 Mice

Neutrophil elastase deficient mice (*Elane*$^{-/-}$) on a C57BL6 background have been described elsewhere[28]. Lox-Stop-Lox K-ras^{G12D} (*LSL-K-ras*) mice provided by Tyler Jacks have been described elsewhere[4] and have subsequently been backcrossed into C57BL6 > five generations. Induction of mutant K-ras expression and the use of ONO-5046 is described in Supplementary Methods. All experiments described herein were approved by the Harvard Standing Committee for Animal Welfare or the University of Pittsburgh IACUC committee.

B.3.2 Tissue Processing

The lungs were inflated with 10% buffered formalin at 25 cm H2O pressure via an intratracheal catheter for 10 min. The lungs were removed and fixed in 10% buffered formalin for 24 hr before embedding in paraffin.

B.3.3 Histology and Immunohistochemistry

Serial mid-sagittal 5 μm sections were used for H&E staining and IHC. Tumor burden was reported as the percentage of lung area occupied by tumor (tumor area μm^2/total area μm^2) on 50 different 10X sections per slide. IHC was performed as described[4] using antibodies against PDGF (Upstate), PDGFRα/β (Upstate), IRS1 (Abcam) and Ki-67 (DAKO). The proliferative index was reported as the number of Ki-67 positive cells per tumor area. Lung tissue immunofluorescence was performed on frozen sections for phospho proteins not amenable to detection on routinely fixed tissues. Detailed methods are located in the Supplementary Methods.

Human lung adenocarcinoma cases (FFPE) obtained from the Lung SPORE tissue bank were subjected to NE and IRS1 IHC (Abcam). These studies were deemed "exempt" by the University of Pittsburgh Institutional Review Board. Four fields identified on the NE slide were imaged, and then the corresponding field in the IRS1 slide was imaged. Images were scored: NE, absent=0, present=2, 1-2 cells=1; and IRS1, absent=0, faint=1, present=2, heavy=3. NE=1 slides were excluded from the analysis. NE and IRS1 were considered discordant when whether one was present but the other absent/faint in the same view. For each tumor sample, the number of discordant views was modeled with a binomial distribution. Likelihood ratio tests determined whether the proportion of discordant views was significantly greater than one-half, the proportion that would be expected by chance.

B.3.4 Cells

The human lung adenocarcinoma cell line A549 (K-ras mutant) was used for in vitro experiments (ATCC). Key experiments were duplicated in K-ras WT 201T lung adenocarcinoma cells (ATCC), and murine lung adenocarcinoma cell lines derived from *LSL-K-ras* tumors as previously described[8]. All cells were maintained in DMEM plus 10% FCS, 1X NEAA, and 1X penicillin/streptomycin.

B.3.5 Thymidine Incorporation

Cells were plated at a concentration of 1×10^5 cells/well in 24-well plates before treatment with NE at concentrations from 4—400 nM (Elastin Products) for 60 min in serum-free media, washing with PBS, and incubation in serum-free media containing 1 μCi/mL of thymidine (Perkin Elmer) for an additional 18 hrs. Assays were terminated by washing with PBS, fixing

with 5% TCA, and washing with H_2O. Cells were then dissolved in 300 mL 200 mM NaOH neutralized with equimolar HCl and transferred to scintillation vials. LY294002 (1.0 μM)(Upstate), U0126 (10 μM)(Cell Signaling), PMSF (1 mM)(Sigma) and dynasore[32] (40 μM)(Sigma) were utilized in a subset of experiments. DMSO was the control vehicle for the LY294002, U0126, and dynasore experiments. Results from representative experiments in triplicate. All experiments were replicated at least three times.

B.3.6 Confocal Microscopy

Confocal Microscopy was employed to determine the location of NE within tumor cells and to identify interaction with other proteins. Detailed procedures are located in the Supplementary Methods.

B.3.7 Western Blotting

Standard 10% SDS-PAGE was performed followed by transfer of proteins to a nitrocellulose membrane. The following antibodies and dilutions were used: pAkt (1:250, Cell Signaling), Akt (1:500, Cell Signaling), p85 (1:500, Upstate), IRS-1 (1:500, Upstate), IRS-2 (1:500, Upstate), PDGF (1:250, Upstate), PDGFRα (1:250, Upstate), pPDGFRα (1:250, Upstate), p44/42-MAPK (1:500, Cell Signaling), phospho-p44/42-MAPK (1:500, Cell Signaling), and pEGFR (1:250, Cell Signaling). β-actin (1:1000, Cell Signaling) served as the endogenous control. All experiments performed in triplicate. All experiments were replicated at least three times.

B.3.8 Co-immunoprecipitation

Lysates from NE-treated A549 cells and controls were immunoprecipitated with anti-p85 or anti-pTyr-p85 antibodies (Upstate) immobilized to protein A/G agarose resin according to manufacturer's instructions (Pierce). Following elution, the samples were subjected to Western blot using anti-PDGFRα (Upstate). All experiments performed in triplicate. All experiments were replicated at least twice.

B.3.9 Protein Expression

IRS-1 protein was over-expressed in A549 cells using a lipofectamine transfection of pcDLSRα containing WT IRS1 [181]. Lipofectamine only transfection served as control. Western blotting confirmed IRS1 expression.

B.3.10 siRNA

A549 cells were plated in 24-well plates at 5×10^4 cells/well. PDGFRα (Invitrogen), IRS-1 (Dharmacon), or SCR siRNA (Invitrogen) (all 40 nM), were transfected using Lipofectamine per manufacturer's instructions (Invitrogen). Cells were washed with PBS 6 hrs later. Western blot analyses and thymidine incorporation assays were performed two days later. All assays were performed in triplicate and replicated at least three times in separate experiments.

B.3.11 Statistics

Data are expressed as the mean value ± SEM. Simple pair-wise comparisons were analyzed using the student's t-test (two tailed distribution with two sample equal variance). For multiple comparisons, one-way ANOVA with Newman-Keuls post-test was employed. A *P* value of

<0.05 was considered significant. The Kaplan-Meier survival curve analysis employed a log-rank test.

B.4 SUPPLEMENTARY FIGURES AND METHODS

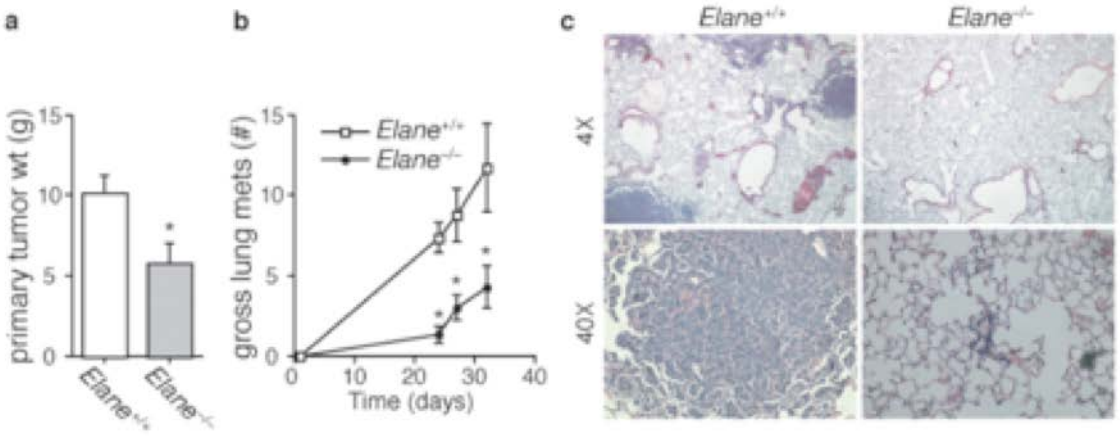

Supplementary Figure 1. Decreased lung metastases in Elane$^{-/-}$ mice: (a) Primary tumor weights of Elane$^{+/+}$ and Elane$^{-/-}$ mice 31 days after subcutaneous injection of 1x10^{6} LLC cells. N=4 mice per group. Bars ± SEM. *P<0.05. (b) Gross LLC lung metastases (#) for Elane$^{+/+}$ and Elane$^{-/-}$ mice. N=3-4 mice per group. Bars ± SEM. *P<0.05. (c) Representative histology from WT and Elane$^{-/-}$ mouse lungs 31 days post-LLC flank injection.

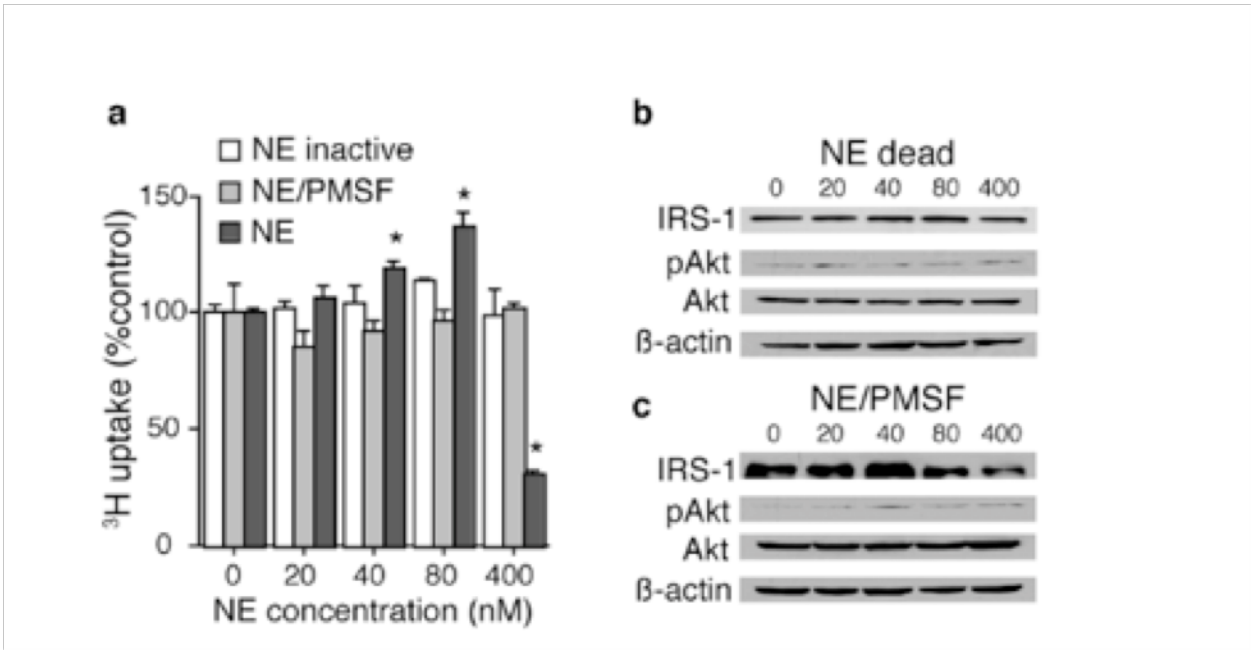

Supplementary Figure 2. NE-induced tumor cell proliferation requires catalytic activity: (a) Thymidine incorporation of A549 cells exposed to NE, heat-inactivated NE, or NE mixed with PMSF (serine proteinase inhibitor). Results from a representative experiment in triplicate. Bars ± SEM. *P<0.05. Wester blots of IRS-1, pAkt, Akt, and B-actin from A549 lysates exposed to (b) heat-inactivated NE or (c) NE/PMSF mixture.

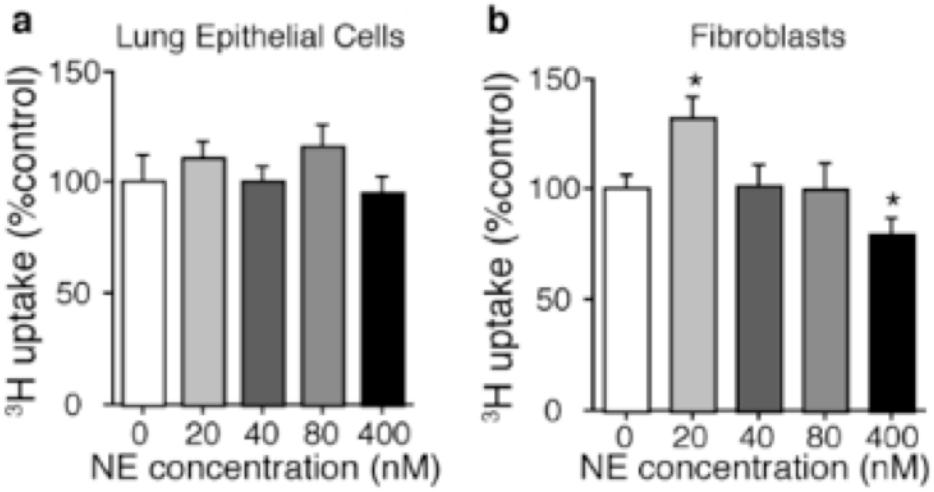

Supplementary Figure 3. NE induces proliferation in fibroblasts, but not lung epithelial cells: Thymidine incorporation of (a) primary mouse lung epithelial cells and (b) primary mouse lung fibroblasts exposed to NE or vehicle control for 60 min. Results from a representative experiment in triplicate. Bars ± SEM. *P<0.05.

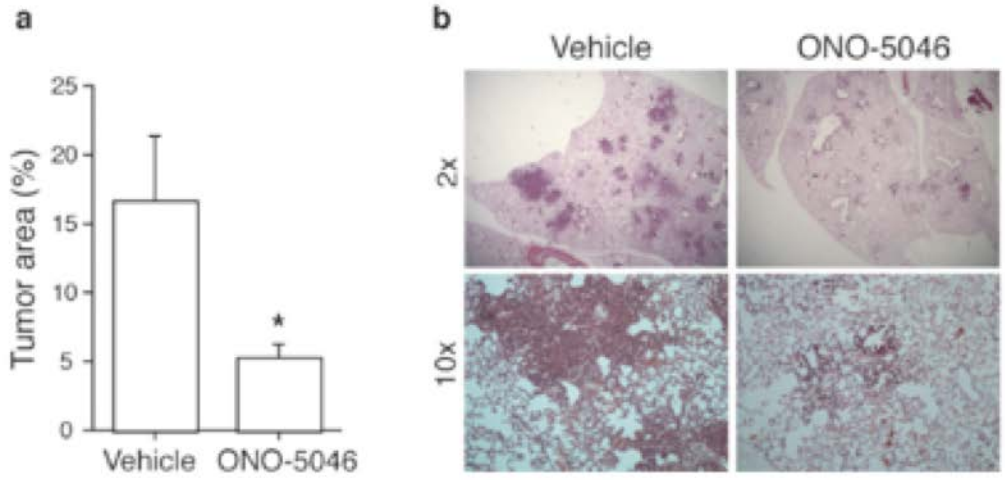

Supplementary Figure 4. NE-inhibition reduces lung tumor growth in vivo: (a) Lung tumor area for LSL-K-ras mice 14 weeks post-AdenoCre exposure treated with ONO-5046 (NE-inhibitor) or vehicle control. N=6 each group. Bars ± SEM. *P<0.05. (b) Representative images for ONO-5046 and vehicle control treated mouse lungs.

Supplementary Table 1: Description of tumor lesions by number, location, and type. Data expressed as mean values Bars ± SEM. N=5 mice each group *P<0.05 (ANOVA).

	Tumor #	AAH (%)	Adenoma (%)	ADCA (%)	Alveolar (%)	Bronchiolar (%)
8 Wks						
K-ras/NE$^{+/+}$	1.47 +/- 0.38	67.7 +/- 5.1	32.3 +/- 5.1	0	55.6 +/- 4.4	44.4 +/- 4.4
K-ras/NE$^{-/-}$	0.76 +/- 0.06	91.5 +/- 1.2*	8.5 +/- 1.2*	0	54.1 +/- 3.2	45.9 +/- 3.2
14 Wks						
K-ras/NE$^{+/+}$	1.99 +/- 0.19	43.0 +/- 7.3	51.6 +/- 5.4	5.42 +/- 2.3	54.1 +/- 1.7	45.9 +/- 1.7
K-ras/NE$^{-/-}$	1.72 +/- 0.12	81.9 +/- 2.3*	16.7 +/- 1.8*	1.4 +/- 0.9	54.6 +/- 4.8	45.4 +/- 4.8
20 Wks						
K-ras/NE$^{+/+}$	2.51 +/- 0.28	26.8 +/- 3.3	63.0 +/- 6.3	10.2 +/- 5.1	48.0 +/- 3.1	52.0 +/- 3.1
K-ras/NE$^{-/-}$	2.43 +/- 0.15	62.7 +/- 1.0*	36.3 +/- 1.0*	0.72 +/- 0.4	48.7 +/- 3.5	51.3 +/- 3.5

Activation of mutant K-ras in vivo. K-ras activation was achieved in vivo by administering 5x106 pfu titer adenoviral Crerecombinase (AdenoCre, University of Iowa) intratracheally to mice at eight weeks of age as previously described4 . Briefly, the mice were anesthetized with avertin and received the titer of adenovirus intranasally in two administrations of 62.5 l volume ten minutes apart. WT mice receiving AdenoCre and LSL-K-ras mice receiving vehicle only (Opti-MEM) served as controls. As these mice did not develop tumors, this data has not been included in the manuscript. The mice were age and sex matched for all experiments. An initial cohort of mice was treated with AdenoCre and followed to establish a life survival curve. This experiment was terminated when all of the mice in the WT group had died, as per our IACUC protocol. Repeat experiments were terminated at pre-determined time points of 8, 14, and 20 weeks.

Administration of NE-inhibitor. An additional cohort of LSL-K-ras mice was administered AdenoCre and subjected to IP injection of an NE-inhibitor (ONO-5046, Elaspol, 50mg/kg/day, ONO Pharmaceutical, Japan) or vehicle, six days/wk for 14 wks.

Bronchoalveolar lavage fluid (BALF). BALFwas obtained by inserting a 22g IV catheter into the trachea and lavaging the lungs with 0.75 mL saline x 4. BAL fluid was centrifuged at 3000 rpm for 3 min. The pellet was treated with red blood cell lysis buffer and resuspended in 1.0 mL saline to determine cellular content. Neutrophil, macrophage, lymphocyte, and total cell counts were measured using a hemocytometer and cytospins stained with Hema3 (Fisher).

Lung tissue immunofluorescence. Lung tissue was inflated with 2% PFA for 1 hr. Fixed tissue was immersed in 2.3 M sucrose in PBS overnight at 4oC and frozen in liquid nitrogen-cooled 2-methylpentane. Sixmm sections wereaffixed to charged slides (Fisher). Tissue was washed with PBS and blocked in 2% BSA for 30 min at RT. Primary antibodies (phospho-Akt

(Cell Signaling) phospho-p44/42 MAPK (Cell Signaling), phospho-IRS1 (Tyr941 and Ser307, Upstate) all diluted 1:100 in 0.5% BSA in PBS (PPB) buffer were added to sections 1 hr at RT. Sections were washed in PPB Buffer then fluorescently tagged secondary antibodies (goat anti-rabbit-Cy3, Jackson ImmunoLabs), diluted 1:1000 in PPB buffer, were added tosections for 1 hr at RT. Tissue was washed in PPB buffer then PBS before counterstaining nuclei with Hoechst 33342. Tissue was coverslipped using Gelvatol. Confocal images were obtained on an Olympus Fluoview 1000 confocal microscope using an oil immersion 40x objective. Quantification of signal was performed using MetaMorph. Six different tumors in each mouse were imaged using a single slice confocal image at 400x and Cy3 signal was evaluated relative to non-immune gated control. Results reported as relative fluorescence intensity.

Visualizing NE uptake by A549 cells. A549 cells were plated at a concentration of 2.5 x 10^4 cells/mL on 12mm circular coverslips within 24-welltissue plates. NE (1 mg, Elastin Products) was covalently labeled with Alex-488 following the manufacturer's instructions (Invitrogen). The cells were exposed to Alexa-488-labeled NE (0 –200 nM) for 60 min, rinsed with PBS and fixed for 60 min in 2% PFA. Cells were washed in labeling buffer (PBG; 0.5% BSA, 0.15% glycine in PBS). After 30 min 20% non-immune goat serum block in PBG, cells were incubated with primary antibody; rabbit anti-human EEA1 (Abcam) or rat anti-human caveolin-1 (Abcam); in PBG for 3 hrs, washed with PBG, and incubated with fluorescently labeled secondary antibodies (goat anti-rat or goat anti-rabbit Cy3, Jackson Immunolabs) in PBG for 60 min. Cells were washed in PBG, then in PBS followed by a 30 sec stain with Hoechst nuclear stain. Cells were then washed in PBS and coverslipped using Gelvatol. In cases where non-labeled NE was used, cells were treated as described above, but immuno-labeled with mouse anti-human NE (Chemicon) and rabbit anti-human IRS1 (Upstate). Goat anti-mouse Cy3

(Jackson Immunolabs) and goat anti-rabbit Alexa488 (Invitrogen) were used as secondary antibodies. All confocal images were taken using an inverted Olympus Fluoview 1000 microscope fitted with a 100x oil immersion objective and digitally zoomed 2x prior to acquiring the image.

Isolation of lung epithelial cells. Primary mouse lung epithelial cells were harvested and cultured from C57BL-6 mice, as previously described [182, 183] and grown on collagen IV coated 24-well plates. Briefly, lungs were perfused with 10ml 0.9% saline. Dispase (3ml) was instilled into the lungs via intratracheal catheter followed immediately by 0.5mLlow melt agarose at 45°C. Lungs were immediately covered with ice for 2min. The lungs were then removed and incubated in 1ml dispase for 45min at 25°C. Lungs were subsequently transferred to a 60-mmculture dish containing 7ml of HEPES-buffered DMEM and 100U/ml DNAse I. Lung tissue was filtered through progressively smaller cell strainers (100 and 40μm) and nylon gauze (20μm). Cells were collected by centrifugation at 130g for 8min (4°C) and placed on prewashed/antibody pre-coated 100-mm tissue culture plates (coated for 24-48 h at 4°C with 42μg CD45 and 16μg CD32 in PBS). After incubation for 1-2 h at 37°C, the cells were gently panned from the plate and collected by centrifugation. The cells were then allowed seven days to differentiate prior to experimentation.

Isolation of murine lung fibroblasts. Primary mouse lung fibroblasts were isolated from C57BL/6 mice, as previously described [184]. Briefly, the lungs were perfused with 10mL sterile saline and placed in ice cold DMEM with 10 IU/ml penicillin, 10 g/ml streptomycin. Each set of lungs was minced into small pieces and placed on scratched 100mm2 culture dishes. The pieces of lung were allowed to adhere to the plate for 10 min then gently submerged in 10 mL of growth media (DMEM with 10% FBS, penicillin, streptomycin). The explants were removed

from the dishes after 7 days in culture, after which the plates were cultures for 7 additional days. The fibroblasts were subsequently passaged to T-75 flasks and cultured on 96-well plates.

Lewis Lung Carcinoma (LLC) cells. Lewis Lung Carcinoma (LLC) cells were utilized in the spontaneous metastasis model as previously described [185]. Briefly, $1x10^6$ LLC cells were injected subcutaneously into the right flank of C57BL6 and NE-/- mice. Primary tumors were removed and weighed 21-days after injection. The number of gross lung metastases (visible on the pleural surface to the naked eye) was tabulated over a time course.

ELISA. BALF was obtained as above. Samples were normalized by volume. The levels of TGFα, VEGF, PDGF-AA, PDGF-AB, and PDGF-BB were determined using the commercially available Quantikine kits (R&D Systems) as per the manufacturer's instructions. Results of PDGF-AB and PDGF-BB were not shown as each was below detection limits of the assay. Each sample was performed in duplicate, n=5 samples

B.5 ACKNOWLEDGEMENTS

This work was supported by grants K08HL085286 and RO1HL054853 from the NIH/NHLBI (A.M.H. and S.D.S.) and by grant RO1DK058259 from the NIH/NIDDK (S.J.F). ONO Pharmaceutical (Osaka, Japan) provided the ONO-5046. AdenoCre was obtained from the University of Iowa Gene Transfer Vector Core. The authors would like to recognize members of the Shapiro lab for their assistance and comments regarding the preparation of this manuscript.

APPENDIX C

NEUTROPHIL ELASTASE PROMOTES MYOFIBROBLAST DIFFERENTIATION IN LUNG FIBROSIS

Alyssa D. Gregory[*,†,‡], Corrine R. Kliment[*,§,‡], Heather E. Metz[*,†,¶], Kyoung-Hee Kim[¶], Julia Kargl[¶], Brittani A. Agostini[*,†], Lauren T. Crum[§], Elizabeth A. Oczypok[§], Tim A. Oury[§], and A. McGarry Houghton[¶,‖]

From the Departments of [*]Medicine and [§]Pathology, [†]Division of Pulmonary, Allergy, and Critical Care Medicine, University of Pittsburgh School of Medicine, Pittsburgh, PA and [¶]Clinical Research Division, Fred Hutchinson Cancer Research Center, Seattle, WA and [‖]Division of Pulmonary and Critical Care, University of Washington, Seattle, WA.

[‡]These authors contributed equally to the work.

Modified from Gregory, A.D., et al. 2015. Neutrophil Elastase Promotes Myofibroblast Differentiation in Lung Fibrosis. *Journal of Leukocyte Biology*. 2015 Aug; 98 (2):143-52.

C.1 SIGNIFICANCE

Idiopathic pulmonary fibrosis (IPF) is a progressive lung disorder characterized by fibroblast proliferation and myofibroblast differentiation. Although neutrophil accumulation within IPF lungs has been negatively correlated with outcomes, the role played by neutrophils in lung fibrosis remains poorly understood. We have previously demonstrated that neutrophil elastase (NE) promotes lung cancer cell proliferation, and hypothesized that it may have a similar effect on fibroblasts. In the current study, we show that *NE*$^{-/-}$ mice are protected from asbestos induced lung fibrosis. *NE*$^{-/-}$ mice displayed reduced fibroblast and myofibroblast content when compared to controls. NE directly promotes both lung fibroblast proliferation and myofibroblast differentiation in vitro as evidenced by proliferation assays, collagen gel contractility assays, and αSMA induction. Furthermore, αSMA induction occurs in a TGF-ß independent fashion. Treatment of asbestos recipient mice with ONO-5046, a synthetic NE antagonist, reduced hydroxyproline content. Thus, the current study points to a key role for neutrophils and NE in the progression of lung fibrosis. Lastly, the study lends rationale to using NE inhibitory approaches as a novel therapeutic strategy for patients with lung fibrosis.

C.2 INTRODUCTION

Idiopathic Pulmonary Fibrosis (IPF) is a rapidly progressive and debilitating lung disease, the most common of several types of interstitial lung diseases that affect humans. There are currently no effective therapies for IPF patients, such that this progressive disorder confers an average survival duration of just three to five years, and accounts for >20,000 deaths annually, in the US alone [186]. Clearly a better understanding of the molecular pathogenesis of lung fibrosis will be required to develop new and effective therapies for IPF subjects [133].

A considerable amount of research has focused on the apparent culprit cell in lung fibrosis, the myofibroblast [187]. The lungs are well stocked with fibroblasts, which maintain the extensive extracellular matrix (ECM) scaffolding required for oxygen exchange. Unfortunately, these lung fibroblasts can take on a hyperfunctioning phenotype with wound healing characteristics. Such myofibroblasts are highly contractile and release substantial quantities of ECM proteins, such as collagen, that results in scarring of the lung, or lung fibrosis. The hallmark of the myofibroblast is the expression of alpha-smooth muscle actin (αSMA), which confers exaggerated contractile properties to myofibroblasts [188]. Despite extensive study, the mechanisms by which lung fibroblasts differentiate into myofibroblasts remain poorly understood. It is certainly clear that transforming growth factor-ß (TGF-ß) can induce myofibroblast formation. Mechanistically, TGF-ß, through interaction with its receptor, induces the generation of phosphorylated mothers against decapentaplegic homolog 3 (pSMAD3) from SMAD3, which then functions as the transcription factor for the production of αSMA [189]. It remains unclear if other factors within the lung environment promote myofibroblast differentiation, and if these factors do so in a TGF-ß-dependent or -independent fashion.

Our group has focused on the role of neutrophils in lung fibrosis. There exists data from human cohorts supporting a role for PMNs in the pathogenesis of IPF [190]. Bronchoalveolar lavage (BAL) fluid content of both neutrophils and of neutrophil elastase (NE) has been shown to correlate with disease severity in IPF [134, 191, 192]. NE is a neutrophil derived serine proteinase with broad substrate specificity, including most components of the ECM [193]. However, the major physiologic function of NE is matrix independent. NE is an essential means of host defense against pulmonary [167], and other, infections. Once neutrophils have phagocytosed bacteria, they rapidly shuttle NE into the phagolysosomes, where it degrades key bacterial cell wall structures, resulting in lysis of bacteria [194].

Once in the extracellular space, NE is capable of degrading essentially all of the ECM proteins found within the lung, including collagens (types I-III), laminin, entactin, fibronectin, type IV collagen, and elastin [195]. NE is best known for its ability to cleave elastic fibers within the lung, which is a key event in the pathogenesis of emphysema [177, 196]. Although it has been reported that NE promotes the development of lung fibrosis [197], the mechanisms remain unclear, and may not involve the processing of ECM substrates. Accordingly, treatment of bleomycin-exposed animals with the serine leukocyte proteinase inhibitor (SLPI, a naturally occurring NE inhibitor) reduced the extent of lung injury [198]. Interestingly, the low dose of SLPI used in this study did not completely abrogate NE enzymatic activity in the lung, suggesting that the mechanism of action was not the simple inhibition of NE-mediated tissue destruction.

Because IPF lungs display enhanced fibroblast content and function, we postulated that NE could be involved in the proliferation and differentiation of these cells. We have previously shown that NE promotes cellular proliferation in multiple different lung cancer cell lines [88].

Recently, other groups have reproduced these findings in breast cancer cells [199], as well. Notably, NE accomplishes this by entering tumor endosomes via classic clathrin pit mediated endocytosis, where it ultimately targets intracellular substrates within the cytosol [200]. The most notable of these is the insulin receptor substrate-1 (IRS-1), a key mediator of phosphoinositol-3 kinase (PI3K) signaling [201]. We detected increased pAkt production and cellular proliferation in A549 lung adenocarcinoma cells (and others) in the absence of IRS-1, whether from NE treatment or IRS-1 silencing [88]. Interestingly, IPF fibroblasts have been demonstrated to display enhanced PI3K activity in vivo [202]. The purpose of the current study, therefore, is to determine if NE promotes fibroblast proliferation in vitro and in vivo, and to identify the mechanisms by which this occurs. Here, we show that NE does in fact induce fibroblast proliferation and, surprisingly, also promotes myofibroblast differentiation, in a novel, TGF-ß-independent fashion.

C.3 MATERIALS AND METHODS

C.3.1 Material

Human neutrophil elastase (NE, also known as human leukocyte elastase) was purified from human sputum and purchased from Elastin Products Co. (Owensville, MO). ONO-5046 was obtained from ONO Pharmaceutical (Osaka, Japan). Crocidolite asbestos was obtained from Andy Ghio (NIEHS).

C.3.2 Mice

NE$^{-/-}$ mice on a pure C57BL/6 background (>10 generations backcrossing) were generated as previously described [177], and provided by Steve Shapiro (University of Pittsburgh). Age and sex-matched wild-type C57BL/6 mice (Jackson, Bar Harbor, ME) were used as the controls. All experiments were approved by the University of Pittsburgh Institutional Animal Care and Use Committee.

C.3.3 Asbestos induced lung injury

Age and sex matched C57BL/6 and *NE*$^{-/-}$ mice between 8-10 weeks of age were anesthetized with 2.5% avertin and intubated using a standard prone technique. By way of an endotracheal catheter, the mice received either 0.1 mg crocidolite asbestos or 0.1 mg titanium dioxide (TiO_2, inert control particulate). Animals were examined at either 7-days or 14-days post asbestos treatment. All mice were weighed daily for the duration of the experiment. At the time of harvest, bronchoalveolar lavage (BAL) was performed on each mouse, the right lung was tied off and excised, and the left lung was inflated with 10% buffered formalin at 25cm H_20 pressure for

10 min, followed by additional formalin fixation for 24 hrs in a 50 cc conical tube. The right lung was flash frozen in liquid nitrogen, homogenized on ice in CHAPS buffer (50 mmol/L Tris-HCl (pH 7.4), 150 mmol/L NaCl, 10 mmol/L CHAPS), with proteinase inhibitors. The lung homogenate was placed in glass vacuoles for hydroxyproline analysis.

C.3.4 Hydroxyproline assay

Lung homogenate samples were dried in glass vacuoles in a 110C oven for 24 hrs. Acid hydrolysis was completed by adding 6M HCl. Vials were vacuumed, sealed and incubated under anoxic conditions for 24 hours at 110C. After drying, the samples were assayed for hydroxyproline using chloramine-T [203], as previously described.

C.3.5 Histology

Formalin fixed lungs (generated above) were embedded in paraffin. Sections were subjected to routine H&E and Masson's Trichrome staining. These images were used to measure the fibrosis index, or the proportion of high-powered lung fields showing evidence of fibrotic involvement. The fibrosis index was generated by scoring fields with >50% alveolar tissue and terminal bronchioles according to the following scale: 0 = no fibrosis, 1 = 0-25%, 2 = 26-50%, 3 = 51-75%, and 4 = 76-100%. A histologic index score was assigned to each sample by dividing the sum of the scores of each field by the total number of scored fields. Lung fibroblasts were quantified using fibroblast specific protein-1 (FSP-1) immunostaining (rat-anti mouse antibody, ab27957, 1:100 dilution, Abcam, Cambridge, MA) on mid-sagittal sections using a standard avidin-biotin HRP technique in which 3,3'-diaminobenzidine was the chromogenic substrate. Results were expressed as the average count from ten hpf per slide, in which only fibrotic lesions

were tabulated. In order to identify myofibroblasts via immunofluorescence staining, lungs were inflated with and embedded in OCT (Sakura, Torrance, CA) prior to sectioning. Six micron mid-sagittal lung tissue sections were adhered to glass slides and fixed with 2% paraformaldehyde (PFA) for 30 min. Tissue was permeabilized by treating with 0.1% Triton X-100 (Sigma, St. Louis, MO) for 5 min and subsequently blocked with 1% BSA for 45 min. Nuclei were stained with 1mg/mL Hoescht and cover glass adhered with gelvatol mounting media. Tissue was stained with anti-smooth muscle actin (1:200, Sigma A5228) and anti-S100A4 (1:200, ab27957, Abcam). Primary antibodies were removed and sections washed three times with PBS before addition of fluorochrome-conjugated secondary antibodies, anti-mouse-Alexa488 and anti-rabbit-Alexa595 (both 1:500, Invitrogen). Stained tissue was imaged using a Fluoview 1000 Confocal Microscope (Olympus, Center Valley, PA) and all laser settings were obtained using secondary antibody-only control sections.

C.3.6 Flow Cytometry

Lung tissue was homogenized into a single cell suspension using a one-hour digestion with 1 mg/mL collagenase type IV and 0.5 mg/mL DNase in DMEM followed by gentle mechanical disruption and passage through a 22-gauge needle. Cells were pre-treated with Fc block (BD Biosciences, San Jose, CA) and then stained with CD45-FITC (eBioscience, San Diego, CA) for one hr at 4C. Cells were then fixed and permeabilized using Cytofix/Cytoperm reagents according to manufacturer's instructions (BD Biosciences). Following permeabilization, cells were incubated with unconjugated anti-S100A4 (ab27957) and αSMA-PE (R&D Systems, Minneapolis, MN) for one hr at 4C. Cells were then washed and stained with anti-rabbit-APC

(Invitrogen, Grand Island, NY) in order to bind unconjugated anti-S100A4. Cells were analyzed using a FacsCalibur flow cytometer (BD Biosciences) using CellQuest Pro acquisition software.

C.3.7 Cells

LL47 human lung fibroblasts were obtained from ATCC and cultured in Dulbecco's modified Eagle's medium (DMEM) + 10% fetal bovine serum (FBS). Primary mouse lung fibroblasts (PMF) were isolated from C57BL/6 mice, as previously described [183], with modifications. Six to eight week old female mice were euthanized before perfusing the right ventricle with 10 mL normal saline to remove blood from the lungs. The lungs were then removed and placed in ice-cold DMEM with 10 IU/mL penicillin and 10 µg/mL streptomycin. The lungs were minced into small pieces and placed on scratched 100 mm^2 culture dishes. The pieces of lung were allowed to adhere to the plate for 10 min then gently submerged in 10 mL DMEM + 10% FBS. The explants were removed from the dishes after seven days in culture, after which the plates were cultured for an additional seven days. The fibroblasts were subsequently passaged to T-75 flasks. The identical procedure was performed using the lungs from insulin receptor substrate-1 (IRS-$1^{fl/fl}$) mice [91] and WT mice on the same genetic background (129/SvJ), with the addition of $1x10^5$ pfu (MOI 100:1) adenoviral cre recombinase (AdCre, University of Iowa Vector Core) on day 14 to both IRS-$1^{fl/fl}$ and IRS-$1^{+/+}$ cultures for the purpose of removing the floxed allele.

C.3.8 Neutrophil elastase treatments

Lung fibroblasts (both LL47 and PMF, in separate experiments) were exposed to NE. The cells were plated at $1x10^5$ cells/well in 24-well plates in serum free media for 24 hrs prior to NE exposure. NE was administered over a dose course (1nM-40nM) for one hour. In some

experiments, NE treatments were accompanied by 30 min pre-treatment with either PI3K inhibitor (LY294002, 50µM, Cell Signaling, Danvers, MA) or type I activin receptor-like kinase (ALK) receptor inhibitor (SB431542, 10µM, Sigma) and with continued exposure during the course of the NE treatment. In other experiments, NE was inactivated either by heating to 100C for 15 minutes or by conjugating with 5mM of the serine proteinase inhibitor phenylmethylsulfonyl fluoride (PMSF, Sigma) at 37C for one hour. Cells were subsequently washed, lysed, and stored at -80C for additional analyses.

C.3.9 Confocal microscopy

LL47 fibroblasts were plated on tissue culture-treated coverslips (Thermo Fisher, Pittsburgh, PA) in 24-well plates, allowed to adhere overnight, and transferred to serum-free media for 24 hr. NE was fluorescently labeled using the Alexa Fluor 488 protein labeling kit (Invitrogen) according to manufacturer's instructions. Cells were treated with Alexa Fluor 488-NE (4nM) for one hr, immediately fixed in 2% PFA in PBS, and permeabilized with 0.1% Triton X-100. Cells were co-stained for early endosomal antigen-1 (EEA-1, 1:200, Abcam), phalloidin (1:200, Invitrogen), or αSMA (A5228, 1:200, Sigma). Donkey anti-rabbit 594 or donkey anti-mouse 488 (Invitrogen) antibodies were used as the secondary antibodies. The identical procedure was repeated using Alexa488-labeled trypsin. Cells were imaged using an Olympus Fluoview 1000 upright confocal microscope. Ten fields per preparation were quantified to determine the percentage of cells displaying intracellular Alexa488 staining.

C.3.10 Fibroblast proliferation assays

Fibroblast proliferation in response to NE treatment was assessed using MTS (Promega) cell viability assays. LL47 or PMF were plated in 96-well plates (4,000 cells/well) and placed in serum-free DMEM for 24 hrs prior to treatment. Cells were treated with media or NE (0 to 40 nM) for 60 min at 37C (both with and without PMSF and heat inactivation). Wst-1 and MTS assays were performed according to manufacturer's instructions and absorbance readings were obtained. All experiments were performed in triplicate and replicated at least three times. Results are expressed as % control +/- SEM.

C.3.11 Would healing (scratch) assay

LL47 fibroblasts were plated on 24 well polystyrene plates and grown to confluence in growth media. Straight wounds were created with a p200 pipet tips, washed, and treated with NE over a dose range. After 1 hr, the cells were washed with PBS. Images were captured using a 4x objective with phase contrast (Nikon, Melville, NY) at time = 0, 18, and 24 hrs. Wound areas were quantified using NIS-Elements Software (Nikon).

C.3.12 Gel contractility assay

Type I rat tail collagen (BD Biosciences) was rapidly mixed with $2x10^5$ LL47 cells in serum free media at a final concentration of 1.8 mg/mL. Cells were treated with NE at the indicated concentrations. The gels were allowed to solidify in a 24 well plate for 20 min at RT and were then gently dissociated from the walls of the plate and incubated in serum free media at 37C with 5% CO2 for 72 hrs. Plates were imaged using an Omega imaging system (UltraLum, Claremont, CA) and areas were quantified using ImageJ software (NIH). To determine the number of

fibroblasts present in the gel matrix, at 72 hrs gels were digested with 0.25 mg/mL collagenase type XI (Sigma) for 1 hr at 37C and the resultant cell pellet was counted using a hemocytometer.

C.3.13 Immunoblotting

Proteins were separated using standard 10% SDS-PAGE followed by transfer of protein to PVDF membranes. Membranes were blocked for 2 hrs at RT or overnight at 4 degrees in 5% dry milk in PBS-tween. Primary antibodies were incubated overnight at 4C followed by secondary antibody incubation (rabbit or mouse IgG HRP conjugated, 1:5000) for 1 hr at RT. The following primary antibodies were used: αSMA (1:250) from Abcam and IRS-1 (1:1000), Akt (1:2000), pAkt (1:1000), p38MAPK (1:2000), phospho-p38MAPK (1:1000), pSMAD3 (1:1000), SMAD2/3 (1:2000), GAPDH (1:2000), all from Cell Signaling Technology.

C.3.14 Statistics

All data were reported as mean value +/- SEM. Statistical significance was determined using either Student's t-test (two-tailed distribution with two-sample equal variance) or ANOVA followed by Tukey's post-test using Graphpad Prism software (Graphpad, San Diego, CA). A P-value of < 0.05 was considered significant.

C.4 RESULTS

C.4.1 NE-deficient mice are protected from asbestos induced lung fibrosis

To determine if NE promotes asbestos induced lung injury, we subjected *NE*$^{-/-}$ mice and C57BL/6 control mice to the intratracheal administration of 0.1 mg crocidolite asbestos, or TiO_2 vehicle control. Both groups of mice were studied at 7 and 14 days post asbestos treatment. Intratracheal delivery of asbestos generated a characteristic fibrotic response within the lungs of C57BL/6 mice that was evident on both H&E and Masson's trichrome staining at the 14-day time point (Figure 1A). Additionally, hydroxyproline measurements similarly demonstrated a statistically significant increase in hydroxyproline content in asbestos treated C57BL/6 mice when compared to TiO_2 controls (Figure 1B) at day 14, a finding that was not present at the earlier time point. In contrast, *NE*$^{-/-}$ mice were completely protected from asbestos induced lung fibrosis. Although there was a scant amount of lung fibrosis present on histological sections, the hydroxyproline content in the lungs of *NE*$^{-/-}$ asbestos treated mice was not statistically different from the TiO_2 treated C57BL/6 or *NE*$^{-/-}$ mice (Figure 1B). Accordingly, histological scores of H&E and trichrome stained slides revealed that the fibrotic index was significantly reduced in asbestos treated *NE*$^{-/-}$ mice as compared to asbestos treated C57BL/6 mice (Figure 1C). Since there has been some speculation that NE may play a role in inflammatory cell trafficking to the lung [204], we analyzed the cellular content of BAL fluid from both groups. As shown in Figure 1D, there was increased BAL inflammation in the asbestos treated mice, though there were not differences observed between WT and *NE*$^{-/-}$ mice.

Figure 1

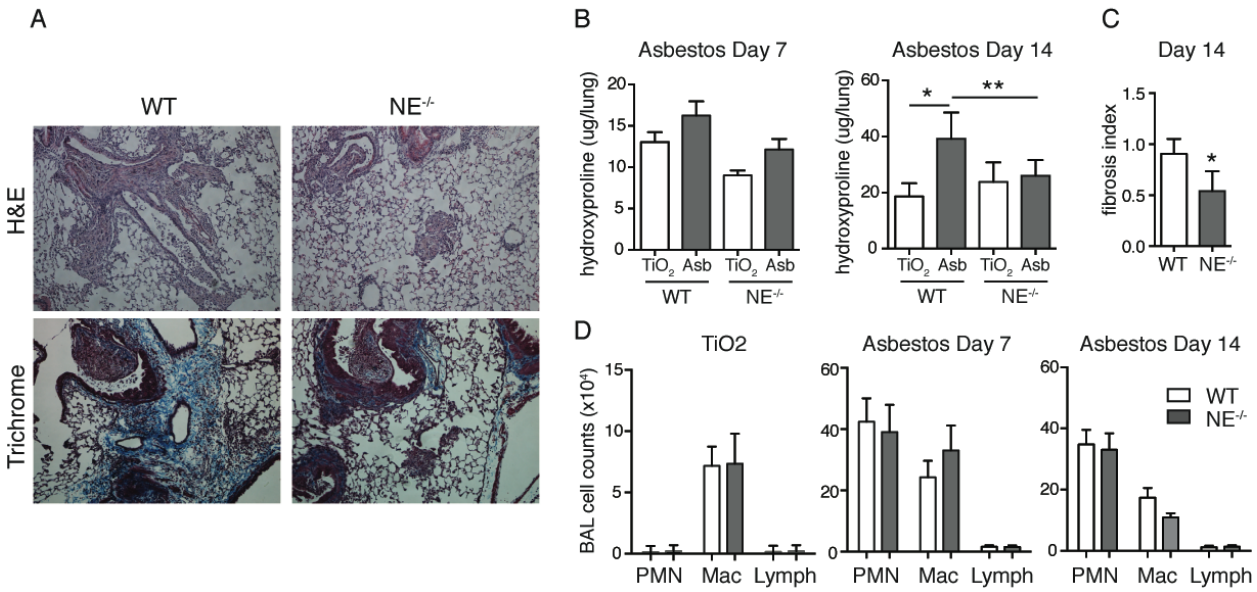

Figure 14. NE-/- mice are protected from asbestos induced lung fibrosis: WT and NE-/- mice were treated with 0.1 mg crocidolite asbestos or TiO2 control. (A) Representative images from H&E (10X) and Masson's Trichrome (20X) stained lung sections 14 days after asbestos treatment. (B) Hydroxyproline content was measured at days 7 (left panel) and 14 (right panel). N=6-8 per group. (C) Fibrosis index was generated according to the criteria described in Materials and Methods. N=6-8 per group. (D) BAL neutrophil, macrophage, and lymphocyte counts for 14 days post-TiO2 treatment (left panel; N=6); day 7 post-asbestos treatment (middle panel; N=8), and day 14 post-asbestos treatment (right panel, N=8). Installations were performed at least two times and the data was pooled. All data presented as mean value +/- SEM. Two-tailed Student's t-test was used to compare differences between groups. *P<0.05.

C.4.2 Reduced fibroblast content in $NE^{-/-}$ mice

Since fibroblasts and myofibroblasts are essential mediators of disease pathogenesis in lung fibrosis, we quantified these cells in asbestos treated WT and *$NE^{-/-}$* mice. FSP-1 stained sections demonstrated a doubling of fibroblast content in WT asbestos treated mice as compared to the NE-deficient arm, which was statistically significant (Figure 2A). We attempted to measure αSMA expression using immunofluorescence staining. We were able to identify some FSP-1/αSMA double-positive cells in WT asbestos treated mice, whereas these cells were virtually undetectable in asbestos treated NE mice (Figure 2B). However, this methodology, and the sparse nature of these cells identified using immunofluorescence did not offer the ability to reliably quantify such cell types.

We performed flow cytometry in order to better quantify the number of fibroblasts and myofibroblasts present in asbestos induced lung injury. Similar to the finding reported for FSP-1 immunohistochemsitry (IHC), we observed an approximate doubling of fibroblasts (by FACS analysis) present in WT asbestos treated mice as compared to *$NE^{-/-}$* mice, even after gating specifically on the $CD45^-$ population (in order to exclude any $FSP\text{-}1^+$ macrophages) (Figure 2C-D).

To quantify lung fibroblasts that had adopted the pro-fibrotic myofibroblast phenotype, we measured the proportion of lung fibroblasts in each treatment group that expressed αSMA by FACS. This involved a permeabilization step, as αSMA is an intracellular protein. Once again, the data showed that there were approximately twice as many myofibroblasts, defined as $CD45^-$ $FSP1^+\alpha SMA^+$ cells, in the lungs of C57BL6 asbestos treated mice when compared to asbestos treated *$NE^{-/-}$* mice (Figure 2C-E). We also quantified pericytes and smooth muscle cells ($CD45^-$ $FSP1^-\alpha SMA^+$ cells) and fibrocytes (Figure 2F-G). Fibrocyte content was determined by

eliminating $CD11c^+$ and $F4/80^+$ cells (macrophages) from the $CD45^+FSP1^+$ population. We were unable to identify significant differences in these populations, suggesting that the major cell types affect by NE deficiency are fibroblasts and myofibroblasts.

Figure 2

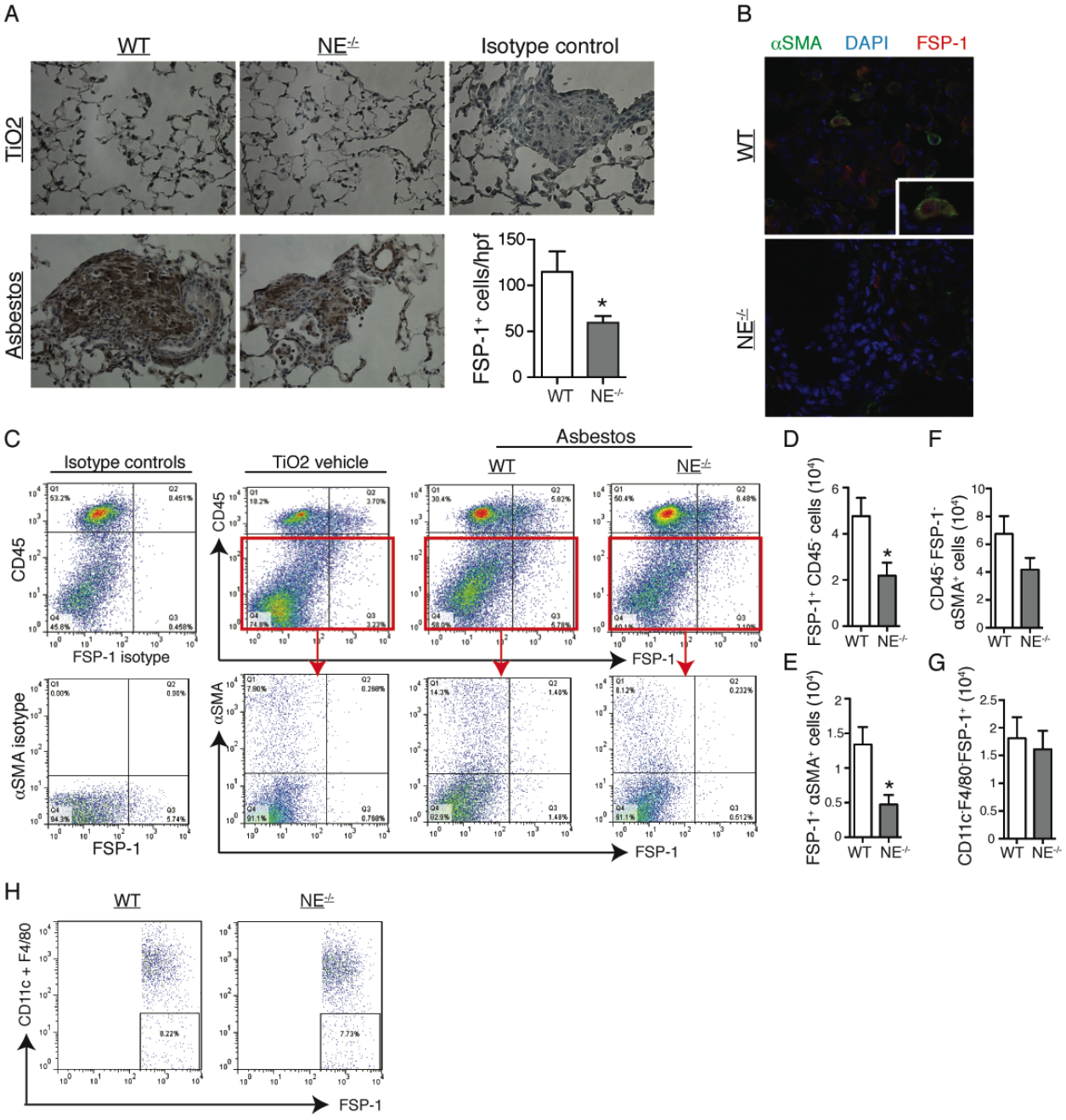

Figure 15. Decreased fibroblast and myofibroblast content in *NE*$^{-/-}$ mice: WT and *NE*$^{-/-}$ mice were treated with 0.1 mg crocidolite asbestos or TiO_2 control and studied 14 days later. (A) Representative images and quantification of IHC staining for FSP-1^{+} cells. Results expressed as positive cells/hpf from ten fields per mouse (N=8 each group). (B) Representative confocal images from αSMA (green), FSP-1 (red), and DAPI (blue) stained frozen lung sections. Laser

voltages were set such that the secondary antibody-only controls exhibited no fluorescence. (C) Representative flow cytometric dot plots of single cell suspensions obtained from day 14 asbestos-treated whole lungs denoting percentages of fibroblasts ($CD45^{-}FSP1^{+}$) and myofibroblasts ($CD45^{-}FSP1^{+}\alpha SMA^{+}$). Gates were set according to isotype controls as illustrated. Total cell numbers of (D) fibroblasts ($CD45^{-}FSP1^{+}$), (E) myofibroblasts ($CD45^{-}FSP1^{+}\alpha SMA^{+}$), (F) pericytes/smooth muscle cells (CD45-$FSP1^{-}\alpha SMA$+) and (G) fibrocytes ($CD45^{+}FSP1^{+}CD11c^{-}F4/80^{-}$) were obtained by multiplying cell percentages by the absolute whole lung cell count obtained by hemacytometer counts (N=7 mice per group). Dot plots in (G) have been gated on $CD45^{+}FSP1^{+}$ cells. All data presented as the mean value +/- SEM. FACS experiments were performed twice with one representative experiment shown. Two-tailed Student's t-test was used to compare differences between the two groups. *P<0.05.

C.4.3 NE induces fibroblast proliferation

Prior studies by our group established the ability of NE to promote the proliferation of lung cancer cells. Based upon the in vivo phenotype above, we suspected that NE might be functioning in a similar capacity with respect to fibroblast proliferation. We exposed both the LL47 human fibroblast cell line and PMFs (primary murine fibroblasts, from C57BL/6 mice) to a dose range of NE. The results showed that NE induced fibroblast proliferation at modest concentrations of NE, very similar to the dosages that induce proliferation in cancer cells (Figure 3A-D). We suspect that similar concentrations of NE are encountered in vivo, although this has proven difficult to determine experimentally. NE is rarely "dumped" into the extracellular space, but rather released from granules in quantum microbursts to overcome the anti-proteinases

prevalent in the extracellular compartment [171]. Therefore, the concentrations encountered at the cell surface are likely to be modest.

The mechanism by which NE induces fibroblast proliferation appears to be quite similar to that previously described for cancer cell proliferation. Exposure of NE to fibroblasts for one hour results in complete loss of insulin receptor substrate-1 (IRS-1), a key mediator of PI3K activity (Figure 3E-F). We suspect that this is a direct proteolytic effect of NE, as we have previously shown that NE degrades recombinant IRS-1 protein at 1:100 molar ratios, and co-localizes with IRS-1 within cancer cells. At the same time that IRS-1 loss is noted, we observed a substantial increase in cellular pAkt production, again, similar to our findings in cancer cells (Figure 3E-F). High concentrations of NE (40nM) produce the opposite effect. Whereas modest concentrations of NE induced proliferation in lung cancer cells and breast cancer cells, high concentrations induce cell death. In this case, the high concentrations simply damage the cell membrane, which results in cellular lysis. The absence of loading control observed on the Western blots (GAPDH) at high NE concentration is simply a reflection of reduced cell content. NE-mediated proliferation (low dose) and toxicity (high dose) require catalytic activity, as both heat- and PMSF-inactivated NE fail to reproduce these effects (Figure 3B-C).

A unique aspect of NE-induced cellular proliferation is that it requires entry into the target cell beyond its plasma membrane. We were able to localize Alexa488-labeled NE within early endosomal antigen-1 (EEA-1) positive endosomes (Figure 3G-H). This finding is specific for NE, as Alexa488-labeled trypsin was unable to enter the endosomes. Based upon our findings, and those of others, NE has been demonstrated to enter multiple different cancer cell lines including lung and breast, and now fibroblasts as well. As is the case for fibroblasts, NE-induced cellular proliferation requires the presence of its catalytic domain [88, 200].

The loss of IRS-1 is a key event in NE-induced fibroblast proliferation. To demonstrate this, we generated IRS-1-deficient fibroblasts. This was accomplished by making PMFs from *IRS-1*$^{fl/fl}$ mice and WT littermate controls and treating them with AdenoCre ($1x10^5$ pfu, MOI 100:1) to remove the floxed allele. IRS-1-deficient fibroblasts generated in this way display increased proliferation when compared to controls (Figure 3I-J).

FIgure 3

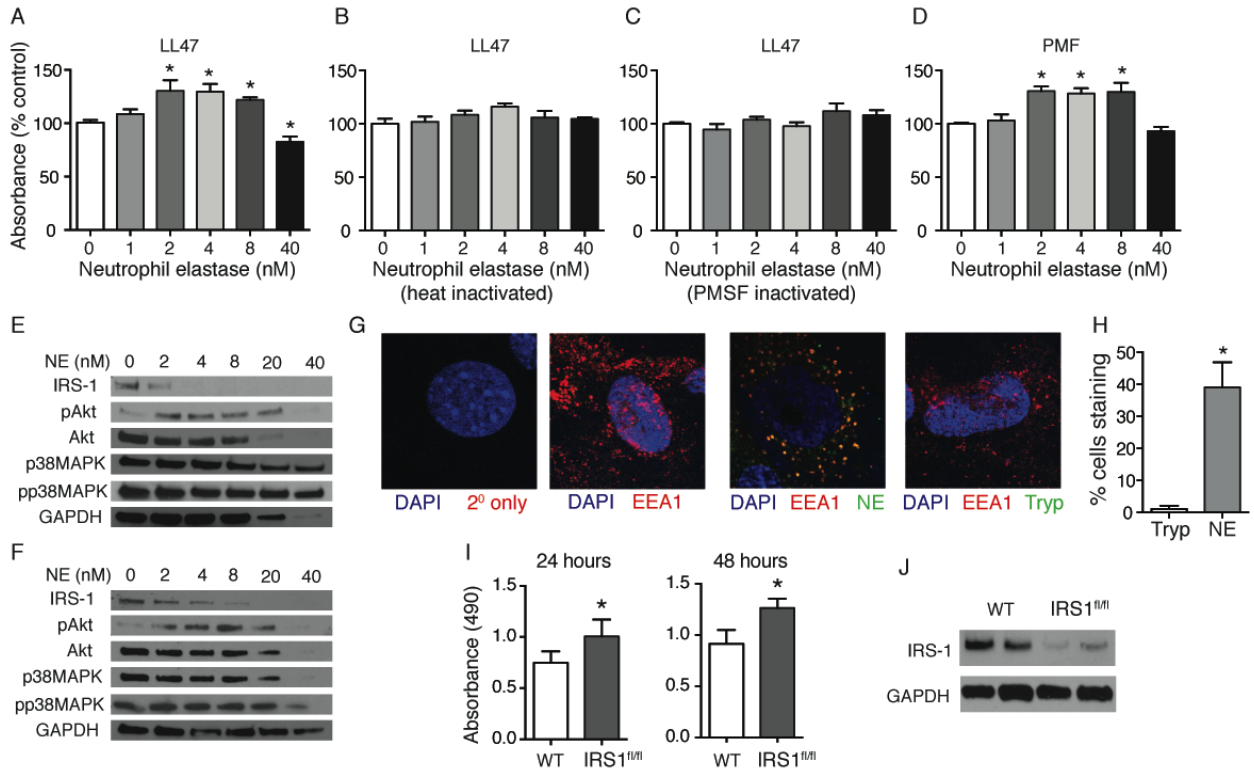

Figure 16. NE induces fibroblast proliferation: MTS proliferation assay for LL47 cells treated with (A) NE, (B) heat-inactivated NE, (C) PMSF-inactivated NE, and (D) PMF fibroblasts treated with NE at the indicated concentrations (N=12 wells per treatment). Western blots performed on (E) LL47 and (F) PMF fibroblast cell lysates for IRS-1, pAkt, Akt, p38MAPK, phospho-p38MAPK, and GAPDH following NE treatment for one hr at the indicated concentrations. (G) Alexa 488-labeled NE (4nM) and trypsin was incubated with LL47 fibroblasts for 60 min and washed with PBS. Cells were stained with anti-EEA1 (red) and counterstained with DAPI (blue) and imaged using confocal microscopy. Magnification = 1200X. (H) The percentage of cells in each field, which contain co-localized NE and EEA1 (yellow) was quantified for both trypsin-Alexa488 and NE-Alexa488. Ten confocal fields per condition (containing at least 75 cells in total) were imaged and quantified. (I) MTS-proliferation assay for WT and IRS-$1^{fl/fl}$ fibroblasts, conducted at 24 (left panel) and 48 (right

panel) hours after an overnight treatment with adenoviral Cre-recombinase (MOI=100:1) (n=4 for each condition, representative of two independent experiments). (J) Western blot depicting knockdown of IRS-1 in primary fibroblasts described in (I). Lysates were prepared at t=0 prior to conducting the 24- and 48-hour proliferation experiments. All data presented as the mean value +/- SEM. Each study was performed twice with one representative experiment shown. Two-tailed Student's t-test was used to compare differences between groups. *P<0.05.

C.4.4 NE promotes myofibroblast differentiation

As demonstrated above, asbestos treated *NE*$^{-/-}$ mice display both reduced fibroblast and myofibroblast content. Therefore, we tested the concept that NE could promote myofibroblast differentiation. NE treatment facilitated wound closure in a simple scratch assay, using the same cell proliferative concentrations as above (Figure 4A-B). To more clearly demonstrate the contractile phenotype of NE exposed fibroblasts, we performed a collagen gel contractility assay. Once again, cell proliferative concentrations of NE enhanced fibroblast contractility, resulting in statistically significant changes in gel area (Figure 4C-D). Furthermore, modest concentrations of NE reduced gel area to a similar extent as witnessed with TGF-ß, serving as a positive control.

The major biochemical feature of myofibroblasts is αSMA production. As suggested from the results of the scratch and contractility assays, exposure of fibroblasts to NE induces the expression of αSMA by western blot (Figure 4F). The contractile nature of NE treated fibroblasts is best illustrated by confocal microscopy. The αSMA expressing stress fibers identified in NE treated fibroblasts were not evident in the control fibroblasts (Figure 4E).

NE-induced αSMA production is associated with significant increases in pSMAD3 production. This is not surprising, given that this is the most commonly reported mechanism for

αSMA gene transcription. Most interestingly, NE-induced αSMA production appears to be independent of TGF-ß signaling, as concomitant administration of SB431542, a TGF-ß receptor antagonist, failed to abrogate αSMA production in the setting of NE exposure, although it did eliminate αSMA production in the absence of NE (Figure 4F). We suspected that the increased generation of pAkt induced by NE treatment might be related to the observed changes in αSMA production. However, this did not turn out to be the case, as co-administration of LY294002 (PI3K inhibitor) failed to abrogate αSMA production, though it did eliminate pAkt production (Figure 4F). Also of note, IRS-1 apparently does not play a significant role in NE-induced myofibroblast differentiation, as IRS-1-deficient fibroblasts fail to upregulate αSMA production (not shown).

Figure 4

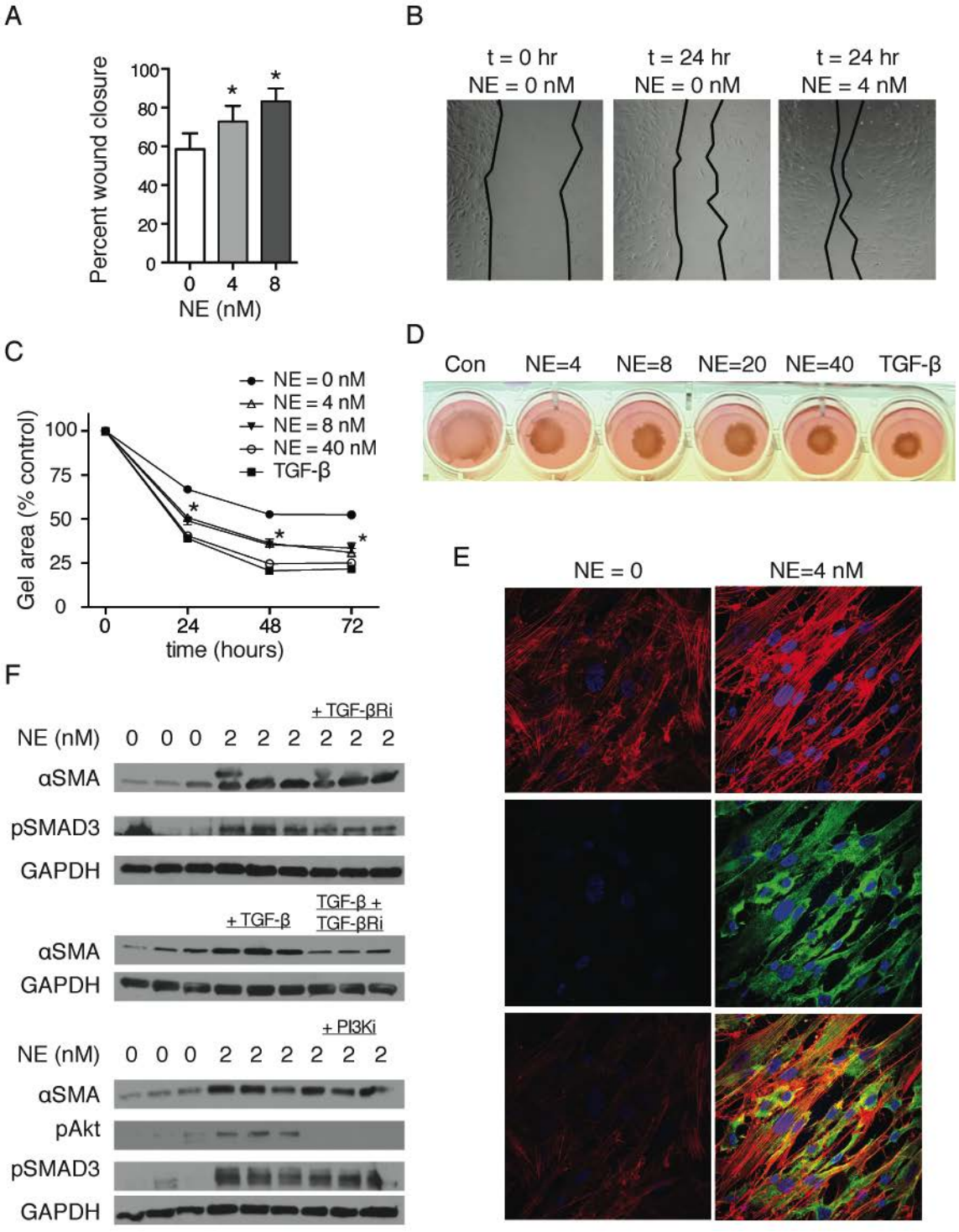

Figure 17. NE promotes myofibroblast differentiation: (A-B) Wound healing assay for LL47 fibroblasts plated on scratched tissue culture plastic and treated with NE (0, 4, or 8nM) for one

hr. Data are mean value of % wound closure +/- SEM from a representative experiment in triplicate. (C-D) LL47 fibroblasts were embedded in a type I collagen matrix in 24-well plates. Gels were treated with NE (0-40nM) or TGF-ß for one hr. Data are mean value of gel area +/- SEM (N=8 wells per condition) pooled from two independent experiments. All NE and TGF-ß treatment groups are significantly different than untreated wells at each time point as indicated by the three asterisks. (E) LL47 fibroblasts were incubated with 4nM NE for one hr. Cells were stained for αSMA (green) and counterstained with phalloidin (red) and DAPI (blue). Magnification = 600X. (F) Representative Western blots for αSMA, pAkt, pSMAD3, and GAPDH for NE treated fibroblasts in the presence and absence of the TGF-ß inhibitor SB431542 (10μM, upper panels) and the PI3K inhibitor, LY294002 (50μM, lower panels). TGF-ß treated fibroblasts in the presence and absence of the TGF-ß inhibitor SB431542 are also depicted (middle panels). One-way ANOVA was performed to determine statistical significance between groups. *P<0.05.

C.4.5 ONO-5046 inhibits asbestos induced lung fibrosis in mice

To demonstrate the therapeutic relevance of NE activity in the setting of lung fibrosis, we repeated our asbestos induced lung injury studies using a synthetic small molecule inhibitor of elastase. ONO-5046 has previously been shown to be an effective antagonist of both mouse and human NE. We previously used this agent to demonstrate that it could reduce tumor growth in the Lox-Stop-Lox (LSL)-K-ras mouse model of lung adenocarcinoma. Here, we administered a large cohort of mice (N=8 each group) either daily IP injections of ONO-5046 (100mg/kg) or vehicle control. After two weeks, the lungs were subjected to histological analysis and

hydroxyproline assay. As depicted in Figure 5, ONO-5046 significantly reduced lung fibrosis, as evidenced by a reduction in hydroxyproline content and fibrosis index.

Figure 5

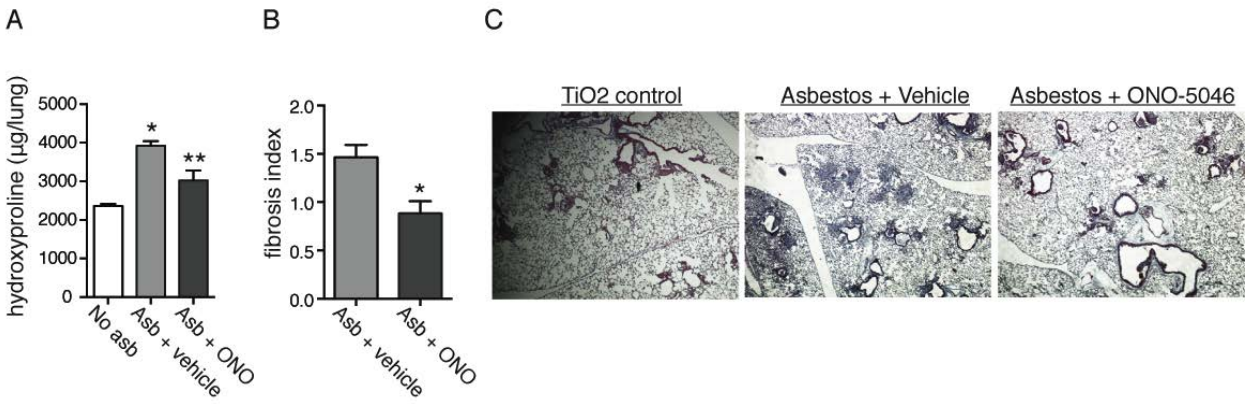

Figure 18. ONO-5046 reduces asbestos induced lung injury: (A) Hydroxyproline assay for asbestos recipient C57BL/6 mice treated with ONO-5046 (100 mg/kg) or vehicle control IP daily for 14 days. N=8 mice per group. This study was performed twice with one representative experiment shown. Data are mean value +/- SEM. *P<0.05. (B) A fibrosis index was generated according to the criteria described in Materials and Methods. N-14 mice per group, pooled from two independent experiments. (C) Representative H&E images (10X) of the lungs from ONO-5046 treated and vehicle control mice. Two-tailed Student's t-test was used to compare differences between groups. *P<0.05.

C.5 DISCUSSION

Fibroproliferative disorders of the lung are surprisingly common and essentially untreatable diseases that result in substantial morbidity and mortality. Although the quantity and quality of lung fibroblasts have long been known to drive lung fibrosis, the origin of these cells remains unclear. Among the possibilities are: local proliferation of lung fibroblasts, recruitment of bone marrow derived cells (fibrocytes) to the lung, and the constellation of myofibroblast differentiation covered under epithelial-mesenchymal transition (EMT) [205]. With respect to proliferation of lung fibroblasts, the factors that drive their proliferation both in vitro and in vivo remain unclear. Since IPF subjects also display robust neutrophil infiltration within their lungs, we hypothesized that NE may contribute to the proliferation of lung fibroblasts in the setting of IPF disease pathogenesis.

Using *NE*$^{-/-}$ mice, we were able to show that the increase in lung fibroblast content induced by the administration of intratracheal asbestos is largely dependent upon elastase. Additionally, the differentiation of a subset of these fibroblasts into myofibroblasts is promoted by the presence of NE. As one would suspect, the quantity of fibroblasts and myofibroblasts correlates with the severity of lung fibrosis, as demonstrated here using trichrome staining and hydroxyproline assay. We used in vitro assays to more directly show that NE can induce fibroblast proliferation and myofibroblast differentiation. Mechanistically, NE drives fibroblast proliferation by targeting IRS-1, which results in PI3K hyperactivity, as has been shown in cancer cells. The ability of NE to promote myofibroblast differentiation does not appear to involve the observed increase in PI3K activity, as the use of a PI3K inhibitor failed to abolish

αSMA production. Similarly, the ability of NE to promote myofibroblast differentiation does not involve IRS-1, as IRS-1 silencing, in and of itself, is not sufficient for αSMA induction.

NE was first reported to promote cellular proliferation in psoriasis, a benign neoplastic disorder of keratinocytes [206]. More recently, we have reported that NE promotes cellular proliferation of lung cancer cells, both in vitro and in vivo [88]. To accomplish this, NE enters tumor endosomes in lung cancer cells via classic clathrin pit mediated endocytosis and targets intracellular substrates [200]. The ability of NE to enter cancer cells while inducing their proliferation has been replicated in other cell types, most notably in breast cancer cells [199]. The NE-IRS-1 axis, described here, has emerged as a key pathophysiologic mechanism in a variety of disease states. In addition to our findings with respect to lung cancer and lung fibrosis, Talukdar and colleagues reported NE-mediated loss of IRS-1 protein in hepatocytes [207]. During a study of glucose intolerance in mice, they showed the complete loss of IRS-1 from hepatocytes in mice fed a high fat diet. Interestingly, high fat diet was associated with increased neutrophilic inflammation within the liver. When the experiment was repeated using $NE^{-/-}$ mice, there was no decrease in hepatocyte IRS-1 content, despite equal amounts of neutrophil influx.

IRS-1 is a signaling adaptor protein best known for its canonical signaling downstream from the insulin receptor (IR) and insulin-like growth factor receptor (IGF-1R), where it mediates glucose metabolism [45]. However, IRS-1 adapts signals for numerous pathways, including PI3K, mitogen activated protein kinase (MAPK), and various cytokine receptors [47]. The impact of IRS-1 loss on intracellular signaling is dependent upon the cell of origin and disease microenvironment. As such, both increases and decreases in PI3K output (pAkt production) have been reported in the setting of IRS-1 deficiency [208]. Determining the detailed

mechanisms by which IRS-1 regulates intracellular signaling cascades is an ongoing area of investigation in our laboratory.

The exact means by which NE promotes myofibroblast differentiation also remains an area of active investigation within our group. The ability of NE to induce αSMA production occurs in a SMAD dependent but TGF-ß independent fashion. Both SMAD and TGF-ß-independent mechanisms promoting myofibroblast differentiation have been reported. SMAD independent generation of the myofibroblast phenotype typically involves PI3K signaling and the participation of a downstream effector molecule, p21 activated kinase-2 [209]. We had initially suspected that PI3K was operative in our cells, given the observed increases in pAkt, but were unable to demonstrate dependence on PI3K using a synthetic antagonist, LY294002. The effects of NE on fibroblasts are likely pleiotropic, and PI3K activity may be important in the migratory phenotype (via Rac1) but not the contractile phenotype [210]. Another identifiable effect of NE is the induction of F-actin. Additional studies are underway in our laboratory to examine the roles of recently described myocardin-related transcription factor (MRTF) and serum-response factor (SRF)-mediated myofibroblast differentiation program, which is potentially TGF-ß independent, and thus represents an attractive potential mechanism for our observed phenotype [211]. TGF-ß independent αSMA production has also been reported, most notably for found in inflammatory zone-1 (Fizz-1). Fizz-1 has specifically been shown to contribute to lung fibrosis and can induce αSMA completely independently of TGF-ß [212]. The mechanism by which this occurs, as with the case for NE here, remains unknown.

Treatment options are scarce for IPF subjects. Traditional immune suppressive therapies, such as systemic corticosteroids and azathioprine, alone or in combination with N-acetylcysteine, have failed to demonstrate any clear benefit [213]. The results presented here carry therapeutic

relevance. Inhibition of NE, using a synthetic antagonist, largely abrogated the development of asbestos induced lung fibrosis. This approach highlights the possibility of using non-traditional approaches to limit fibroblast growth and function, which holds promise as a potential therapeutic strategy for lung fibrosis patients.

C.6 ACKNOWLEDGMENTS

This work was supported by: American Lung Association Senior Fellowship Research Award (ADG), NIH/NHLBI R01HL108979 (AMH), and the Sidney Kimmel Foundation (AMH).

BIBLIOGRAPHY

1. Jemal, A., et al., *Global cancer statistics.* CA Cancer J Clin.

2. Jemal, A., et al., *Cancer statistics, 2010.* CA Cancer J Clin, 2010. **60**(5): p. 277-300.

3. Youlden, D.R., S.M. Cramb, and P.D. Baade, *The International Epidemiology of Lung Cancer: geographical distribution and secular trends.* J Thorac Oncol, 2008. **3**(8): p. 819-31.

4. Witschi, H., *A short history of lung cancer.* Toxicol Sci, 2001. **64**(1): p. 4-6.

5. Warren, G.W., et al., *The 2014 Surgeon General's report: "The health consequences of smoking--50 years of progress": a paradigm shift in cancer care.* Cancer, 2014. **120**(13): p. 1914-6.

6. Ferlay, J., et al., *Estimates of worldwide burden of cancer in 2008: GLOBOCAN 2008.* Int J Cancer, 2010. **127**(12): p. 2893-917.

7. Couraud, S., et al., *Lung cancer in never smokers--a review.* Eur J Cancer, 2012. **48**(9): p. 1299-311.

8. Herbst, R.S., J.V. Heymach, and S.M. Lippman, *Lung cancer.* N Engl J Med, 2008. **359**(13): p. 1367-80.

9. Cagle, P.T., et al., *Revolution in lung cancer: new challenges for the surgical pathologist.* Arch Pathol Lab Med. **135**(1): p. 110-6.

10. Devarakonda, S., D. Morgensztern, and R. Govindan, *Genomic alterations in lung adenocarcinoma.* Lancet Oncol, 2015. **16**(7): p. e342-51.

11. Skoulidis, F., et al., *Co-occurring Genomic Alterations Define Major Subsets of KRAS-Mutant Lung Adenocarcinoma with Distinct Biology, Immune Profiles, and Therapeutic Vulnerabilities.* Cancer Discov, 2015. **5**(8): p. 860-77.

12. Russo, A., et al., *A decade of EGFR inhibition in EGFR-mutated non small cell lung cancer (NSCLC): Old successes and future perspectives.* Oncotarget, 2015. **6**(29): p. 26814-25.

13. Brosseau, S., et al., *[Resistances to targeted therapies and strategy for following therapeutic lines in metastatic NSCLC]*. Bull Cancer, 2015. **102**(6 Suppl 1): p. S27-33.

14. Landi, L. and F. Cappuzzo, *Experience with erlotinib in the treatment of non-small cell lung cancer.* Ther Adv Respir Dis, 2015. **9**(4): p. 146-63.

15. Waller, A., *LVIII. Microscopic observation on the perforation of the capillaries by the corpuscles of the blood, and on the origin of mucus and pus-globules.* The London, Edinburgh, and Dublin Philosophical Magazine and Journal of Science, 1846. **29**(195): p. 397-405.

16. Metchnikoff, E., *Lectures on the Comparative Pathology of Inflammation, London, Keegan, Paul, Trench, Trubner, 1893*, 1968, Reprinted by Dover, New York.

17. Silverstein, A.M., *Cellular versus humoral immunity: Determinants and consequences of an epic 19th century battle.* Cellular Immunology, 1979. **48**(1): p. 208-221.

18. Metchnikoff, E., *Immunity in infective diseases*1905: University Press.

19. Balkwill, F. and A. Mantovani, *Inflammation and cancer: back to Virchow?* Lancet, 2001. **357**(9255): p. 539-45.

20. Heidland, A., et al., *The contribution of Rudolf Virchow to the concept of inflammation: what is still of importance?* J Nephrol, 2006. **19 Suppl 10**: p. S102-9.

21. Dunn, G.P., et al., *Cancer immunoediting: from immunosurveillance to tumor escape.* Nat Immunol, 2002. **3**(11): p. 991-8.

22. Burnet, F.M., *The concept of immunological surveillance.* Prog Exp Tumor Res, 1970. **13**: p. 1-27.

23. Burnet, M., *Immunological Factors in the Process of Carcinogenesis.* Br Med Bull, 1964. **20**: p. 154-8.

24. Philip, M., D.A. Rowley, and H. Schreiber, *Inflammation as a tumor promoter in cancer induction.* Semin Cancer Biol, 2004. **14**(6): p. 433-9.

25. Coussens, L.M., L. Zitvogel, and A.K. Palucka, *Neutralizing tumor-promoting chronic inflammation: a magic bullet?* Science, 2013. **339**(6117): p. 286-91.

26. Lu, H., W. Ouyang, and C. Huang, *Inflammation, a key event in cancer development.* Mol Cancer Res, 2006. **4**(4): p. 221-33.

27. Hanahan, D. and R.A. Weinberg, *Hallmarks of cancer: the next generation.* Cell, 2011. **144**(5): p. 646-74.

28. Coussens, L.M. and Z. Werb, *Inflammation and cancer.* Nature, 2002. **420**(6917): p. 860-7.

29. Smith, J.A., *Neutrophils, host defense, and inflammation: a double-edged sword.* J Leukoc Biol, 1994. **56**(6): p. 672-86.

30. Gregory, A.D. and A.M. Houghton, *Tumor-associated neutrophils: new targets for cancer therapy.* Cancer Res, 2011. **71**(7): p. 2411-6.

31. Kruger, P., et al., *Neutrophils: Between host defence, immune modulation, and tissue injury.* PLoS Pathog, 2015. **11**(3): p. e1004651.

32. Cools-Lartigue, J., et al., *Neutrophil extracellular traps in cancer progression.* Cell Mol Life Sci, 2014. **71**(21): p. 4179-94.

33. Donskov, F., *Immunomonitoring and prognostic relevance of neutrophils in clinical trials.* Semin Cancer Biol, 2013. **23**(3): p. 200-7.

34. Polonsky, K.S., *The past 200 years in diabetes.* N Engl J Med, 2012. **367**(14): p. 1332-40.

35. Banting, F.G., W.R. Campbell, and A.A. Fletcher, *Further Clinical Experience with Insulin (Pancreatic Extracts) in the Treatment of Diabetes Mellitus.* Br Med J, 1923. **1**(3236): p. 8-12.

36. Banting, F.G., et al., *Pancreatic Extracts in the Treatment of Diabetes Mellitus.* Can Med Assoc J, 1922. **12**(3): p. 141-6.

37. Lee, J. and P.F. Pilch, *The insulin receptor: structure, function, and signaling.* Am J Physiol, 1994. **266**(2 Pt 1): p. C319-34.

38. Rosenfeld, L., *Insulin: discovery and controversy.* Clin Chem, 2002. **48**(12): p. 2270-88.

39. De Meyts, P., *Insulin and its receptor: structure, function and evolution.* Bioessays, 2004. **26**(12): p. 1351-62.

40. White, M.F., R. Maron, and C.R. Kahn, *Insulin rapidly stimulates tyrosine phosphorylation of a Mr-185,000 protein in intact cells.* Nature, 1985. **318**(6042): p. 183-6.

41. Sun, X.J., et al., *Structure of the insulin receptor substrate IRS-1 defines a unique signal transduction protein.* Nature, 1991. **352**(6330): p. 73-7.

42. Araki, E., et al., *Alternative pathway of insulin signalling in mice with targeted disruption of the IRS-1 gene.* Nature, 1994. **372**(6502): p. 186-90.

43. Sun, X.J., et al., *Role of IRS-2 in insulin and cytokine signalling.* Nature, 1995. **377**(6545): p. 173-7.

44. Withers, D.J., et al., *Disruption of IRS-2 causes type 2 diabetes in mice.* Nature, 1998. **391**(6670): p. 900-4.

45. White, M.F., *IRS proteins and the common path to diabetes.* Am J Physiol Endocrinol Metab, 2002. **283**(3): p. E413-22.

46. Yamauchi, T., et al., *Growth hormone and prolactin stimulate tyrosine phosphorylation of insulin receptor substrate-1, -2, and -3, their association with p85 phosphatidylinositol 3-kinase (PI3-kinase), and concomitantly PI3-kinase activation via JAK2 kinase.* J Biol Chem, 1998. **273**(25): p. 15719-26.

47. White, M.F. and L. Yenush, *The IRS-signaling system: a network of docking proteins that mediate insulin and cytokine action.* Curr Top Microbiol Immunol, 1998. **228**: p. 179-208.

48. Dearth, R.K., et al., *Oncogenic transformation by the signaling adaptor proteins insulin receptor substrate (IRS)-1 and IRS-2.* Cell Cycle, 2007. **6**(6): p. 705-13.

49. Smith-Hall, J., et al., *The 60 kDa insulin receptor substrate functions like an IRS protein (pp60IRS3) in adipose cells.* Biochemistry, 1997. **36**(27): p. 8304-10.

50. Fantin, V.R., et al., *Characterization of insulin receptor substrate 4 in human embryonic kidney 293 cells.* J Biol Chem, 1998. **273**(17): p. 10726-32.

51. Cai, D., et al., *Two new substrates in insulin signaling, IRS5/DOK4 and IRS6/DOK5.* J Biol Chem, 2003. **278**(28): p. 25323-30.

52. Yenush, L., et al., *The pleckstrin homology and phosphotyrosine binding domains of insulin receptor substrate 1 mediate inhibition of apoptosis by insulin.* Mol Cell Biol, 1998. **18**(11): p. 6784-94.

53. Taniguchi, C.M., B. Emanuelli, and C.R. Kahn, *Critical nodes in signalling pathways: insights into insulin action.* Nat Rev Mol Cell Biol, 2006. **7**(2): p. 85-96.

54. Fruman, D.A., R.E. Meyers, and L.C. Cantley, *Phosphoinositide kinases.* Annu Rev Biochem, 1998. **67**: p. 481-507.

55. Yu, J., et al., *Regulation of the p85/p110 phosphatidylinositol 3'-kinase: stabilization and inhibition of the p110alpha catalytic subunit by the p85 regulatory subunit.* Mol Cell Biol, 1998. **18**(3): p. 1379-87.

56. Backer, J.M., et al., *Phosphatidylinositol 3'-kinase is activated by association with IRS-1 during insulin stimulation.* EMBO J, 1992. **11**(9): p. 3469-79.

57. Datta, S.R., A. Brunet, and M.E. Greenberg, *Cellular survival: a play in three Akts.* Genes Dev, 1999. **13**(22): p. 2905-27.

58. Fresno Vara, J.A., et al., *PI3K/Akt signalling pathway and cancer.* Cancer Treat Rev, 2004. **30**(2): p. 193-204.

59. Baldin, V., et al., *Cyclin D1 is a nuclear protein required for cell cycle progression in G1.* Genes Dev, 1993. **7**(5): p. 812-21.

60. Diehl, J.A., et al., *Glycogen synthase kinase-3beta regulates cyclin D1 proteolysis and subcellular localization.* Genes Dev, 1998. **12**(22): p. 3499-511.

61. Graff, J.R., et al., *Increased AKT activity contributes to prostate cancer progression by dramatically accelerating prostate tumor growth and diminishing p27Kip1 expression.* J Biol Chem, 2000. **275**(32): p. 24500-5.

62. Stambolic, V., et al., *Negative regulation of PKB/Akt-dependent cell survival by the tumor suppressor PTEN.* Cell, 1998. **95**(1): p. 29-39.

63. Li, J., et al., *PTEN, a putative protein tyrosine phosphatase gene mutated in human brain, breast, and prostate cancer.* Science, 1997. **275**(5308): p. 1943-7.

64. Hu, T.H., et al., *Expression and prognostic role of tumor suppressor gene PTEN/MMAC1/TEP1 in hepatocellular carcinoma.* Cancer, 2003. **97**(8): p. 1929-40.

65. Alimov, A., et al., *Somatic mutation and homozygous deletion of PTEN/MMAC1 gene of 10q23 in renal cell carcinoma.* Anticancer Res, 1999. **19**(5B): p. 3841-6.

66. Wang, S.I., et al., *Somatic mutations of PTEN in glioblastoma multiforme.* Cancer Res, 1997. **57**(19): p. 4183-6.

67. Celebi, J.T., et al., *Identification of PTEN mutations in metastatic melanoma specimens.* J Med Genet, 2000. **37**(9): p. 653-7.

68. Forgacs, E., et al., *Mutation analysis of the PTEN/MMAC1 gene in lung cancer.* Oncogene, 1998. **17**(12): p. 1557-65.

69. Cully, M., et al., *Beyond PTEN mutations: the PI3K pathway as an integrator of multiple inputs during tumorigenesis.* Nat Rev Cancer, 2006. **6**(3): p. 184-92.

70. Rodriguez-Viciana, P., et al., *Phosphatidylinositol-3-OH kinase as a direct target of Ras.* Nature, 1994. **370**(6490): p. 527-32.

71. Engelman, J.A., et al., *Effective use of PI3K and MEK inhibitors to treat mutant Kras G12D and PIK3CA H1047R murine lung cancers.* Nat Med, 2008. **14**(12): p. 1351-6.

72. Nave, B.T., et al., *Compartment-specific regulation of phosphoinositide 3-kinase by platelet-derived growth factor and insulin in 3T3-L1 adipocytes.* Biochem J, 1996. **318 (Pt 1)**: p. 55-60.

73. Ceresa, B.P. and J.E. Pessin, *Insulin regulation of the Ras activation/inactivation cycle.* Mol Cell Biochem, 1998. **182**(1-2): p. 23-9.

74. D'Ambrosio, C., et al., *Transforming potential of the insulin receptor substrate 1.* Cell Growth Differ, 1995. **6**(5): p. 557-62.

75. Tanaka, S., T. Ito, and J.R. Wands, *Neoplastic transformation induced by insulin receptor substrate-1 overexpression requires an interaction with both Grb2 and Syp signaling molecules.* J Biol Chem, 1996. **271**(24): p. 14610-6.

76. Ito, T., Y. Sasaki, and J.R. Wands, *Overexpression of human insulin receptor substrate 1 induces cellular transformation with activation of mitogen-activated protein kinases.* Mol Cell Biol, 1996. **16**(3): p. 943-51.

77. DeAngelis, T., et al., *Transformation by the simian virus 40 T antigen is regulated by IGF-I receptor and IRS-1 signaling.* Oncogene, 2006. **25**(1): p. 32-42.

78. Boissan, M., et al., *Overexpression of insulin receptor substrate-2 in human and murine hepatocellular carcinoma.* Am J Pathol, 2005. **167**(3): p. 869-77.

79. Nehrbass, D., F. Klimek, and P. Bannasch, *Overexpression of insulin receptor substrate-1 emerges early in hepatocarcinogenesis and elicits preneoplastic hepatic glycogenosis.* Am J Pathol, 1998. **152**(2): p. 341-5.

80. Tanaka, S. and J.R. Wands, *Insulin receptor substrate 1 overexpression in human hepatocellular carcinoma cells prevents transforming growth factor beta1-induced apoptosis.* Cancer Res, 1996. **56**(15): p. 3391-4.

81. Tanaka, S. and J.R. Wands, *A carboxy-terminal truncated insulin receptor substrate-1 dominant negative protein reverses the human hepatocellular carcinoma malignant phenotype.* J Clin Invest, 1996. **98**(9): p. 2100-8.

82. Nolan, M.K., et al., *Differential roles of IRS-1 and SHC signaling pathways in breast cancer cells.* Int J Cancer, 1997. **72**(5): p. 828-34.

83. Surmacz, E. and J.L. Burgaud, *Overexpression of insulin receptor substrate 1 (IRS-1) in the human breast cancer cell line MCF-7 induces loss of estrogen requirements for growth and transformation.* Clin Cancer Res, 1995. **1**(11): p. 1429-36.

84. Dearth, R.K., et al., *Mammary tumorigenesis and metastasis caused by overexpression of insulin receptor substrate 1 (IRS-1) or IRS-2.* Mol Cell Biol, 2006. **26**(24): p. 9302-14.

85. Rosner, A., et al., *Pathway pathology: histological differences between ErbB/Ras and Wnt pathway transgenic mammary tumors.* Am J Pathol, 2002. **161**(3): p. 1087-97.

86. Ma, Z., et al., *Suppression of insulin receptor substrate 1 (IRS-1) promotes mammary tumor metastasis.* Mol Cell Biol, 2006. **26**(24): p. 9338-51.

87. Rocha, R.L., et al., *Insulin-like growth factor binding protein-3 and insulin receptor substrate-1 in breast cancer: correlation with clinical parameters and disease-free survival.* Clin Cancer Res, 1997. **3**(1): p. 103-9.

88. Houghton, A.M., et al., *Neutrophil elastase-mediated degradation of IRS-1 accelerates lung tumor growth.* Nat Med, 2010. **16**(2): p. 219-23.

89. Jackson, E.L., et al., *Analysis of lung tumor initiation and progression using conditional expression of oncogenic K-ras.* Genes Dev, 2001. **15**(24): p. 3243-8.

90. Antoniades, H.N., et al., *Malignant epithelial cells in primary human lung carcinomas coexpress in vivo platelet-derived growth factor (PDGF) and PDGF receptor mRNAs and their protein products.* Proc Natl Acad Sci U S A, 1992. **89**(9): p. 3942-6.

91. Dong, X.C., et al., *Inactivation of hepatic Foxo1 by insulin signaling is required for adaptive nutrient homeostasis and endocrine growth regulation.* Cell Metab, 2008. **8**(1): p. 65-76.

92. Hardy, S., et al., *Construction of adenovirus vectors through Cre-lox recombination.* J Virol, 1997. **71**(3): p. 1842-9.

93. Roxburgh, C.S. and D.C. McMillan, *Therapeutics targeting innate immune/inflammatory responses through the interleukin-6/JAK/STAT signal transduction pathway in patients with cancer.* Transl Res, 2015.

94. Kiu, H. and S.E. Nicholson, *Biology and significance of the JAK/STAT signalling pathways.* Growth Factors, 2012. **30**(2): p. 88-106.

95. Stark, G.R. and J.E. Darnell, Jr., *The JAK-STAT pathway at twenty.* Immunity, 2012. **36**(4): p. 503-14.

96. Schindler, C., et al., *Interferon-dependent tyrosine phosphorylation of a latent cytoplasmic transcription factor.* Science, 1992. **257**(5071): p. 809-13.

97. Sadowski, H.B., et al., *A common nuclear signal transduction pathway activated by growth factor and cytokine receptors.* Science, 1993. **261**(5129): p. 1739-44.

98. Zhong, Z., Z. Wen, and J.E. Darnell, Jr., *Stat3: a STAT family member activated by tyrosine phosphorylation in response to epidermal growth factor and interleukin-6.* Science, 1994. **264**(5155): p. 95-8.

99. Quelle, F.W., et al., *Cloning of murine Stat6 and human Stat6, Stat proteins that are tyrosine phosphorylated in responses to IL-4 and IL-3 but are not required for mitogenesis.* Mol Cell Biol, 1995. **15**(6): p. 3336-43.

100. Azam, M., et al., *Interleukin-3 signals through multiple isoforms of Stat5.* EMBO J, 1995. **14**(7): p. 1402-11.

101. Wilks, A.F., et al., *Two novel protein-tyrosine kinases, each with a second phosphotransferase-related catalytic domain, define a new class of protein kinase.* Mol Cell Biol, 1991. **11**(4): p. 2057-65.

102. Harpur, A.G., et al., *JAK2, a third member of the JAK family of protein tyrosine kinases.* Oncogene, 1992. **7**(7): p. 1347-53.

103. O'Shea, J.J. and R. Plenge, *JAK and STAT signaling molecules in immunoregulation and immune-mediated disease.* Immunity, 2012. **36**(4): p. 542-50.

104. Bromberg, J., *Stat proteins and oncogenesis.* J Clin Invest, 2002. **109**(9): p. 1139-42.

105. Levy, D.E. and J.E. Darnell, Jr., *Stats: transcriptional control and biological impact.* Nat Rev Mol Cell Biol, 2002. **3**(9): p. 651-62.

106. Rane, S.G. and E.P. Reddy, *Janus kinases: components of multiple signaling pathways.* Oncogene, 2000. **19**(49): p. 5662-79.

107. Murray, P.J., *The JAK-STAT signaling pathway: input and output integration.* J Immunol, 2007. **178**(5): p. 2623-9.

108. Liu, F., et al., *Genetic polymorphisms and plasma levels of interleukin-22 contribute to the development of nonsmall cell lung cancer.* DNA Cell Biol, 2014. **33**(10): p. 705-14.

109. Sabat, R., W. Ouyang, and K. Wolk, *Therapeutic opportunities of the IL-22-IL-22R1 system.* Nat Rev Drug Discov, 2013. **13**(1): p. 21-38.

110. Catlett-Falcone, R., W.S. Dalton, and R. Jove, *STAT proteins as novel targets for cancer therapy. Signal transducer an activator of transcription.* Curr Opin Oncol, 1999. **11**(6): p. 490-6.

111. Xu, Y.H. and S. Lu, *A meta-analysis of STAT3 and phospho-STAT3 expression and survival of patients with non-small-cell lung cancer.* Eur J Surg Oncol, 2014. **40**(3): p. 311-7.

112. Mukohara, T., et al., *Expression of epidermal growth factor receptor (EGFR) and downstream-activated peptides in surgically excised non-small-cell lung cancer (NSCLC).* Lung Cancer, 2003. **41**(2): p. 123-30.

113. Gao, S.P., et al., *Mutations in the EGFR kinase domain mediate STAT3 activation via IL-6 production in human lung adenocarcinomas.* J Clin Invest, 2007. **117**(12): p. 3846-56.

114. Looyenga, B.D., et al., *STAT3 is activated by JAK2 independent of key oncogenic driver mutations in non-small cell lung carcinoma.* PLoS One, 2012. **7**(2): p. e30820.

115. Rodenhuis, S. and R.J. Slebos, *The ras oncogenes in human lung cancer.* Am Rev Respir Dis, 1990. **142**(6 Pt 2): p. S27-30.

116. Harvey, J.J., *Replication of murine sarcoma virus-Harvey (MSV-H) in tissue cultures of virus-induced sarcomas.* J Gen Virol, 1968. **3**(3): p. 327-36.

117. Kirsten, W.H. and L.A. Mayer, *Morphologic responses to a murine erythroblastosis virus.* J Natl Cancer Inst, 1967. **39**(2): p. 311-35.

118. Scolnick, E.M., et al., *Studies on the nucleic acid sequences of Kirsten sarcoma virus: a model for formation of a mammalian RNA-containing sarcoma virus.* J Virol, 1973. **12**(3): p. 458-63.

119. Scolnick, E.M. and W.P. Parks, *Harvey sarcoma virus: a second murine type C sarcoma virus with rat genetic information.* J Virol, 1974. **13**(6): p. 1211-9.

120. Cox, A.D. and C.J. Der, *Ras history: The saga continues.* Small GTPases, 2010. **1**(1): p. 2-27.

121. Campbell, S.L., et al., *Increasing complexity of Ras signaling.* Oncogene, 1998. **17**(11 Reviews): p. 1395-413.

122. Koera, K., et al., *K-ras is essential for the development of the mouse embryo.* Oncogene, 1997. **15**(10): p. 1151-9.

123. Ebi, H., et al., *Not just gRASping at flaws: finding vulnerabilities to develop novel therapies for treating KRAS mutant cancers.* Cancer Sci, 2014. **105**(5): p. 499-505.

124. Fang, B., *RAS signaling and anti-RAS therapy: lessons learned from genetically engineered mouse models, human cancer cells, and patient-related studies.* Acta Biochim Biophys Sin (Shanghai), 2015.

125. Scheffzek, K., et al., *The Ras-RasGAP complex: structural basis for GTPase activation and its loss in oncogenic Ras mutants.* Science, 1997. **277**(5324): p. 333-8.

126. Ihle, N.T., et al., *Effect of KRAS oncogene substitutions on protein behavior: implications for signaling and clinical outcome.* J Natl Cancer Inst, 2012. **104**(3): p. 228-39.

127. O'Hagan, R.C. and J. Heyer, *KRAS Mouse Models: Modeling Cancer Harboring KRAS Mutations.* Genes Cancer, 2011. **2**(3): p. 335-43.

128. Johnson, L., et al., *K-ras is an essential gene in the mouse with partial functional overlap with N-ras.* Genes Dev, 1997. **11**(19): p. 2468-81.

129. Johnson, L., et al., *Somatic activation of the K-ras oncogene causes early onset lung cancer in mice.* Nature, 2001. **410**(6832): p. 1111-6.

130. Li, J., et al., *Idiopathic pulmonary fibrosis will increase the risk of lung cancer.* Chin Med J (Engl), 2014. **127**(17): p. 3142-9.

131. Tzouvelekis, A., F. Bonella, and P. Spagnolo, *Update on therapeutic management of idiopathic pulmonary fibrosis.* Ther Clin Risk Manag, 2015. **11**: p. 359-70.

132. Raghu, G., et al., *Incidence and prevalence of idiopathic pulmonary fibrosis.* Am J Respir Crit Care Med, 2006. **174**(7): p. 810-6.

133. Gross, T.J. and G.W. Hunninghake, *Idiopathic pulmonary fibrosis.* N Engl J Med, 2001. **345**(7): p. 517-25.

134. Obayashi, Y., et al., *The role of neutrophils in the pathogenesis of idiopathic pulmonary fibrosis.* Chest, 1997. **112**(5): p. 1338-43.

135. Bagnato, G. and S. Harari, *Cellular interactions in the pathogenesis of interstitial lung diseases.* Eur Respir Rev, 2015. **24**(135): p. 102-14.

136. Darby, I.A., et al., *Fibroblasts and myofibroblasts in wound healing.* Clin Cosmet Investig Dermatol, 2014. **7**: p. 301-11.

137. Myers, M.G., Jr., et al., *The pleckstrin homology domain in insulin receptor substrate-1 sensitizes insulin signaling.* J Biol Chem, 1995. **270**(20): p. 11715-8.

138. Eck, M.J., et al., *Structure of the IRS-1 PTB domain bound to the juxtamembrane region of the insulin receptor.* Cell, 1996. **85**(5): p. 695-705.

139. Yenush, L., et al., *The pleckstrin homology domain is the principal link between the insulin receptor and IRS-1.* J Biol Chem, 1996. **271**(39): p. 24300-6.

140. Yu, H., D. Pardoll, and R. Jove, *STATs in cancer inflammation and immunity: a leading role for STAT3.* Nat Rev Cancer, 2009. **9**(11): p. 798-809.

141. Johnston, J.A., et al., *Interleukins 2, 4, 7, and 15 stimulate tyrosine phosphorylation of insulin receptor substrates 1 and 2 in T cells. Potential role of JAK kinases.* J Biol Chem, 1995. **270**(48): p. 28527-30.

142. Yin, T., et al., *Interleukin-9 induces tyrosine phosphorylation of insulin receptor substrate-1 via JAK tyrosine kinases.* J Biol Chem, 1995. **270**(35): p. 20497-502.

143. Houghton, A.M., et al., *Elastin fragments drive disease progression in a murine model of emphysema.* J Clin Invest, 2006. **116**(3): p. 753-9.

144. Siegfried, J.M., et al., *Evidence for autocrine actions of neuromedin B and gastrin-releasing peptide in non-small cell lung cancer.* Pulm Pharmacol Ther, 1999. **12**(5): p. 291-302.

145. Chang, S.H., et al., *T helper 17 cells play a critical pathogenic role in lung cancer.* Proc Natl Acad Sci U S A, 2014. **111**(15): p. 5664-9.

146. Weathington, N.M., et al., *Glycogen synthase kinase-3beta stabilizes the interleukin (IL)-22 receptor from proteasomal degradation in murine lung epithelia.* J Biol Chem, 2014. **289**(25): p. 17610-9.

147. Tsuji, Y., et al., *Subcellular localization of insulin receptor substrate family proteins associated with phosphatidylinositol 3-kinase activity and alterations in lipolysis in primary mouse adipocytes from IRS-1 null mice.* Diabetes, 2001. **50**(6): p. 1455-63.

148. Huang, Y.H., et al., *Th22 cell accumulation is associated with colorectal cancer development.* World J Gastroenterol, 2015. **21**(14): p. 4216-24.

149. Chang, Q., et al., *Constitutive activation of insulin receptor substrate 1 is a frequent event in human tumors: therapeutic implications.* Cancer Res, 2002. **62**(21): p. 6035-8.

150. Han, C.H., et al., *Clinical significance of insulin receptor substrate-I down-regulation in non-small cell lung cancer.* Oncol Rep, 2006. **16**(6): p. 1205-10.

151. Gregory, A.D., et al., *Neutrophil elastase promotes myofibroblast differentiation in lung fibrosis.* J Leukoc Biol, 2015. **98**(2): p. 143-52.

152. Brahmer, J.R. and D.M. Pardoll, *Immune checkpoint inhibitors: making immunotherapy a reality for the treatment of lung cancer.* Cancer Immunol Res, 2013. **1**(2): p. 85-91.

153. Bustamante Alvarez, J.G., et al., *Advances in immunotherapy for treatment of lung cancer.* Cancer Biol Med, 2015. **12**(3): p. 209-22.

154. Lim, C. and R. Savan, *The role of the IL-22/IL-22R1 axis in cancer.* Cytokine Growth Factor Rev, 2014. **25**(3): p. 257-71.

155. Cortes de Miguel, S., et al., *Granulocyte colony-stimulating factors as prophylaxis against febrile neutropenia.* Support Care Cancer, 2015. **23**(2): p. 547-59.

156. Kalluri, R. and M. Zeisberg, *Fibroblasts in cancer.* Nat Rev Cancer, 2006. **6**(5): p. 392-401.

157. Nakao, M., et al., *Prognostic significance of carbonic anhydrase IX expression by cancer-associated fibroblasts in lung adenocarcinoma.* Cancer, 2009. **115**(12): p. 2732-43.

158. Jemal, A., et al., *Cancer statistics, 2009.* CA Cancer J Clin, 2009. **59**(4): p. 225-49.

159. Karin, M., *Inflammation and cancer: the long reach of Ras.* Nat Med, 2005. **11**(1): p. 20-1.

160. Sparmann, A. and D. Bar-Sagi, *Ras-induced interleukin-8 expression plays a critical role in tumor growth and angiogenesis.* Cancer Cell, 2004. **6**(5): p. 447-58.

161. Haqqani, A.S., J.K. Sandhu, and H.C. Birnboim, *Expression of interleukin-8 promotes neutrophil infiltration and genetic instability in mutatect tumors.* Neoplasia, 2000. **2**(6): p. 561-8.

162. Nozawa, H., C. Chiu, and D. Hanahan, *Infiltrating neutrophils mediate the initial angiogenic switch in a mouse model of multistage carcinogenesis.* Proc Natl Acad Sci U S A, 2006. **103**(33): p. 12493-8.

163. Ji, H., et al., *K-ras activation generates an inflammatory response in lung tumors.* Oncogene, 2006. **25**(14): p. 2105-12.

164. Bellocq, A., et al., *Neutrophil alveolitis in bronchioloalveolar carcinoma: induction by tumor-derived interleukin-8 and relation to clinical outcome.* Am J Pathol, 1998. **152**(1): p. 83-92.

165. Foekens, J.A., et al., *The prognostic value of polymorphonuclear leukocyte elastase in patients with primary breast cancer.* Cancer Res, 2003. **63**(2): p. 337-41.

166. Lee, W.L. and G.P. Downey, *Leukocyte elastase: physiological functions and role in acute lung injury.* Am J Respir Crit Care Med, 2001. **164**(5): p. 896-904.

167. Belaaouaj, A., et al., *Mice lacking neutrophil elastase reveal impaired host defense against gram negative bacterial sepsis.* Nat Med, 1998. **4**(5): p. 615-8.

168. Weinrauch, Y., et al., *Neutrophil elastase targets virulence factors of enterobacteria.* Nature, 2002. **417**(6884): p. 91-4.

169. Lee, S., et al., *Processing of VEGF-A by matrix metalloproteinases regulates bioavailability and vascular patterning in tumors.* J Cell Biol, 2005. **169**(4): p. 681-91.

170. Wada, Y., et al., *Neutrophil elastase induces cell proliferation and migration by the release of TGF-alpha, PDGF and VEGF in esophageal cell lines.* Oncol Rep, 2007. **17**(1): p. 161-7.

171. Liou, T.G. and E.J. Campbell, *Quantum proteolysis resulting from release of single granules by human neutrophils: a novel, nonoxidative mechanism of extracellular proteolytic activity.* J Immunol, 1996. **157**(6): p. 2624-31.

172. Rubino, M., et al., *Selective membrane recruitment of EEA1 suggests a role in directional transport of clathrin-coated vesicles to early endosomes.* J Biol Chem, 2000. **275**(6): p. 3745-8.

173. Macia, E., et al., *Dynasore, a cell-permeable inhibitor of dynamin.* Dev Cell, 2006. **10**(6): p. 839-50.

174. Gual, P., Y. Le Marchand-Brustel, and J.F. Tanti, *Positive and negative regulation of insulin signaling through IRS-1 phosphorylation.* Biochimie, 2005. **87**(1): p. 99-109.

175. Sentinelli, F., et al., *The G972R variant of the insulin receptor substrate-1 gene impairs insulin signaling and cell differentiation in 3T3L1 adipocytes; treatment with a PPARgamma agonist restores normal cell signaling and differentiation.* J Endocrinol, 2006. **188**(2): p. 271-85.

176. Neuhausen, S.L., et al., *Prostate cancer risk and IRS1, IRS2, IGF1, and INS polymorphisms: strong association of IRS1 G972R variant and cancer risk.* Prostate, 2005. **64**(2): p. 168-74.

177. Shapiro, S.D., et al., *Neutrophil elastase contributes to cigarette smoke-induced emphysema in mice.* Am J Pathol, 2003. **163**(6): p. 2329-35.

178. Wilson, D.O., et al., *Association of radiographic emphysema and airflow obstruction with lung cancer.* Am J Respir Crit Care Med, 2008. **178**(7): p. 738-44.

179. Houghton, A.M., M. Mouded, and S.D. Shapiro, *Common origins of lung cancer and COPD.* Nat Med, 2008. **14**(10): p. 1023-4.

180. Peto, R., Z.M. Chen, and J. Boreham, *Tobacco--the growing epidemic.* Nat Med, 1999. **5**(1): p. 15-7.

181. Tu, Y., et al., *Src homology 3 domain-dependent interaction of Nck-2 with insulin receptor substrate-1.* Biochem J, 2001. **354**(Pt 2): p. 315-22.

182. Rice, W.R., et al., *Maintenance of the mouse type II cell phenotype in vitro.* Am J Physiol Lung Cell Mol Physiol, 2002. **283**(2): p. L256-64.

183. Kliment, C.R., et al., *Oxidative stress alters syndecan-1 distribution in lungs with pulmonary fibrosis.* J Biol Chem, 2009. **284**(6): p. 3537-45.

184. Yasuoka, H., et al., *Insulin-like growth factor-binding protein-5 induces pulmonary fibrosis and triggers mononuclear cellular infiltration.* Am J Pathol, 2006. **169**(5): p. 1633-42.

185. Houghton, A.M., et al., *Macrophage elastase (matrix metalloproteinase-12) suppresses growth of lung metastases.* Cancer Res, 2006. **66**(12): p. 6149-55.

186. *American Thoracic Society. Idiopathic pulmonary fibrosis: diagnosis and treatment. International consensus statement. American Thoracic Society (ATS), and the European Respiratory Society (ERS).* Am J Respir Crit Care Med, 2000. **161**(2 Pt 1): p. 646-64.

187. Hinz, B., et al., *The myofibroblast: one function, multiple origins.* Am J Pathol, 2007. **170**(6): p. 1807-16.

188. Hinz, B., *Formation and function of the myofibroblast during tissue repair*. J Invest Dermatol, 2007. **127**(3): p. 526-37.

189. Hu, B., Z. Wu, and S.H. Phan, *Smad3 mediates transforming growth factor-beta-induced alpha-smooth muscle actin expression.* Am J Respir Cell Mol Biol, 2003. **29**(3 Pt 1): p. 397-404.

190. Hunninghake, G.W., et al., *Mechanisms of neutrophil accumulation in the lungs of patients with idiopathic pulmonary fibrosis.* J Clin Invest, 1981. **68**(1): p. 259-69.

191. Yamanouchi, H., et al., *Neutrophil elastase: alpha-1-proteinase inhibitor complex in serum and bronchoalveolar lavage fluid in patients with pulmonary fibrosis.* Eur Respir J, 1998. **11**(1): p. 120-5.

192. Ziegenhagen, M.W., et al., *Serum level of interleukin 8 is elevated in idiopathic pulmonary fibrosis and indicates disease activity.* Am J Respir Crit Care Med, 1998. **157**(3 Pt 1): p. 762-8.

193. Baugh, R.J. and J. Travis, *Human leukocyte granule elastase: rapid isolation and characterization.* Biochemistry, 1976. **15**(4): p. 836-41.

194. Belaaouaj, A., K.S. Kim, and S.D. Shapiro, *Degradation of outer membrane protein A in Escherichia coli killing by neutrophil elastase.* Science, 2000. **289**(5482): p. 1185-8.

195. Hedstrom, L., *Serine protease mechanism and specificity.* Chem Rev, 2002. **102**(12): p. 4501-24.

196. Senior, R.M., et al., *The induction of pulmonary emphysema with human leukocyte elastase.* Am Rev Respir Dis, 1977. **116**(3): p. 469-75.

197. Chua, F., et al., *Mice lacking neutrophil elastase are resistant to bleomycin-induced pulmonary fibrosis.* Am J Pathol, 2007. **170**(1): p. 65-74.

198. Mitsuhashi, H., et al., *Administration of truncated secretory leukoprotease inhibitor ameliorates bleomycin-induced pulmonary fibrosis in hamsters.* Am J Respir Crit Care Med, 1996. **153**(1): p. 369-74.

199. Mittendorf, E.A., et al., *Breast cancer cell uptake of the inflammatory mediator neutrophil elastase triggers an anticancer adaptive immune response.* Cancer Res, 2012. **72**(13): p. 3153-62.

200. Gregory, A.D., et al., *Clathrin pit-mediated endocytosis of neutrophil elastase and cathepsin G by cancer cells.* J Biol Chem, 2012. **287**(42): p. 35341-50.

201. Myers, M.G., Jr., et al., *IRS-1 is a common element in insulin and insulin-like growth factor-I signaling to the phosphatidylinositol 3'-kinase.* Endocrinology, 1993. **132**(4): p. 1421-30.

202. White, E.S., et al., *Negative regulation of myofibroblast differentiation by PTEN (Phosphatase and Tensin Homolog Deleted on chromosome 10).* Am J Respir Crit Care Med, 2006. **173**(1): p. 112-21.

203. Woessner, J.F., Jr., *The determination of hydroxyproline in tissue and protein samples containing small proportions of this imino acid.* Arch Biochem Biophys, 1961. **93**: p. 440-7.

204. Kaynar, A.M., et al., *Neutrophil elastase is needed for neutrophil emigration into lungs in ventilator-induced lung injury.* Am J Respir Cell Mol Biol, 2008. **39**(1): p. 53-60.

205. McAnulty, R.J., *Fibroblasts and myofibroblasts: their source, function and role in disease.* Int J Biochem Cell Biol, 2007. **39**(4): p. 666-71.

206. Wiedow, O., et al., *Lesional elastase activity in psoriasis, contact dermatitis, and atopic dermatitis.* J Invest Dermatol, 1992. **99**(3): p. 306-9.

207. Talukdar, S., et al., *Neutrophils mediate insulin resistance in mice fed a high-fat diet through secreted elastase.* Nat Med, 2012. **18**(9): p. 1407-12.

208. Metz, H.E. and A.M. Houghton, *Insulin receptor substrate regulation of phosphoinositide 3-kinase.* Clin Cancer Res, 2011. **17**(2): p. 206-11.

209. Wilkes, M.C., et al., *Transforming growth factor-beta activation of phosphatidylinositol 3-kinase is independent of Smad2 and Smad3 and regulates fibroblast responses via p21-activated kinase-2.* Cancer Res, 2005. **65**(22): p. 10431-40.

210. Qian, Y., et al., *ILK mediates actin filament rearrangements and cell migration and invasion through PI3K/Akt/Rac1 signaling.* Oncogene, 2005. **24**(19): p. 3154-65.

211. Haak, A.J., et al., *Targeting the myofibroblast genetic switch: inhibitors of myocardin-related transcription factor/serum response factor-regulated gene transcription prevent fibrosis in a murine model of skin injury.* J Pharmacol Exp Ther, 2014. **349**(3): p. 480-6.

212. Liu, T., et al., *FIZZ1 stimulation of myofibroblast differentiation.* Am J Pathol, 2004. **164**(4): p. 1315-26.

213. Raghu, G., et al., *Prednisone, azathioprine, and N-acetylcysteine for pulmonary fibrosis.* N Engl J Med, 2012. **366**(21): p. 1968-77.